University of Pretoria

X-RAY AND NMR SPECTROSCOPIC STUDIES OF SELECTED HETEROCYCLIC COMPOUNDS OF PHOSPHORUS AND NITROGEN

BY

R.M. MAMPA

X-RAY AND NMR SPECTROSCOPIC STUDIES OF SELECTED HETEROCYCLIC COMPOUNDS OF PHOSPHORUS AND NITROGEN.

A thesis submitted by

RICHARD MOKOME MAMPA

In partial fulfilment for the degree of

MAGISTER SCIENTIAE

(CHEMISTRY)

Faculty of Natural and Agricultural Sciences

UNIVERSITY OF PRETORIA

SUPERVISOR : PROF. T.A. MODRO

CO-SUPERVISOR : PROF. K.R. KOCH

(UNIVERSITY OF STELLENBOSCH)

November 2000

DECLARATION

I hereby declare that this thesis submitted to the University of Pretoria for the degree of Master of Science in Chemistry has not been previously submitted by me for the degree at this university or any other university, that this is my own work in design and execution, and that all materials contained therein have been duly acknowledged.

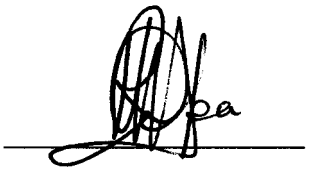

Signature

28 MAY 2001

Date

TABLE OF CONTENTS

ABSTRACT

A full ^{1}H, ^{13}C and ^{31}P NMR assignments of phosphoric triamides 1-oxo-2,8-diphenyl-2,5,8-triaza-1-phosphabicyclo [3.3.0]octane (**1**), 1-oxo-10-phenyl-4,7,10-triaza-2.3-benzo-1-phoshabicyclo [5.3.0]decane (**2**) and 1-oxo-4,7,10-triaza-2,3,11,12-dibenzo-1-phosphabicyclo[5.5.0]dodecane (**3**) which have been recently synthesised was accomplished. The solution state NMR analysis of these compounds showed a number of interesting spin systems upon moving from **1**→**2**→**3**, spanning from ABC to ABCDX spin systems where X is phosphorus nucleus. The three systems showed a high degree of rigidity in solution state, which made it possible to compare dihedral/torsion angles determined from solution state NMR with those of X-ray diffraction data. Both X-ray diffraction and NMR analysis supported the molecular conformations. A significant solvent effect was observed for solutions of compounds **1**, **2** and **3** in benzene-d_6 compared to solutions in chloroform-d_1 and acetone. Benzene-d_6 showed a generally upfield chemical shift of methylene protons in particular, and this is assumed to be due to different solvent-substrate interactions and to the magnetic anisotropic effect of the solvent.

LIST OF TABLES

LIST OF FIGURES

ABRIVIATIONS/SYMBOLS

1. BuLi = Butyllithium
2. COSY = Correlated Spectroscopy
3. LAOCOON = Least squares Adjustment Of Calculated On Observed NMR transitions.
4. NMR = Nuclear Magnetic Resonance
5. ORTEP = X-ray structure determination computer programme.
6. ppm = parts per million
7. SHELX = Crystal structure determination programme.
8. SHELXL = Solution refinement X-ray structure determination computer programme.
9. RSC = Royal Society of Chemistry
10. δ = Chemical shift
11. θ = Dihedral angle
12. ϕ = Valence angle

ACKNOWLEDGEMENTS

I wish to express my sincere gratitude and appreciation to my supervisor, Professor T.A. Modro for suggesting the problem and providing continuous guidance and support. I also wish to direct my sincere thanks to co-supervisor, Professor K Koch for his technical assistance with the NMR spectroscopy at University of Stellenbosch. A word of thanks goes to Professor J.J. Prinsloo for his vision and support as the then head of the Chemistry Department at the University of the North. A special thanks goes to all my colleagues in the Chemistry Department and Mrs M.S Thomas in the Unify Department, both of University of the North for their support.

Finally, I wish to acknowledge my parents and friends, for their continuous spiritual and moral support. Last but least, I wish to express my deepest gratitude to my wife, Joyce for all the time and sacrifices she endured during my entire academic period.

I also wish to acknowledge the financial assistance from the National Research Foundation (NRF) as well as the University of the North.

CHAPTER 1

INTRODUCTION

The appropriate theme for nuclear magnetic resonance spectroscopy is nuclear induction, springing from the first, but simple demonstration during the winter of 1945-46 by Professors F. Bloch and W. Hansen, and their associates at Stanford, and by another independent group at Harvard, directed by Dr. E.M. Purcell[1], and gaining momentum and strength from its application to structural chemistry. An introduction of superconducting magnets, Fourier-transform and multiple-pulse excitation made the NMR today to be the only known method for determining structure and conformation of complex molecules in solution. Nuclear Magnetic Resonance has wrought a revolution in biological sciences and in medicine through magnetic resonance imaging and will continue to do so as results of its non-invasive and selective NMR spectroscopic analysis of biological systems, including humans.

1.1 NMR SPECTROSCOPY IN STRUCTURAL ASSIGNMENT OF ORGANIC CYCLIC SYSTEMS

Proton nuclear magnetic resonance (^{1}H NMR) has been the powerful method of conformational analysis ever since the discovery of magnetic resonance phenomenon in solution state of matter. The success of ^{1}H NMR hinged upon several features, principally the higher natural abundance (99.98%), high sensitivity of the ^{1}H nucleus

and its spin quantum number of half (i.e. I= ½, leading to simpler spectra). Hydrogen atoms are present in the vast majority of organic compounds at strategic positions. The ubiquitousness of hydrogen atoms in organic molecules also makes it a ready to focus at in the analysis of organic compounds. Not much about the ^{1}H NMR spectroscopy can be said without in depth analysis of what spin-spin splitting or spin-spin coupling is.

1.1.1 Spin-spin coupling/ spin-spin splitting.

The theory of spin-spin coupling is complex; hence only a simplified version of the theory is treated here. Spin–spin coupling interaction between nuclei of spin quantum number not equal to zero ($I \neq 0$), arises principally from the electron-spin interactions, not from the orbital interaction[2]. The coupling interaction is proportional to the product of the magnetogyric ratios of the coupled nuclei[3]; the same is true of the electron orbital and electron-dipole terms. For comparison of the magnitude of coupling constant between different nuclei, and to compensate for the negative sign introduced in some cases by magnetogyric ratios, a reduced coupling constant K_{AB} can be defined as follows:

$$K_{AB} == \frac{2\pi}{\gamma_A \gamma_B} J_{AB} \quad \text{.....[1]}$$

where the dependence of J in cycles per second or Hz and γ (the magnetogyric ratio of the coupling nuclei) represents changes in coupling constant with isotopic substitution even-though the electron distribution in the molecule remain unchanged[2].

The terms spin-spin splitting or spin-spin coupling are used interchangeably due to the fact that coupling results from spin splitting[1]. The spin-spin coupling phenomenon is called scalar coupling when coupling is carried through chemical bonds by electrons in an isotropic liquid phase and not through space[4] as is the case with dipole-dipole interactions. Spin-spin splitting occurs between magnetically non-equivalent protons attached to the same carbon or adjacent carbon atoms that exhibit spin-spin coupling. The theory of spin coupling is in accord with an interaction of the form $I_1.I_2$ (where I_1 and I_2 are nuclear spin vectors) which depends on the orientation of one spin with respect to the other, but does not depend on the orientation of the spin with respect to magnetic field[4]. The theoretical development of the electron-coupled spin-spin interaction has been carried out principally by second-order pertubation theory[3]. Coupling between protons occurs as a result of the difference in the chemical shifts between nuclei of the type (homonuclear) and between nuclei of different type (heteronuclear). However two or more nuclei can be either chemically equivalent or magnetically equivalent, the former being due to identical chemical environment and the latter being due to not only chemical environment but also having the same coupling constant with every other nuclei in the molecule. As the nuclei interact, they produce different coupling patterns which, can be simplified by the letters of alphabet, e.g AMX.

Assuming that AMX is as a result of interaction between three homonulear nuclei, this means that one falls at low field (X), another at an intermediate value (M), and the third at a high-field position (A). Interpretation of spin-spin splitting or spin-spin coupling systems can be treated by first order analysis only if:

(i) the chemical shift difference between nuclei is much larger than the coupling between them ($\Delta E/J > 10$),

(ii) and that the coupling must involve groups of nuclei that are magnetically equivalent and not just chemically equivalent

It is for this reason that the splitting does not interfere or affect the overall integrated intensities of the multiplets, which have to correspond with the number of underlying protons. Hence, coupling constant, $^{\#}J_{ab}$ (where # is the number of bonds between the coupling nuclei and, a and b are the coupling nuclei) are extremely useful in recognising stereochemical relationships between carbons to which protons are attached. Moreover, in complicated cases, the coupling constants are utilised in tracking sequences of protons around a molecule by means of shared J values. It was earlier reported that protons attached to adjacent carbon atoms tend to have antiparallel nuclear moments with respect to one another in the lower energy state. By definition, the coupling constants between such protons attached to the same carbon tend to have their nuclear moments parallel to one another in the lower-energy state and from that, coupling constants between such as geminal methylene protons are usually negative[5, 6] (see figure 1.1). Couplings are generally transmitted more effectively through multiple bonds than

through single bonds[5,7,8], to an extent that coupling through four bonds ($^4J_{HH}$) are often reported. For example, vicinal couplings for ethane derivative are usually < 10Hz, while in ethylene derivatives $^3J_{(cis)}$ ≈10Hz and $^3J_{(trans)}$ ≈17Hz as illustrated in Figure 1.2 according "w" pattern.

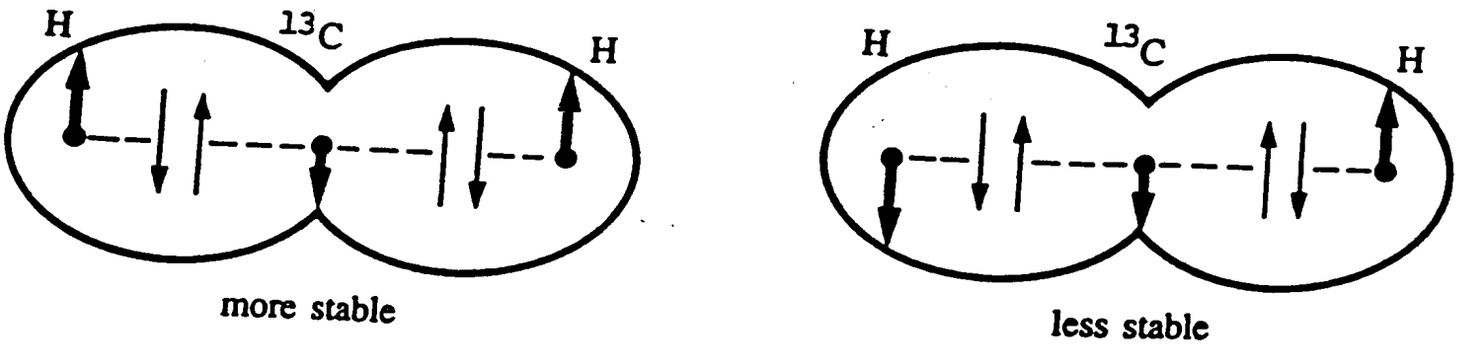

Figure 1.1 Nuclear and electronegative spin orientation in an H – C – H unit. Boldface arrows represent nuclear spins, while regular arrows represent the electronic spins.

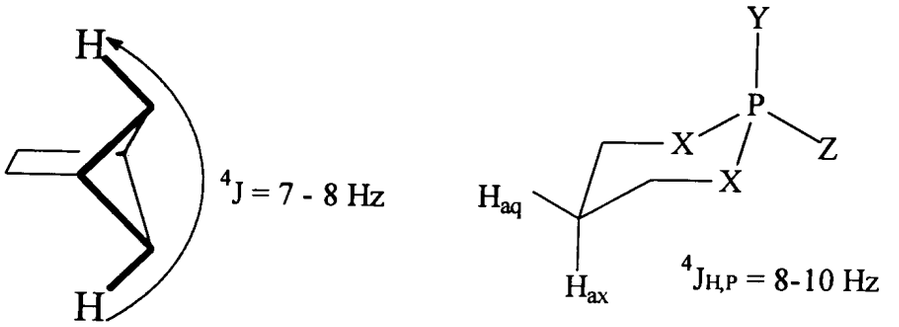

Figure 1.2. An illustration of long range coupling constant through bonds.

1.1.2. Analysis of $^3J_{HH}$ vicinal systems in cyclic organic systems.

Vicinal proton-proton couplings in saturated compounds have been studied extensively both experimentally and theoretically and the factors influencing $^3J_{HH}$ are therefore very well understood. Coupling constants, measured as frequency differences in Hertz between individual peaks of multiplets, are not affected or dependent on the strength of magnetic field, unlike chemical shifts. However there are several factors affecting vicinal coupling constants. Among the most important physical factors, which affect the magnitude of $^3J_{HH}$ coupling constant are [7,8]

i. Hybridization of the atoms in the spin system,

ii. dihedral bond angle or torsion angle (θ) on the H-C-C-H moiety,

iii. electronegativity of the substituents X and Y on the H-C(X)-C(Y)-H moiety,

iv. bond length between the two carbon atoms bearing the protons and

v. H-C-C-H valence angles ϕ and ϕ' e.g. cyclic olifines, in which the dihedral angles is zero, i.e. $\phi = \phi$' and the ^3J decreases with decreasing ring size.

The dependence of coupling constant on the electron density (i.e. electronegativity and hybridisation) of the nucleus suggests a relation between J and the amount of shared *s* character in the bond. Such a relation is indeed found for ^{13}C-^1H couplings in *sp*, sp^2, sp^3 hybridized systems[3,9].

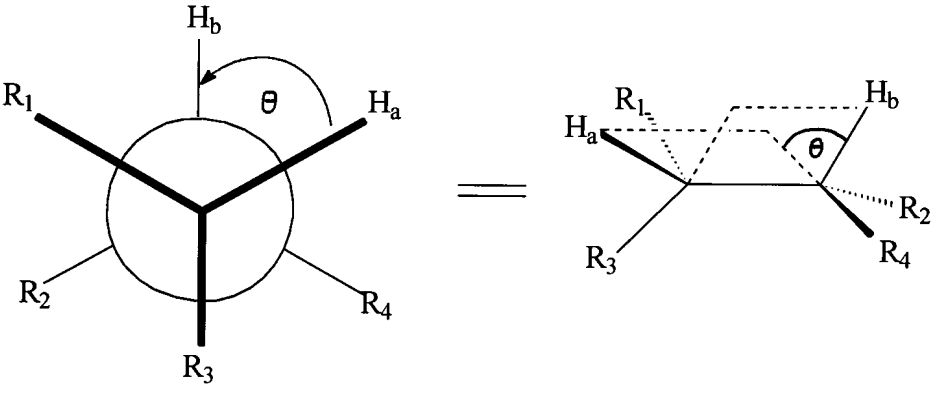

Figure 1.3 Schematic representation of vicinal system $^{3}J_{H(a)H(b)}$, where the angle between H_a and H_b represents the vicinal dihedral angle.

One of the most important factors that affect vicinal coupling relationships is the dihedral angle, θ. Valence bond theory has been of great success in qualitatively describing trends in $^{3}J_{HH}$[7]. Torsion or dihedral angle can be defined as the angle of rotation about a carbon-carbon bond viewed end on with the lower numbered carbon nearest the viewer and hydrogen eclipsed; a clockwise rotation of the carbon farthest away corresponding to a positive dihedral angle (figure 1.3). The dependence of the coupling constant on dihedral angles can approximately be determined by the Karplus equation[10] as in equation [3] and [4] and some of its variation[11]. By employing an appropriate set of parameters, the Karplus equation can be used to describe some of the heterocyclic system conformations in terms of dihedral angles. Normally the sign of coupling constant (illustrated in figure 1.1) has no effect on the appearance of the NMR spectrum[6] and therefore has no effect on the Karplus equations.

$$^{3}J_{HH} = 9.5\ cos^{2}\ \theta - 0{,}28 \text{ for } \theta = 90° - 180^{0} \quad \ldots\ldots\ldots\ldots\ldots\ldots [4]$$

where the value of θ is the dihedral angle represented in figure 1.4

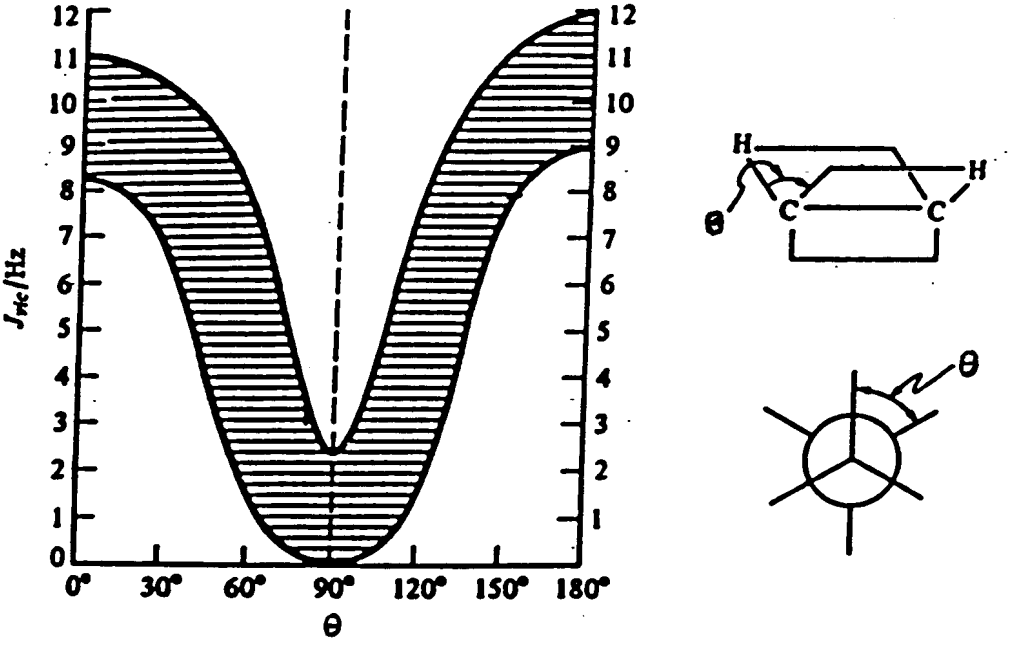

Figure 1.4 Graphical representation of Karplus equation.

The experience has shown however that the ^{3}J values for θ = 0° and θ = 180° are in general are about 2-4 Hz larger than the calculated values, although the prediction $^{3}J_{180°} > {}^{3}J_{0°}$ is always confirmed [12]. Alternatively the dependence of vicinal J values can be predicted by the semiempirical equation 5:

$$^{3}J_{HH} = A + B\ cos\ \theta + C\ cos\ 2\theta \quad \text{.....[5]}$$

where A, B and C are constant with approximate values 4.0 Hz, -0.5 Hz and 4.5 Hz respectively[3,9]. However use of these values usually underestimates ^{3}J, and a better set for hydrocarbons is found to be A = 7 Hz, B = -1 Hz and C = 5 Hz. Equations 3, 4 and 5 are named after M Karplus[10,13]. Although the exact values of the Karplus parameters A,B, and C depend on the detailed structure of the compound under consideration, and may vary depending on the specific H-C-C-H fragment being considered, an empirical set of parameters for all fragments can be determined if acceptable error limits are placed on the dihedral or torsion angle to be calculated. Such an approach has also been taken for the five-membered rings in poly(L-proline)II[14] and specific proline derivatives[15,16]. Coupling constants in three bonds systems has usually a positive sign because of orbital energy stabilization. It is for that reason that a rough idea of how the dihedral angle affects the magnitude of the coupling may be obtained. Figure 1.4, shows that the coupling constant is largest when the vicinal protons are *trans*-coplanar (i.e. θ = 180°), zero when the respective H-C-C-H are at 90° to one another, and larger when the protons are *cis*-coplanar (i.e. θ = 60°). This can be explained by the stereochemical interaction between the two vicinal molecular orbitals (bonds) is at its maximum when the orbitals are parallel (dihedral angle of 0^0 and 180^0), which decreases to nearly zero when the orbitals are perpendicular (a dihedral angle of 90^0)[5]. This is analogous to the requirement for *p*-orbital to be parallel to form a π bond system. It should, however be

noted that since most single bonds that are not part of the ring structure, these can rotate constantly and rapidly (on the NMR time scale), so that the observed values of ^3J represent a weighted average over all conformations. Such a scalar coupling constant can also show a dependence on the temperature, because the ratio of the various conformations (of different energy) can vary with temperature according to the Boltzman distribution equation[17] [6].

$$\frac{P_{(m=-1/2)}}{P_{(m=½)}} == e^{-\Delta E/KT} \quad \text{.....[6]}$$

Where $P_{(m=-1/2)}$ and $P_{(m=1/2)}$ are the number of nuclei in the ground and excited sates respectively of either the minor or the major conformer, ΔE is the energy difference between them, *k* is the Boltzman constant, and T is the absolute temperature.

The relationship between the dihedral angle and vicinal coupling constant is of particular importance in the stereochemistry of groups attached to cyclic systems, e.g. triterpernoids, steroids, etc. In the cyclohexane ring, the hydrogens can be either axial or equatorial, forming with their neighbours a dihedral angle of between 60^0 and 180^0, thus rendering the application of the Karplus equation and some its variations a straightforward procedure to find out the stereochemistry of the products through coupling constant between vicinal hydrogens which could otherwise not be determined with ease.

Since the dihedral angle is the largest when the vicinal protons are diaxial, thus *trans*-coplanar with respect to one another, the coupling constants are accordingly larger, but when the vicinal protons are in an axial-equatorial or equatorial-equatorial relationship, the dihedral angle is about 60^0 or less and the coupling constant are correspondingly smaller[8]. Table 1.1; demonstrates the geometrical effect by the coupling nuclei positioned axial-equatorial (*gauche*) and equatorial-equatorial (*cis*) to each other.

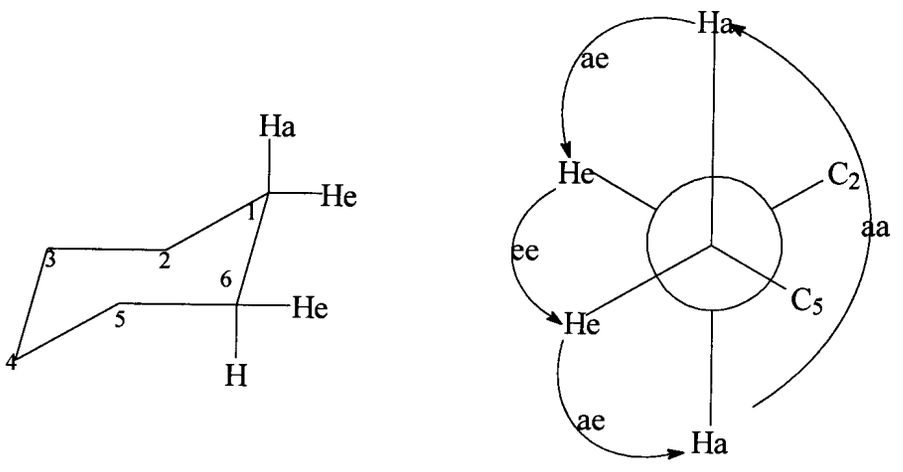

Figure 1.5 Newman projection of C_6 in C1 of cyclohexane ring showing axial-axial (aa), axial-equatorial (ae), and equatorial-equatorial (ee) interaction

An estimation of coupling constants or dihedral angles by Karplus equation does not necessarily end up with only saturated systems, but also applies in olefins, where a modified Karplus equation predicts larger *trans*-coupling than *cis*-coupling.

Table 1.1 Relationship between dihedral angles and vicinal coupling constants for cyclohexane ring.

Dihedral relationship	J (Hz) Calculated	J (Hz) Observed
Axial- Axial (θ_{aa}= 180^0)	9	8-14
Axial-equatorial (θ_{ae}= 60^0)	1.8	1-7
Equatorial-equatorial (θ_{ee}= 60^0)	1.8	1-7

The NMR analysis of the derivatives of cyclic phosphines (e.g. 10-Oxo-10-phospha-1,4,7-triazatricyclo[5.2.1.0]decane) with pyramidal nitrogens is of particular importance in a sense that a similar phenomenon due to vicinal coupling constants as in cyclohexane derivatives is observed [18] (Figure 1.6).

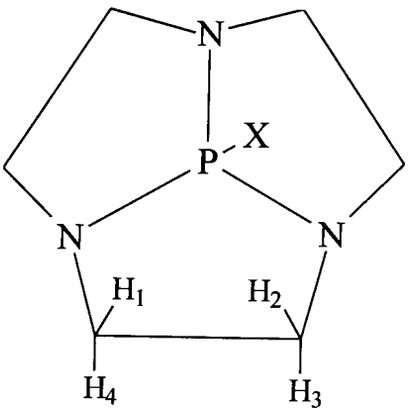

Where X represents O, Se and S.

Figure 1.6. Molecular structure of 10-X-10-phospha-1,4,7-triazacyclo[5.2.1.0]decane.

Table 1.2 LAOCOON III ^{1}H analysis of 10-X-10-phospha-1,4,7-triazatricyclo[5.2.1.0]decane. This is illustrated by LAOCOON III analysis of ^{1}H NMR spectrum as recorded in Table 1.2. The interchange of vicinal coupling, (which assumes $AA^{1}BB^{1}X$ system, where X is ^{31}P) causes no change in any of the NMR spectra since the assignment given are considered positive, although H-C-H geminal coupling have been shown to be generally negative, i.e. $^{2}J_{H(1)H(4)}$ = -12Hz and $^{2}J_{H(2)H(3)}$ = -12Hz. The complexities of structural analysis of this acyclic tri(dialkylamino) phosphines are due to the planarity or pyramidiality of nitrogens in the PNR moiety. Although nitrogen has three bonds plus a "lone pair" of electrons, one might expect sp^3 hybridisation and thus a tetrahedral arrangement, in this case nitrogen is found from X-ray diffraction studies to be generally planar or nearly so (i.e. the sum of the angles around nitrogen is > 355°)[17].

Table 1.2 LAOCOON III analysis of cyclic (dialkylamino) phosphine with pyramidal Nitrogen (Figure 1.6).

	$\delta_{H(1)}$, $\delta_{H(2)}$	$\delta_{H(3)}$, $\delta_{H(4)}$	$^{3}J_{H(1)P}$ $^{3}J_{H(2)P}$	$^{3}J_{H(3)P}$ $^{3}J_{H(4)P}$	$^{3}J_{H(2)\,H(1)}$	$^{3}J_{H(3)\,H(4)}$	$^{3}J_{H(1)H(3)}$ $^{3}J_{H(2)H(4)}$	$^{2}J_{H(1)H(4)}$ $^{2}J_{H(2)H(3)}$
X=O	3,19	3.55	11.8	10.2	6.0	6.0	6.3	-12.0
X=S	3.25	3.63	13.1	11.7	6.1	6.0	6.4	-12.2
X=Se	3.21	3.62	13.4	12.2	6.2	6.2	6.3	-12.2

The validity of the results from reference ([18]) stems from the fact that Karplus equation can be applied to confirm the conformation and configuration of heterocyclic systems since the coupling is transmitted through nitrogen (also oxygen and sulphur atoms) provided that no exchange of protons attached to the heteroatom occurs. It should therefore be noted that the Karplus equation is not limited to conformation analysis of six-membered ring heterocyclic systems but, also to a large number of five-membered ring of phosphorus heterocyclic systems, which have also been analyzed by NMR techniques. Tricovalent 1,2,3-dioxaphospholanes show coupling constants which, are in agreement with the Karplus equation.[19,20], figure 1.7.

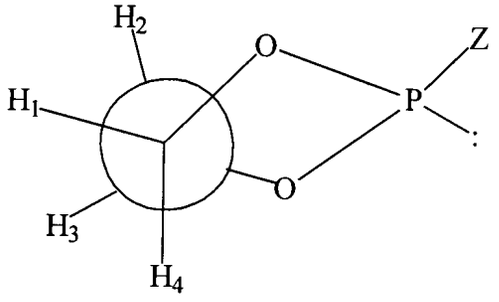

$^3J_{PH(1)} = 3 - 4$ Hz
$^3J_{PH(2)} = -1$ to 0.4 Hz
$^3J_{PH(3)} = 4 - 5$ Hz
$^3J_{PH(4)} = 13 - 15$ Hz

Figure 1.7. Five membered heterocyclic ring with Z representing a variety of substituents.

The largest coupling, i.e. $^3J_{PH(4)}$ = 13-15 Hz, was observed for the proton *syn* to the lone pair[21,22]. Three bond proton-phosphorus coupling through nitrogen [$^3J_{P-H}$] in cyclic systems follow similar Karplus-like relationship, which have been largely derived from 2-oxo and 2-thio-1,2,3-oxazaphosphorinane system [23] .

In general, it has been found that the vicinal coupling constant decreases if electronegative substituent is attached to the H-C(X)-C(H)-H moeity[24] (figure 1.8a). The relationship between the electronegativity of the substituent X and the coupling constant between vicinal proton on a freely rotating alkyl chain is given by equation 7.

$$J = 7.9 - (0.7\Delta E) \quad \text{.....[7]}$$

where ΔE is the difference in Haggins electronegativities between the substituent X and H atom [8].

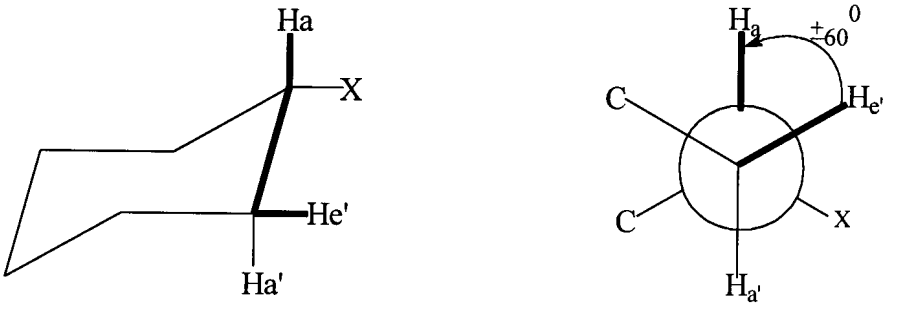

(a) $^3J_{H(a)H(e')} = 5.5$ Hz (*cis*-coplanar)

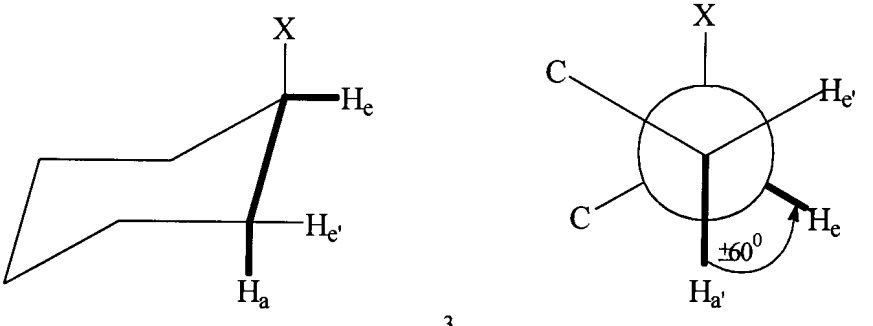

(b) $^3J_{H(a)H(e)} = 2.5$ Hz (*trans*- coplanar)

Figure 1.8. Electronegativity effect on the vicinal coupling constant.

The effect is additive if more than one electronegative substituent is attached to the vicinal carbon atoms. The maximum effect of the substituent in reducing the vicinal coupling constant is observed when the substituent and the proton on the vicinal carbon are *trans*-coplanar[8,25], as shown in figure 1.8(b). In system (a) (figure 1.8) the electronegative substituent (X) is not trans-coplanar to either H(a^1) or H(e^1) whereas in system (b) X and Ha^1 are trans-coplanar, hence $^3J_{H(a)H(c)}$ is reduced to 2.5 Hz. It does appear that the electron-withdrawing effect of X in reducing the coupling constant is more effectively transmitted through the bonds when X and one of the coupling protons are *trans*-coplanar. This information helps in deducing the stereochemistry of X-substituent from the magnitude of the axial-equatorial coupling constant. The electronegativity of the substituent alters the values of geminal coupling only if the two interacting nuclei are magnetically non-equivalent while the ^2J (geminal coupling constant) increases algebraically with increasing electronegativity of the substituent.

One more factor that is of significance in the determination of ^3J (vicinal coupling constant) values is the presence of heteronuclear atom, which is magnetically active ($I \neq 0$). The presence of a heteronuclear atom in the organic molecule can introduce additional complications into the spectrum, since this nuclei will take up spin orientation with respect to the applied field in the same way was a neighbour proton does[4]. Vicinal heteronuclear coupling constant also depends on the dihedral angles. Curves similar to those in figure 1.4, Karplus curves, have been developed for $^3J_{(HCOP)}$ and $^3J_{(NCCH)}$[26]. In molecules where nonbonding electrons are localized in a specific

direction, as in some nitrogen and phosphorus-containing compounds, geminal couplings are also dependent on the angular orientation. In such cases, molecular orbital approach has also been used to calculate proton-proton coupling constants[27].

1.1.4. Stereochemistry of five membered ring compounds.

Five membered rings are common in natural products[28], e.g. carbocylic rings in the D ring of steroids [29, 30] and in prostaglandins[31]; oxygen containing rings in furanose sugars, nucleosides, nucleotides and nucleic acids[32], nitrogen containing rings in the amino acids proline, hydroxyproline and in alkaloids, such as nicotine[33] can serve as examples. A carbocylic planar five membered ring would have valence angles of 108° and thus be nearly free of angle strains. However the torsional strains in such systems is sizeable (estimated at 10 kcal mol^{-1} for 10 pairs of H-H eclipsings) and to minimize this strain, cyclopentane becomes nonplanar[34], thus reducing the sum of residual torsional plus angular strain to the about 60% of the value in a planar ring[34]. The most stable conformations of cyclopentane are therefore the envelope (C_2, naming it after its symmetry point group) and the half-chair (C_s) conformation as shown in figure 1.9

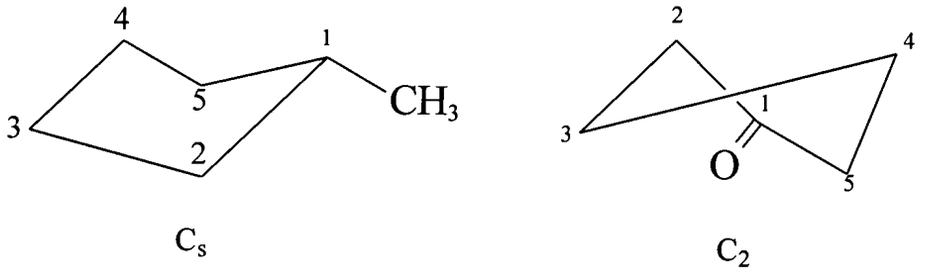

C_s C_2

Figure 1.9. Envelope (C_s) and half-chair (C_2) conformation of cyclopentane derivatives.

The implications of this in the conformational analysis of cyclopentanes are two fold[28]. One stems from the low energy barriers between envelope and half-chair which make it impossible to freeze out, to individual conformers. It is for this reason that cyclopentanes (or heterocyclo-pentanes) are totally different from cyclohexane derivatives in which their chair conformation is located in deep energy valley[28], which contribute towards their relative stability. In cyclopentane, there is little if any energy difference between the envelope and the half-chair, i.e. about 0.5 kcal mol^{-1} (2.1 kJ mol^{-1}). The molecule is thus in rapid state of conformational flux among various C_2 and C_s as well intermediate conformations[35]. Internal substitution of the five-membered ring with a heteroatom seems to introduce small energy barrier in the conformation interchange circuit[36,37]. A few studies of heterocyclic five-membered rings have been reviewed by Fuschs[38] and Riddel[39,40]. Both oxygen and nitrogen containing rings, like cyclopentane itself, seem to interchange conformations freely, where equilibrium and NMR studies have been carried out for 2,4-disubstituted and 2,4,5-trisubstituted 1,3-dioxolanes[41].

1.1.5. Stereochemistry of seven ring compounds.

Several reviews of the conformation of seven membered, as well as other medium and larger rings are available [42]. Unlike cyclohexane, which has basically two families of conformations; the chair and the twist-boat family, whereas cycloheptane on the other hand, has many different possible conformations[43].

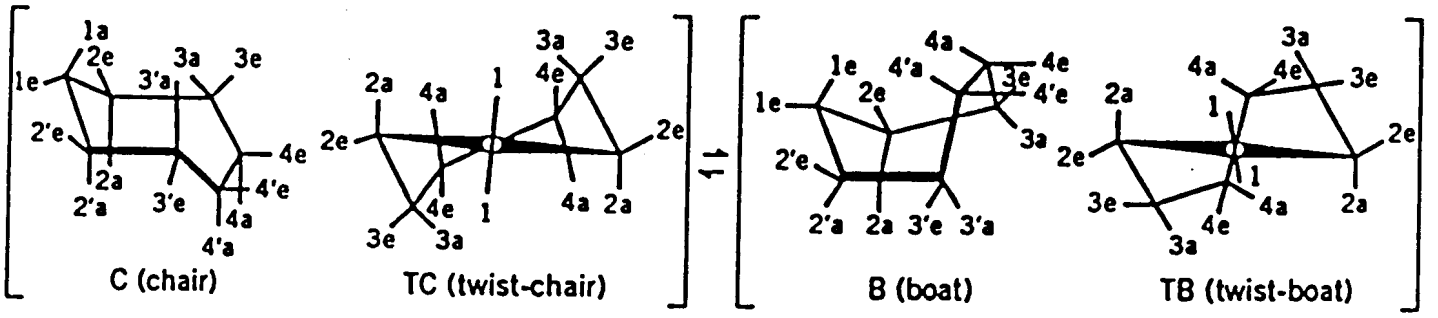

Figure 1.10. Conformations of cycloheptane[44].

The principal methods of conformational studies in seven-membered and larger rings have been NMR spectroscopy, force field calculations, and to a lesser extent, study of vibrational spectra, electron diffraction and X-ray study. The conformational analysis of cycloheptane[45,46,47,48] was first unravelled by the classical study of Hendrickson[46,47,48], which represents one of the first application of molecular mechanics calculation. As shown in figure 1.10, there are basically two families of conformations in cycloheptane wherein the twist-chair and twist-boat represent the most stable conformations of cycloheptane in either family[48]. However a more complicated situation arises as more substituents are introduced into the seven-member ring compound. It rapidly becomes clear that there are more variables in cycloheptane conformations upon substitution than in familiar chair cyclohexane, which has primarily one stable conformation, i.e. chair form, owing to its energy stability. The high symmetry of the chair form of cyclohexane allows the distinguishing of only two kinds of positions for the sustituent, i.e. axial and equatorial. By contrast, there are seven possible sustituent positions distinguishable in the twist-chair cycloheptane and eight in the chair form, with corresponding seven and

eight in the twist-boat and boat respectively, so that conformational analysis of substituted cycloheptanes is notably more complex than in cyclohexane[44].

1.2 X-RAY DIFFRACTION STUDIES OF ORGANIC CYCLIC SYSTEMS.

X-ray diffraction is by far the most powerful technique for the structure determination of crystalline materials varying from the smallest molecules that can be conveniently crystallized to molecules as large as proteins. Crystals are therefore defined as solids in which a basic arrangement of atoms or molecules are repeated periodically by translation vectors in a three nonplanar directions to generate a three dimensional structure formed by small building blocks, called unit cell[28]. Crystals, with their long range ordered structure, provide an excellent diffraction grating for X-rays, giving rise thereby to a discontinuous pattern that is dependent on the relative positions and scattering powers of the individual atoms. Disregarding the generally small atomic motions in molecules, crystals may thus be considered rigid objects with well-defined shape, symmetry and dimension[28]. X-ray diffraction dominates the methods of structural analysis at a level of molecular visualization. X-ray diffraction furnishes two types of stereochemical information: relative to configuration of chiral centres, both intra- and intermolecular, and absolute configuration can be established when the wavelength of the chosen X-ray is to the absorption of an inner-shell electron of one of the atoms in the crystal[49].

Of importance to this research are the torsional angles, as analyzed by the X-ray diffraction method. A torsional angle is a useful conformational parameter of a molecule. The angle θ according to X-ray spectroscopy is defined as the angle between planes ABC and BCD; and lies in the range $-180° < \theta \leq 180°$ where the sign is an important parameter[50] (Fig. 1.11).

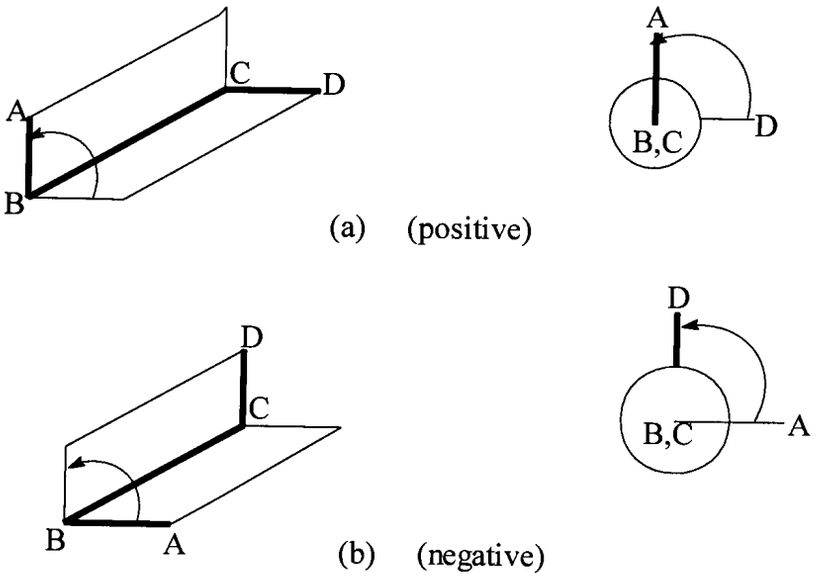

Figure 1.11. Positive and negatively rotated angles as viewed on the X-ray instrument.

There is often confusion in the literature over the use of torsion angle in conformational analysis. It is often convenient to quote values of torsion angles as lying within certain angles. For example, $0^0 \leq \theta \leq 90^0$ as *cis*, $90^0 \leq \theta \leq 180°$ as *trans* and $\theta \approx \pm 60°$ as *gauche*. Therefore it becomes very important and convenient to quote the exact torsion angle to eliminate confusions.

1.3 SHORT REVIEW OF PREPARATION OF SYSTEM 1, 2 AND 3.

The preparation of cyclic phosphoric triamides was achieved in our laboratory before[51]. A series of N-bis(2-chloroethyl) phosphoric triamides (and diamido esters) were prepared by using a phosphoryl chloride as a common starting material (Scheme 1).

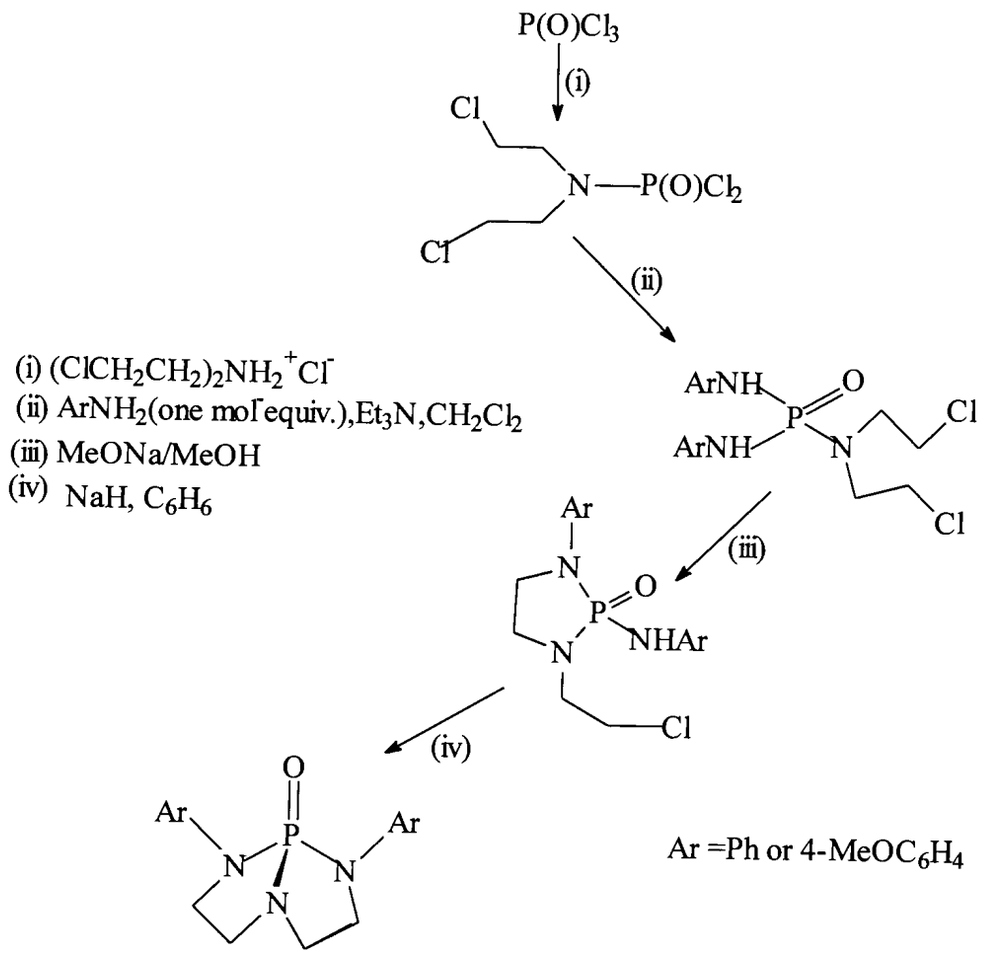

Scheme 1.1

Structural changes in the sequence (ii) → (iii) → (iv) (Scheme 1) were accompanied by a significant deshielding effect in the ^{31}P NMR spectra. Those effects together with the X-ray diffraction analysis, were interpreted in terms of these structural changes in the N-P-N bond angles and the corresponding hybridization changes[52]. Goresnstein reported similar correlation of the ^{31}P NMR chemical shifts with O-P-O bond angles in phosphates.

Regioselective cleavage of a P-N bond in compound **1**[53] can lead to either eight-membered (2,5,8-triaza-1λ^5-phosphacyclooctane) [cleavage of the P-N(5) bond] or the five-membered (1,3,2-λ^5-diazaphospholidine) monocyclic product, [cleavage of the P-N(2) bond]. It was discovered in our laboratory[54] that the bicyclic phosphoric triamide **1** undergoes metallation-induced rearrangement to a new, bicyclic phosphonic diamide **2**, which can undergo further rearrangement to a new, bicyclic phosphinic amide system **3** (Scheme 1.2).

A similar rearrangement involving migration of phosphorus from nitrogen to aromatic carbon was reported with LDA for simple phosphoric N-phenylamide[55]. The structures of the compounds **1, 2, 3** were deduced from NMR (^1H, ^{13}C, ^{31}P) spectroscopy and fully confirmed by X-ray diffraction studies.

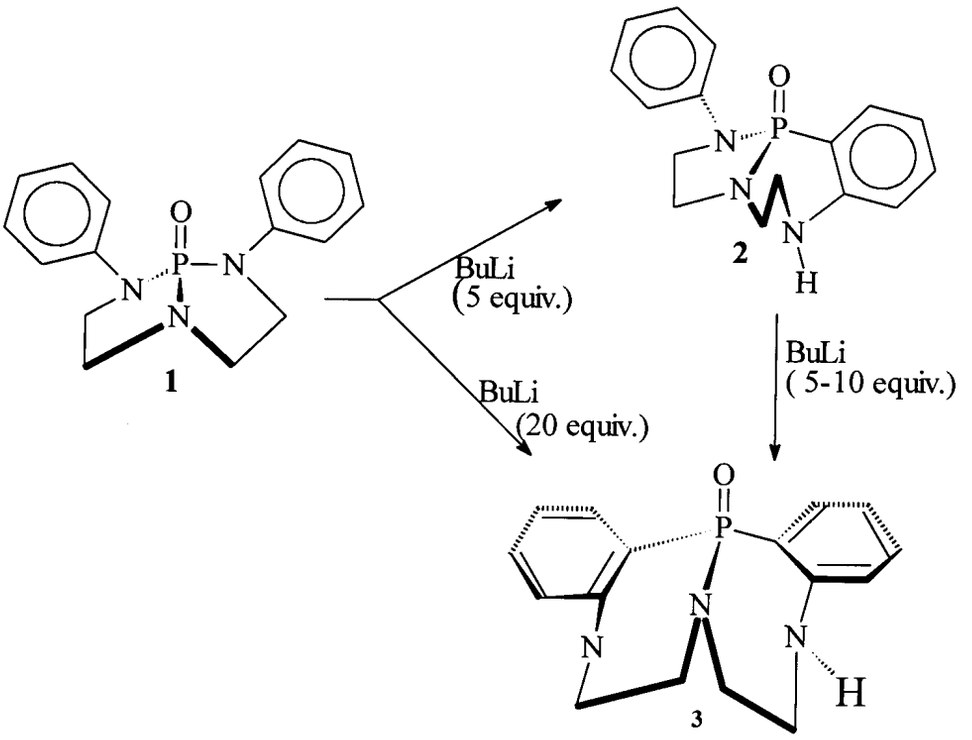

Scheme 1.2

Compounds [**1**], [**2**], and [**3**] represent an interesting series of bicyclic compounds with structural changes that take place at the phosphorus centre during transformation **1→2→3** that lead to unusual bonding parameters of the phosphoryl function in the final product **3** (scheme 1.2).

1.4. OBJECTIVES AND RATIONALE OF THE PROJECT.

The objective of this project was to apply NMR spectroscopic and X-ray analysis in order to get a clear insight into the molecular structures of the new heterocyclic compound which as part of their ring structure contain carbon, nitrogen and phosphorus

atoms. These phosphoric amides (tri-, di-, monoamides) belong to three systems of fused rings (system **1**, **2**, and **3**) as shown in scheme 1.2 and **1a**, **2a**, and **3a** as in figure 1.12 below. Because of the rigid structures of these systems there is high non-equivalency of the individual hydrogen atoms of the ring methylene groups, which have been observed in the ^{1}H NMR spectra of these compounds.

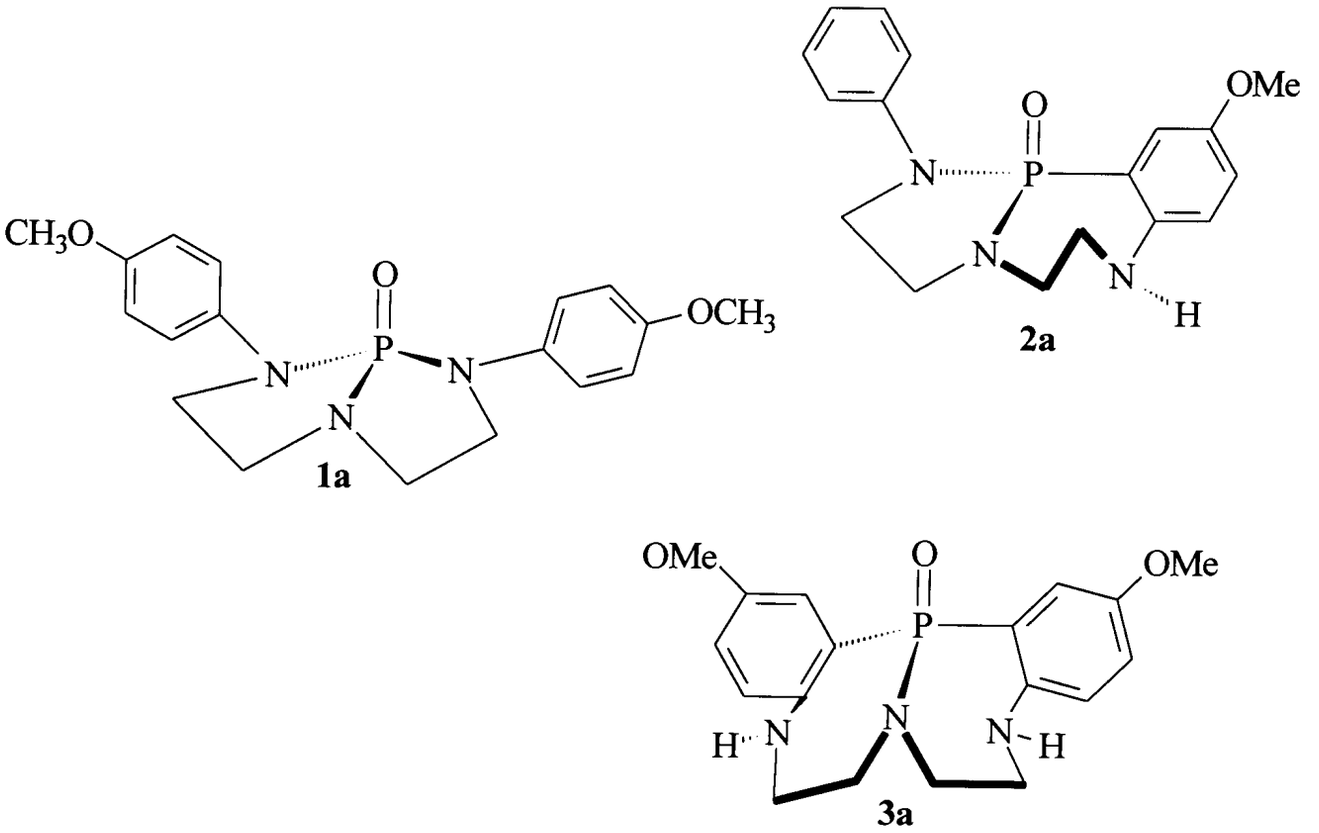

Figure 1.12. Molecular structures of system derivatives, **1a**, **2a**, and **3a**.

The specific objectives therefore were therefore to:

i. assign all the ring methylene protons

i. calculate the dihedral angle of the vicinal protons by Karplus equations

ii. Correlate where possible the NMR spectroscopic data with the molecular geometry information available from X-ray diffraction analysis.

iii. Determine the solvent effect on the NMR characteristics of the phosphoamidate skeleton and

iv. To perform simulation experiments to confirm the NMR spectroscopic data in solution.

1.5 SCOPE OF THE PROJECT

A full NMR analysis was performed on the following compounds, **1**, **1a**, **2**, **2a**, **3** and **3a** i.e. compounds **1**, **2**, and **3** as in scheme 1.2, and **1a**, **2a**, and **3a** as in figure 1.12 . In each case the ^{1}H, ^{13}C, ^{31}P NMR data were obtained and only in selected compounds the ^{1}H NMR spectra were ^{31}P-decoupled. COSY experiments and simulation experiments were also carried out. Solvent effect experiments were performed for each representative compound of the series in deuterated chloroform ($CDCl_3$) deuterated benzene (C_6D_6) and deuterated acetone (CD_3COCD_3). A wide range of NMR instruments were used, starting from as low field as 200 MHz to 600 MHz instrument.

The following instruments were used in different stages of the project:

i. Varian 200 MHz, broad-band Gemini 2000 instrument

ii. Bruker AC 300 MHz spectrometer

iii. Varian VXR-S 400 MHz spectrometer

iv. Bruker DRX 500 MHz spectrometer and

v. Varian ^{UNITY}INOVA 600 MHz spectrometer

CHAPTER 2

CONFORMATIONAL AND STRUCTURAL ANALYSIS OF COMPOUND 1

2.1 ^{1}H NMR assignment of system 1

Compound **1** has an approximate molecular mass of 299.1 g/mol. The compound consists of two five-member rings, which share the phosphorus atom and the bridgehead nitrogen (Figure 2.1). The compound has a C_1 symmetry with a rigid conformational structure on the NMR time scale, and gives only four sets of multiplets for the aliphatic hydrogens of the molecule.

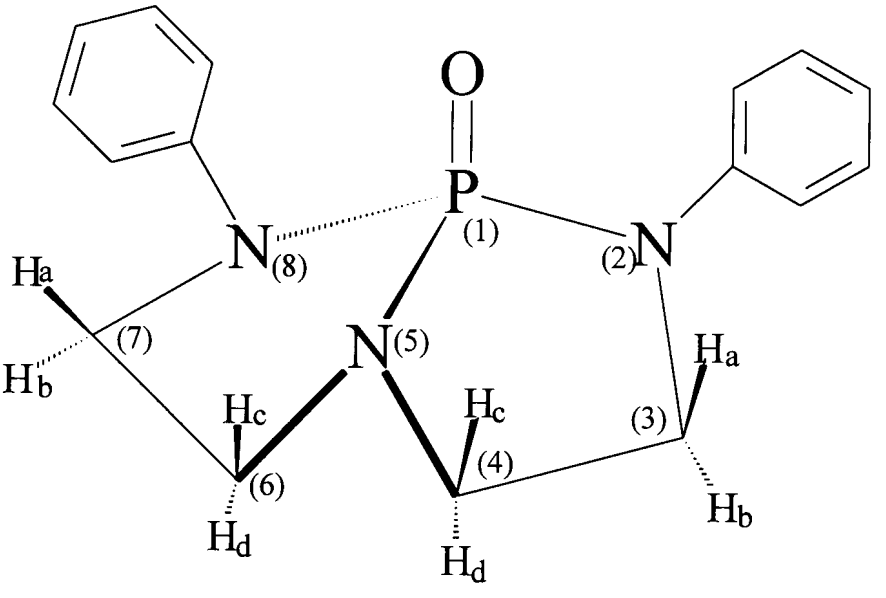

Figure 2.1. A schematic representation of compound **1**

The stereochemistry of the nitrogen atoms at position 2 (N-2) and 8 (N-8) are approximately planar while the nitrogen at position 5 (N-5) is pyramidal. This particular phoshoramidate is characterised by a specific ^{31}P NMR chemical shift of 32.2 ppm and ^{1}H NMR data as in Table 2.1 and figure 2.2a. Similar correlations were done by Gorenstein[27] for ^{31}P chemical shift with O-P-O bond angle in various phosphates and found that a decrease in the bond angle results in the deshielding of the P nucleus. Similar corrections were demonstrated for compounds with the S-P-S bonds[51].

Table 2.1. ^{1}H NMR chemical shifts in deuterated chloroform-d, benzene-d_6 and acetone-d_6.

Proton	δ/ppm (400 MHz) Chloroform-d_1	δ/ppm (200 MHz) Acetone-d_6	δ/ppm (200 MHz) Benzene-d_6
H_a	3.91	3.9	3.0
H_b	3.62	3.6	2.8
H_c	3.77	3.6	3.0
H_d	3.17	3.3	2.1

It was not possible to do full ^{1}H NMR assignment with compound **1** dissolved in acetone-d_6 and benzene-d_6 because of poor solubility. However, deuterated benzene and acetone at 200 MHz field provided a valuable

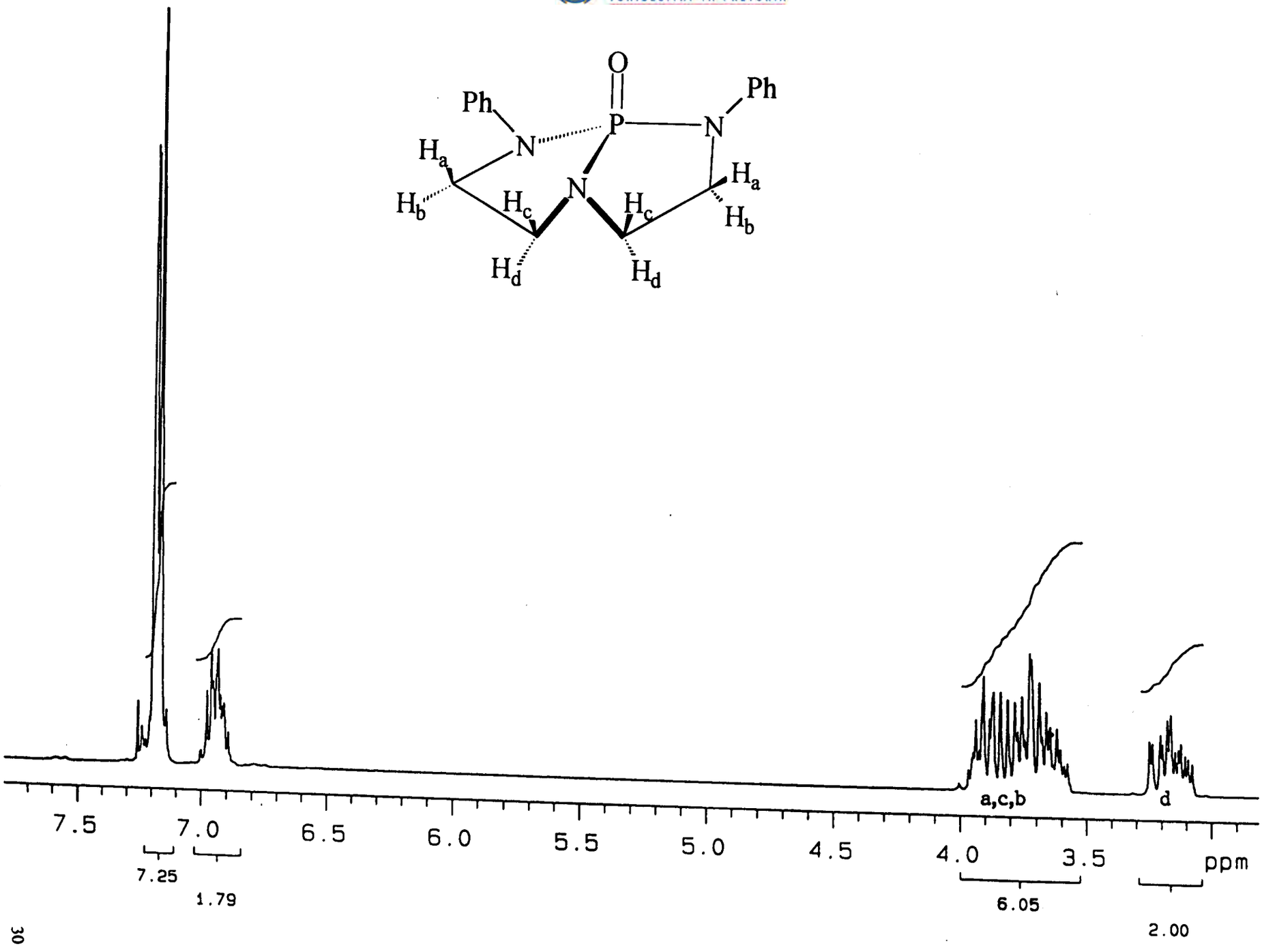

Figure 2.2a. ^{1}H spectrum of **1** at 200 MHz field in chloroform-d_1.

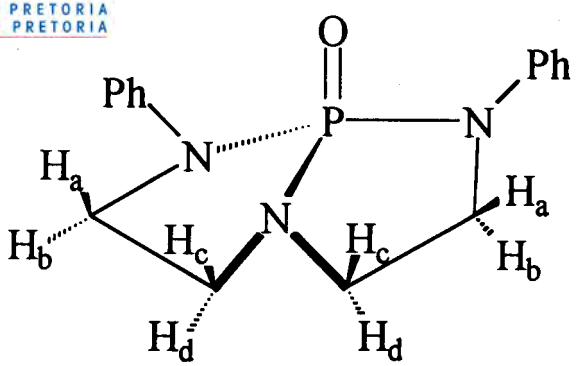

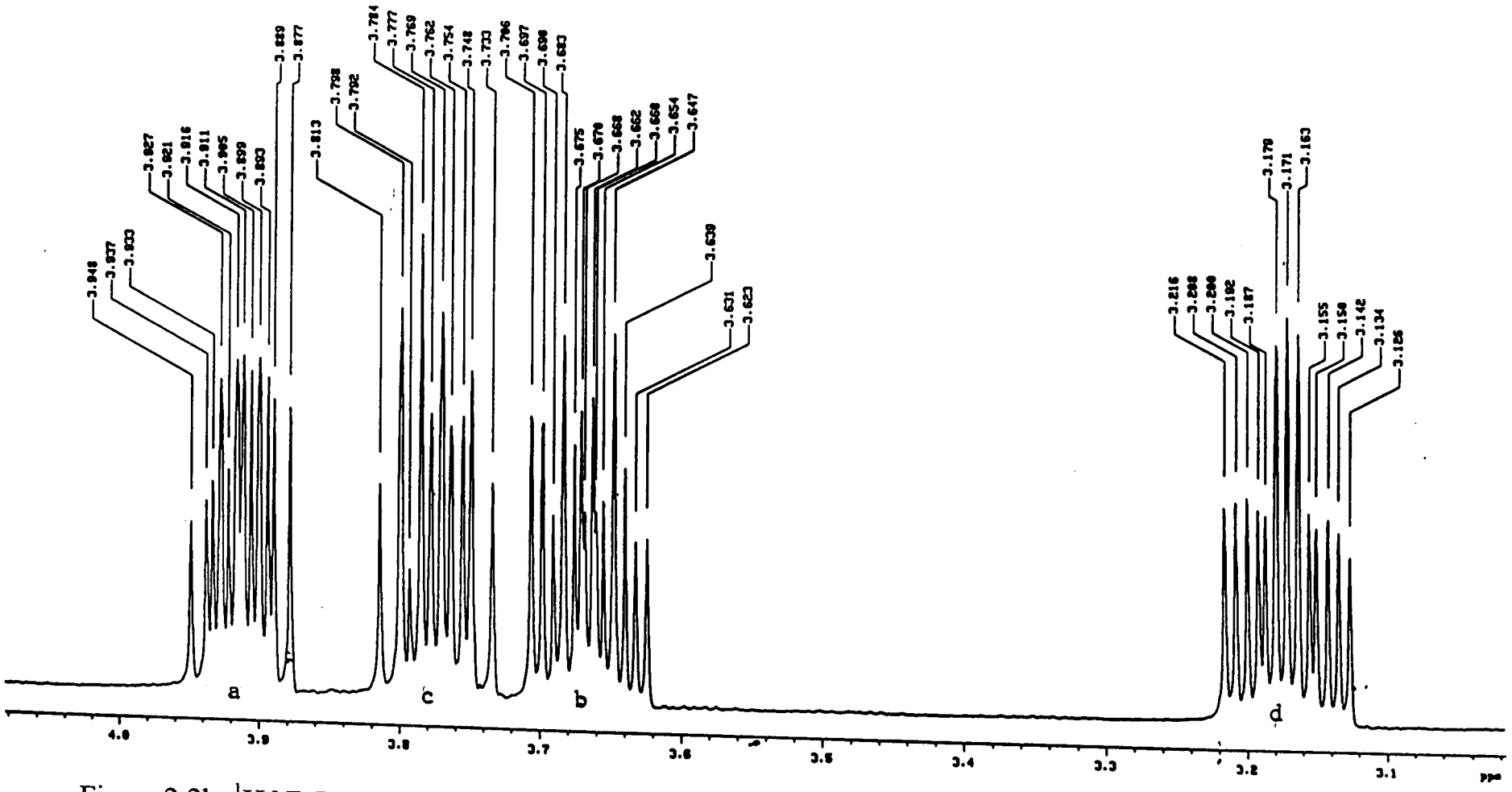

Figure 2.2b. ^{1}H NMR spectrum of the aliphatic region of **1** at 400 MHz field in chloroform-d_1.

information in terms of solvent effects about collective chemical shifts of both aromatic and aliphatic protons. ^{1}H NMR spectrum of the system **1** shows a number of resonances at high field (400 MHz) of interesting features. For the aliphatic protons, there is dramatic separation into the high-field and most high field spectral regions (δ_H 3.1 ppm and δ_H 3.67-3.92 ppm). Figure 2.2b gives a first order spectrum of those protons. Figure 2.2b is hereby used for the analysis and is discussed below. A particular attention is hereby made to the aliphatic spectral region in figure 2.2b to make full assignment of all aliphatic protons.

The appearance of four sets of multiplets brings into picture the molecular plane of symmetry, which divides the protons into two groups of four protons of the vicinal system, which gives an ABCDX spin system, where X represents ^{31}P. According to Atta-ur-Rahman[8], theoretically up to 240 lines can result from five spin interacting nuclei with low $\Delta\delta/J$ ratios, but usually most of these lines are not easy to observe. In comparison, a monosustituted benzene, which has a five spin system where two sets of protons are chemically equivalent but magnetically non-equivalent represent an AA'BB'C spin system that produce as many as 110 lines at high resolution. An ABCDX spin system of **1** results from a ^{31}P-coupled interaction whereas

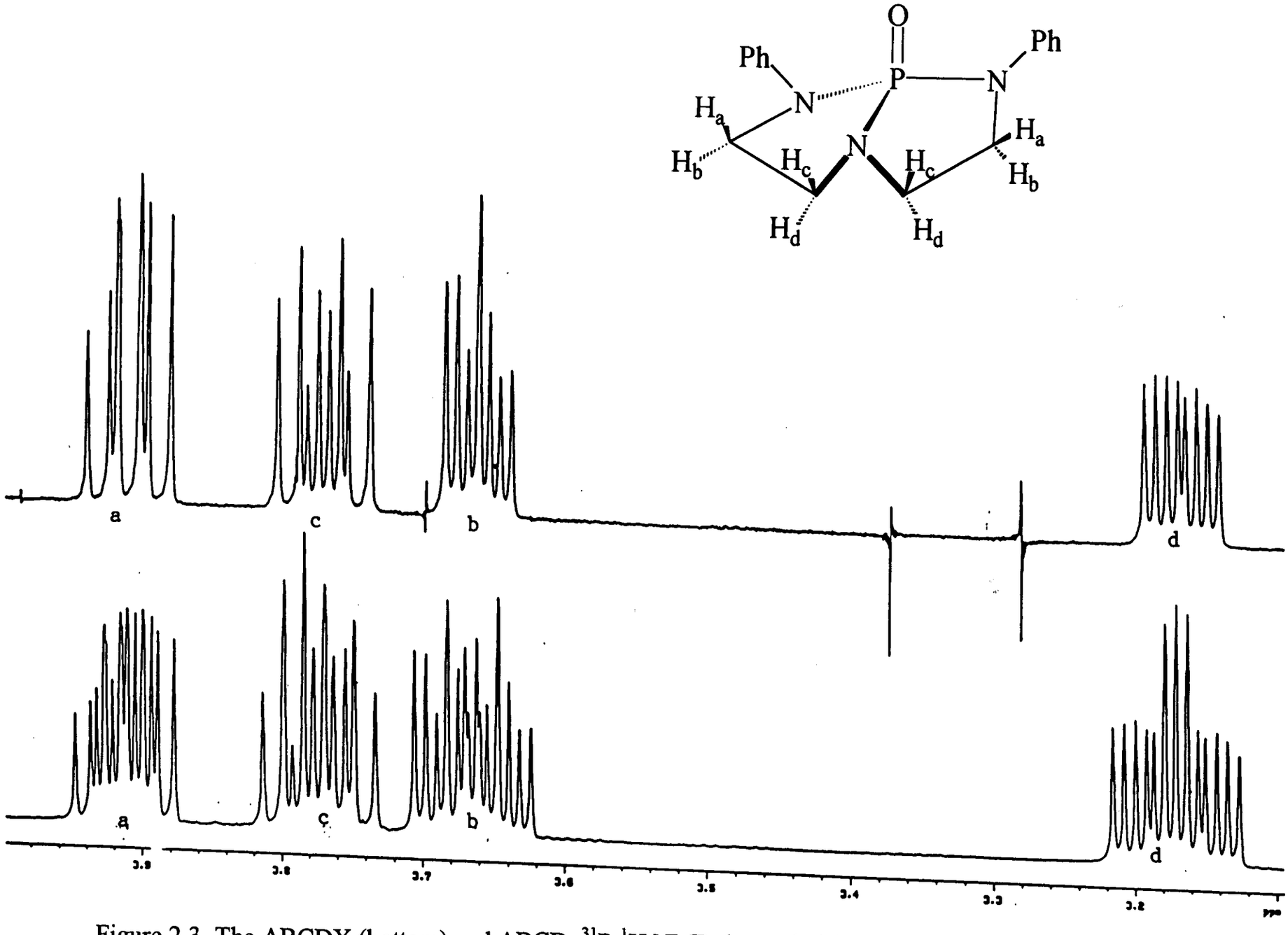

Figure 2.3. The ABCDX (bottom) and ABCD, ^{31}P-^{1}H NMR decoupled (top) spectra of the aliphatic protons of **1** at 400 MHz field in chloroform-d_1.

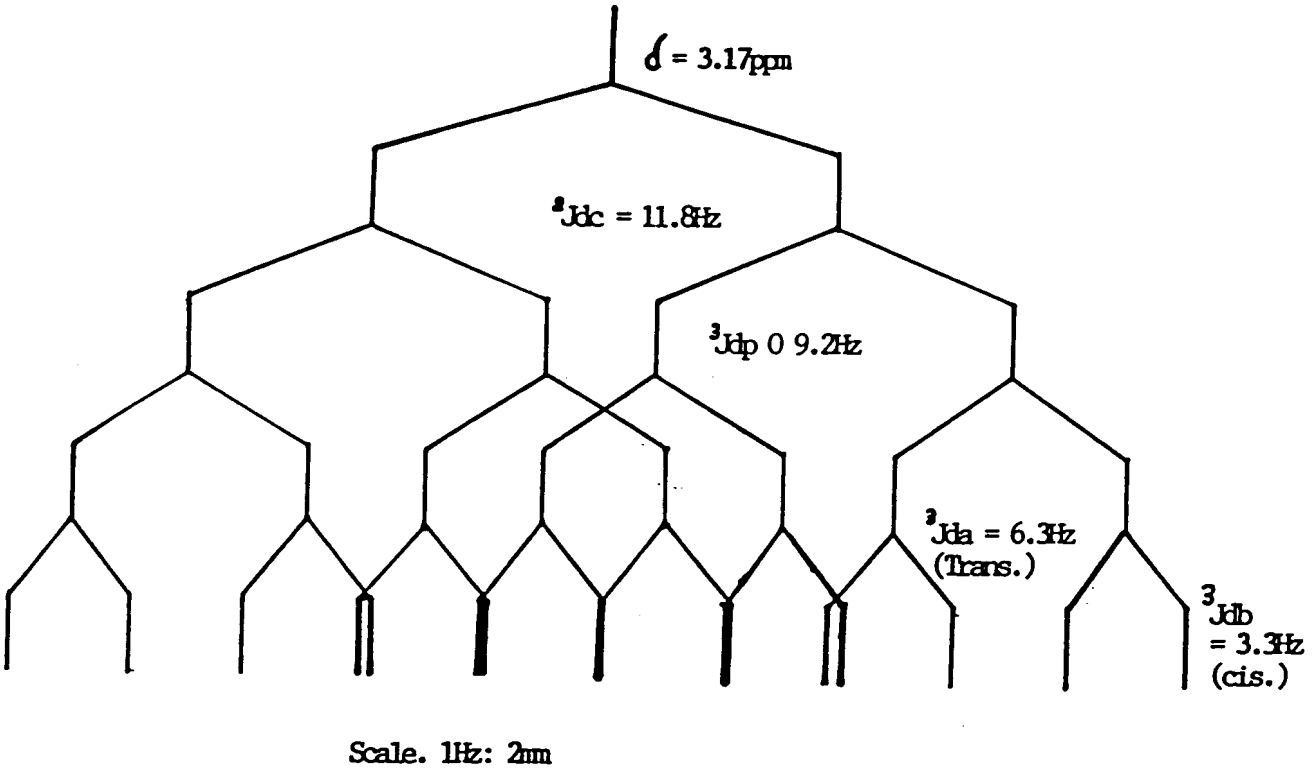

Figure 2.4. Coupling tree structure of an ABCDX spin system of the high field proton in **1**.

an ABCD is as a result of ^{31}P-decoupled interactions (Figure 2.3). However, in this particular case, an ABCDX spin system produces 16 lines (with due consideration of signal overlaps) which can be accounted for by the coupling tree (Figure 2.4). Moreover, upon ^{31}P decoupling, only eight (8) lines are observed. It should be noted that despite the complexity of the system, all four sets of protons each producing sixteen (16) signals appear within a chemical shift range of about 1ppm nevertheless, it was still possible to assign all the multiplets to individual protons. The assignment of all vicinal

hydrogens was done by considering the most probable geometry of the molecule and by measuring the coupling constants. The existence of only one (1) ABCDX splitting pattern in the aliphatic region i.e. the two N-CH_2-CH_2-N moieties, suggest that the two halves of the molecule are equivalent in terms of NMR time scale. Thus the molecule exists in solution as a unique conformation of C_s symmetry or as a mixture of two or more enantiomeric conformers in fast exchange[57]. The symmetry of the compound is again made clear by the equivalent interaction of the two most high field protons, H_d (δ_H 3.17 ppm) with the ^{31}P resulting into a very clear triplet from the partially decoupled ^{31}P NMR spectrum, with a coupling constant of $^3J_{PH}$ of 9.4 Hz, which compares well with the literature value[18] of 10.1 Hz for *trans* relationship (Figure 2.5). If the system was not as symmetrical as it is, we should be observing two sets of doublets of doublet upon selective magnetic irradiation between (3.6 – 3.9) ppm range due. Since the ^1H NMR spectra were recorded at room temperature, the symmetry element of the molecule still remains to be observed at low temperatures, were the exchange rates would be slow to lead to a rigid system .The high field signal was identified as proton H_d for a number of reasons. First, H_d is the proton located at the opposite side of the molecule with respect to the strong deshielding oxygen atom of the phosphoryl group.

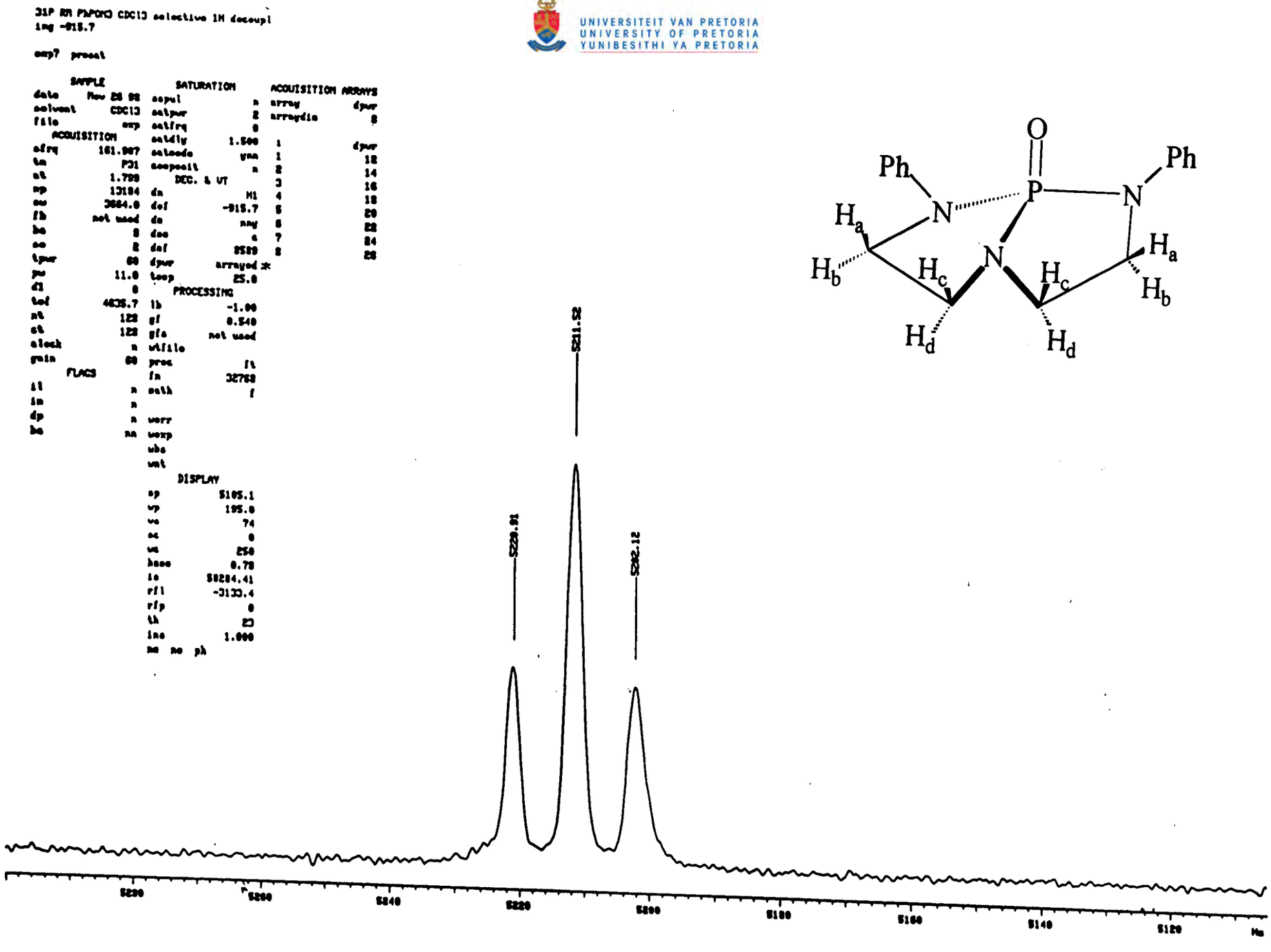

Figure 2.5 Partially decoupled ^{31}P NMR of **1**.

As expected a geminal proton to H_d (H_c) is exposed to both phosphorus and oxygen in space (*cis* to P=O), thus being deshielded. Second, H_d is bonded to a carbon next to the pyramidal nitrogen atom (N_5), which is predominantly of sp^3 hybridization. The same trend is expected of H_a and H_b for the same reasons as for H_d and H_c. Protons H_a and H_b on the other hand, are relatively deshielded because they are in proximity of more planar nitrogen atom derived from the aromatic amine. Despite the fact that all the vicinal protons are three bond distance away from phosphorus and that nitrogen atoms act as a bridge, the geminal protons are very much different from each other (H_a, H_c being *cis*, and H_b, H_d *trans* to the P=O group).

Table 2.2 Calculated dihedral angles according to Karplus equation.

Coupling interactions	J value (Hz)	Dihedral angle (θ)	Orientation
$^2J_{H(a)H(b)}$	9.3	-	Geminal
$^2J_{H(c)H(d)}$	11.8	-	Geminal
$^3J_{H(a)H(d)}$	6.3	146	*Trans*
$^3J_{H(b)H(c)}$	6.2	145.7	*Trans*
$^3J_{H(b)H(d)}$	3.3	49	*Cis*
$^3J_{H(a)H(c)}$	3.3	49	*Cis*

Using the Karplus equation[10] and the measured coupling constants, it was then possible to calculate the dihedral angle between the vicinal protons (Table 2.2). The proton-phosphorus relationship helps in assigning the protons of N-CH_2-CH_2-N moiety in terms of *cis*- or *trans*- coplanar relationship[57] in figure 2.6. The results given in table 2.2 agree to a large extent with the reported angular relationship of the vicinal protons in related organophosphorus systems[18,57,58]. Depending on the geometry of the molecule, the coupling constants of the methylene group in a vicinal moiety give a clear indication as to whether the hydrogen atoms are *trans*- or *cis*-

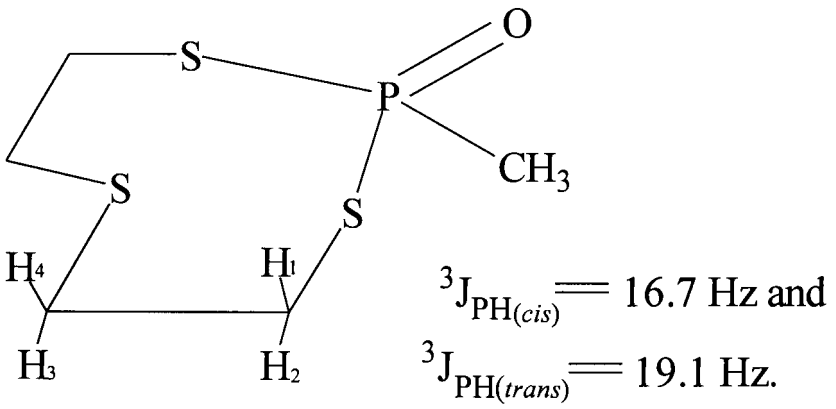

Figure 2.6. Vicinal ^{1}H coupling constants for a cyclic system[57].

coplanar with respect to each other. It is for this reason that we can safely assign the vicinal protons according to how they are related to each other

and also how they are orientated with respect to phosphoryl group. An analogous trend was observed for a cyclic thiophosphoryl compounds, as illustrated[57] figure 2.6.

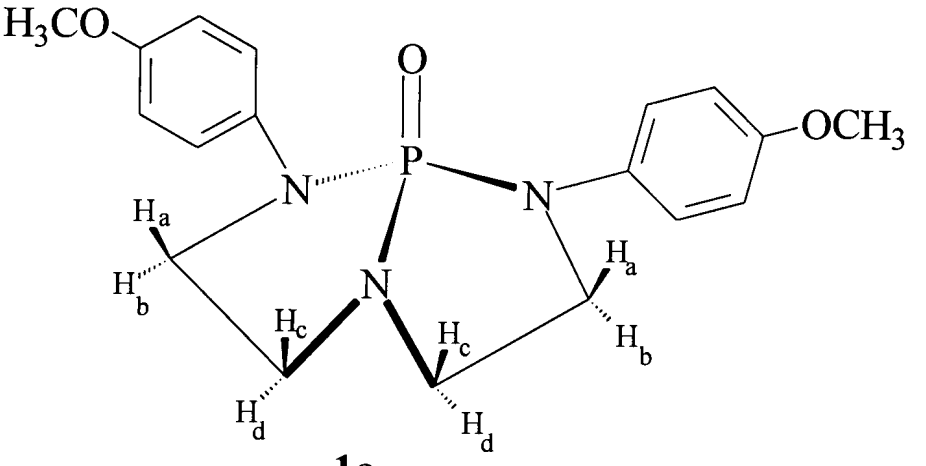

1a

Figure 2.7 A *para*-substituted derivative of system **1**

A simulated ^{1}H NMR spectrum, illustrated in figure 2.8 which, proved to be a clear replica of the experimental spectrum[59] finally, confirmed the assignment of vicinal protons in **1**. Figure 2.8 represents a nearly perfect agreement between the experimental and the calculated spectra, even though a ^{31}P-decoupled spectrum (ABCD spin pattern) was simulated and compared with the ^{31}P-decoupled experimental spectrum. The same phenomenon is to be expected of the fully coupled system, i.e. ABCDX spin system.

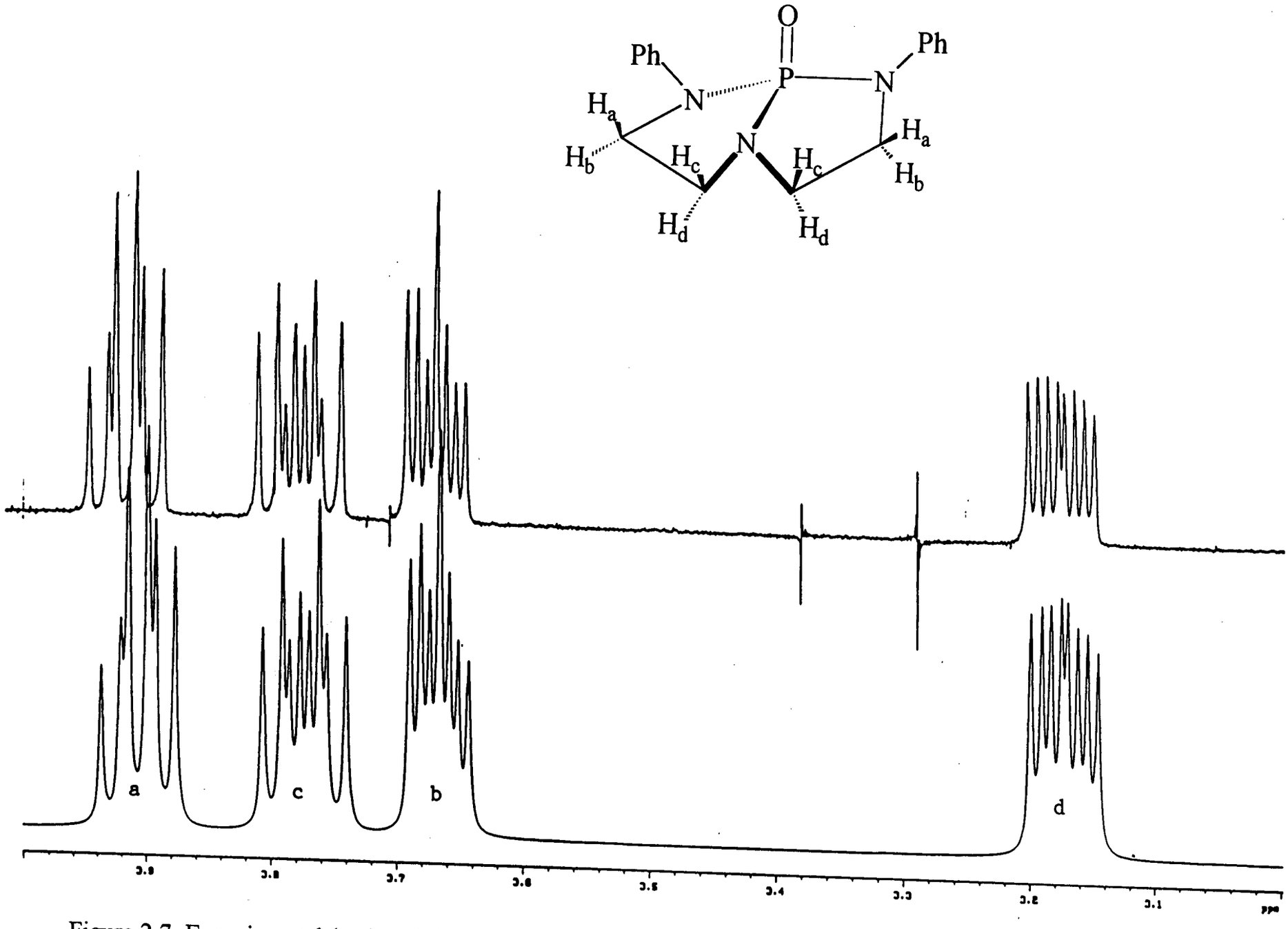

Figure 2.7. Experimental (top) and the simulated ^{1}H NMR spectra of the aliphatic protons in **1** in chloroform-d_1 at 400 MHz field.

^{1}H NMR spectrum of system **1a** (figure2.8), a derivative of system **1,** agrees to large extent with the splitting patterns observed for system **1**(figure 2.3), particularly in the aliphatic region where the vicinal system is present. Both compounds (**1** and **1a**) have the same spin system (ABCDX) for the N-CH_2-CH_2-N moiety and the same attachment of phenyl group on the planar nitrogen atoms, however in this case the phenyl ring is *para* substituted. Interestingly, we can still identify four sets of multiplets accounting to the four chemically non-equivalent protons of the vicinal moiety. All the protons are equidistant in terms of bonds from ^{31}P, thus a similar coupling pattern as for system **1** is observed. Similar to **1**, H_d (δ 3.1 ppm) splits into sixteen (16) signals (i.e. considering signal overlapping). The small chemical shift difference (ca. 0.02 ppm) is so insignificant that it can be accepted that both systems have the same spin system for vicinal moiety in all respects.

2.2 Comparison of NMR analysis with X-ray structural analysis.

A comparison between solution state NMR analysis and solid state X-ray analysis can be regarded as intrinsically difficult because a solution state represents a dynamic environment within which molecules must conform, whereas a solid state represents a different environment with limited external

influences. Thus the X-ray relates to a rigid state of the molecules. The X-ray molecular structure of **1** is shown in Figure 2.9. The X-ray diffraction data (Table 2.3) confirmed the planarity of the aromatic nitrogen atoms.

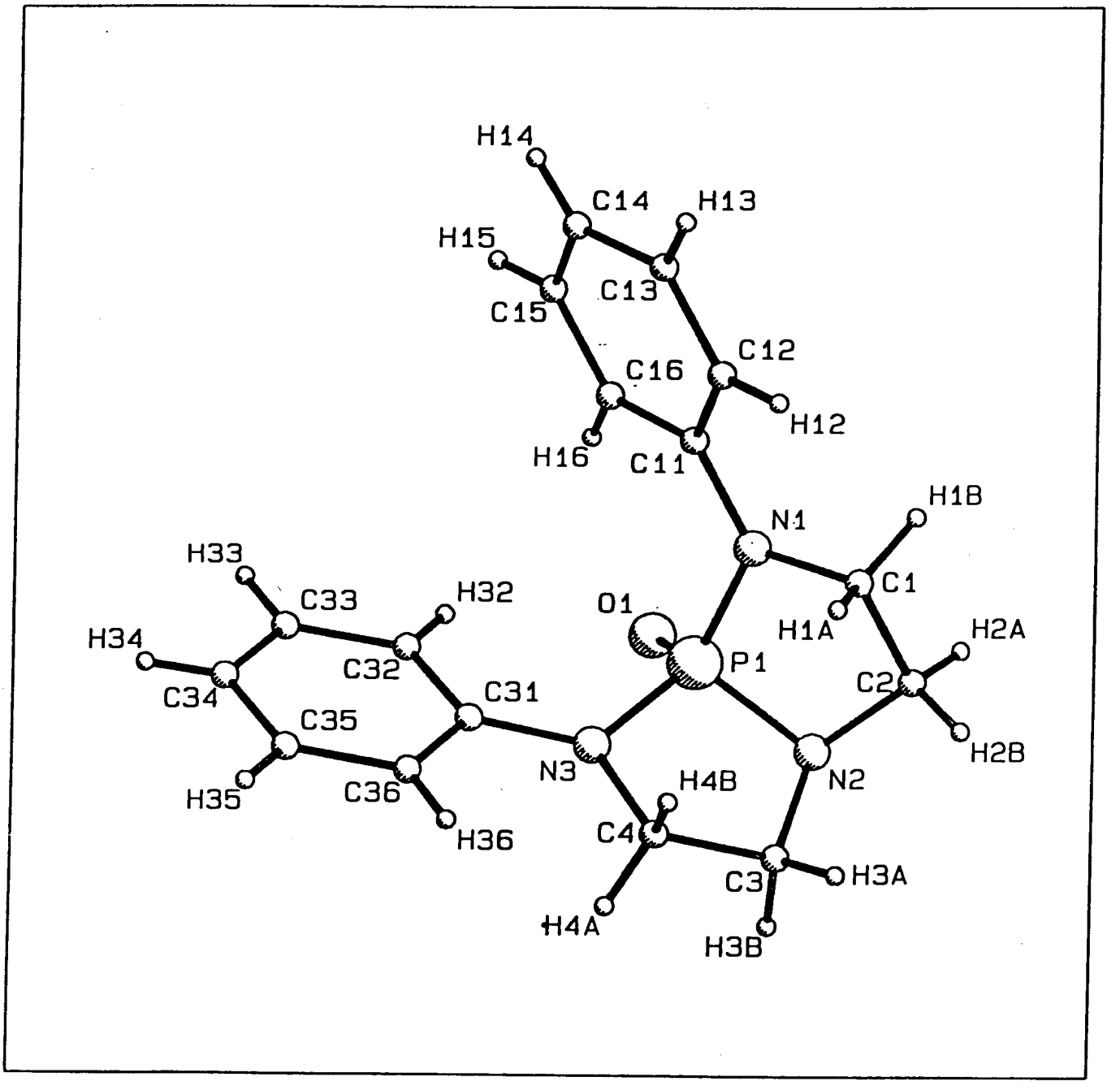

Figure 2.9. An X-ray molecular structure of **1**.

This difference in nitrogen atom's geometry supports our conclusions about the high field chemical shift of H_d, i.e. H(3A) and H(2B) according to the ORTEP X-ray structure plot (Table 2.3). From this crystal structure, we can easily visualise the effect of the lone pair of electrons on the nitrogen (N2) to the *cis*-coplanar proton to it, thus proton H_d.

An interesting feature comes out of crystal structure in terms of torsion angle difference between the two halves of the molecule (Table 2.4, Ring A and B). There is a remarkable difference in the vicinal proton orientation for each ring, which definitely accounts for the difference in the geometrical relationship between the individual rings. Assuming the X-ray crystal structure to be the most ideal one, we can conclude that, the NMR data represent an average of the two rings, so they appear similar on the NMR time-scale. This conclusion is arrived at with due consideration of the limitations involved in the calculation of dihedral angles. One of the limitations of this procedure (dihedral angle calculation) is that, coupling constant should properly be integrated over the whole rotation circuit of conformationaly mobile molecules rather than just summed over the most stable conformation.

Table 2.3. Selected bond lengths [A] and angles [deg.] for **1**.

Bond angles [deg]		Bond lengths [A]	
O(1)-P(1)-N(1)	114.4	P(1)-O(1)	1.437
O(1)-P(1)-N(2)	121.3	P(1)-N(1)	1.653
N(1)-P(1)-N(2)	96.3	P(1)-N(2)	1.661
O(1)-P(1)-N(3)	112.7	P(1)-(N(3)	1.676
N(1)-P(1)-N(3)	114.4	N(1)-C(11)	1.407
N(2)-P(1)-N(3)	95.7	N(1)-C(1)	1.473
C(11)-N(1)-C(1)	120.6	N(2)-C(2)	1.451
C(11)-N(1)-P(1)	127.4	N(2)-C(3)	1.475
C(1)-N(1)-P(1)	110.3	N(3)-C(31)	1.420
C(2)-N(2)-C(3)	115.9	N(3)-C(4)	1.470
C(2)-N(2)-P(1)	109.2	C(1)-C(2)	1.504
C(3)-N(2)-P(1)	110.9	C(3)-C(4)	1.497
C(31)-N(3)-C(4)	121.2		
C(31)-N(3)-P(1)	126.0		
C(4)-N(3)-P(1)	111.1		
N(1)-C(1)-C(2)	104.5		
N(2)-C(2)-C(1)	107.1		
N(2)-C(3)-C(4)	109.0		
N(3)-C(4)-C(3)	106.3		

Table 2.4. The observed torsion angles of vicinal hydrogens according to X-ray diffraction method in figure 2.9.

RING A		RING B	
Bond connection	Torsion angle, θ	Bond connection	Torsion angle, θ
H(IA)-C(1)-C(2)-H(2B)	37.6^0	H(3A)-C(3)-C(4)-H(4B)	27.4^0
H(1A)-C(1)-C(2)-H(2A)	157.5^0	H(3B)-C(3)-C(4)-H(4B)	146.5^0
H(1B)-C(1)-C(2)-H(2B)	83.4^0	H(3A)-C(3)-C(4)-H(4B)	92.9^0
H(1B)-C(1)-C(2)-H(2A)	36.4^0	H(3B)-C(3)-C(4)-H(4A)	26.2^0

Table 2.5 shows a comparison between the NMR spectroscopic and the X-ray diffraction results in terms of the observed torsion/dihedral angle. For the H_a/H_c, H_b/H_c, H_b/H_d pairs of protons, the difference between two values is reasonably small. For the H_a/H_d pair, on the other hand, the agreement is quite unsatisfactory. However, quantitatively speaking, the information we

could extract from the NMR results suggests similar structural features as the X-ray crystal analysis does.

Table 2.5. Comparison of the dihedral angles obtained for **1** from the NMR and the X-ray diffraction method.

Coupling interactions	Dihedral angle, (°) (from ^{1}H NMR)	Torsion angle, (°) (average, from X-ray diffraction)	Orientation
$^{3}J_{H(a)H(c)}$	49.0	31.2	*Cis*
$^{3}J_{H(a)H(d)}$	146.0	88.2	*Trans*
$^{3}J_{H(b)H(c)}$	145.7	151.2	*Trans*
$^{3}J_{H(b)H(d)}$	49.0	32.5	*Cis*

2.3 Solvent effect for 1.

The extent of solubility of a compound in a given solvent depends on a number of factors, such as the atomic geometry, polarity, density, electronic character, etc. of both the solute and the solvent. NMR spectroscopy is helpful in that we can observe directly some of these solvent effects. It is

solvent-substrate interaction that we are able to observe by monitoring the changes in the chemical shift position(s). An interesting picture of solvent effect was observed when system **1** was dissolved in the acetone-d_6 and benzene-d_6, and the ^{1}H NMR spectra were compared with those obtained in chloroform-d_1. A dramatic effect was observed on the vicinal hydrogens in benzene-d_6 where there was a general upfield chemical shift of nearly 1ppm while for acetone-d_6 we observed some upfield shift of selected protons on the N-CH_2CH_2-N moiety, (Figure 2.10). Benzene-d_6 is a flat molecule, which has a ring current, which affects the chemical shifts of the neighbouring hydrogen atoms. This chemical shift effect, depends on whether these hydrogen atoms are above the plane of the benzene ring or in the plane of the benzene molecule. This up-field chemical shift effect is assumed to be caused by interaction of **1** and benzene-d_6 molecules simply implies an increase in electron density on the vicinal moiety resulting in high resonance frequencies. For the operating frequency at which the ^{1}H NMR spectra were recorded, thus (200 MHz), there is less separation of signals into four sets of multiplets. However, a very clear similarity in terms of chemical shift is observed with both acetone-d_6 and chloroform-d_1. There is a selective solvent effect in a sense that only the aliphatic region seems to be strongly

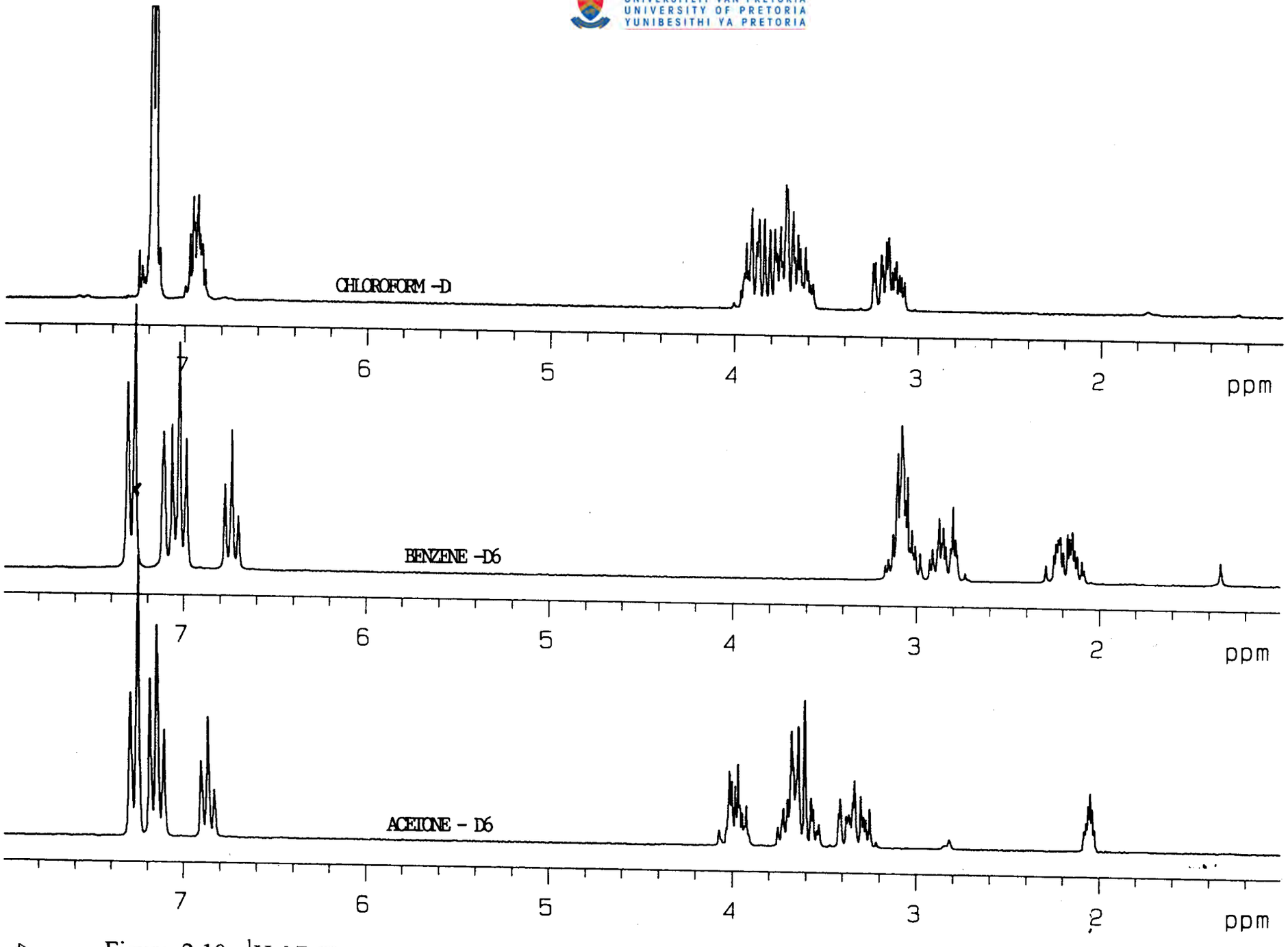

Figure 2.10. ^{1}H NMR spectrum of **1** in: chloroform-d_1 (top), benzene-d_6 (middle) and acetone-d_6 (bottom) obtained at 200MHz.

affected while the aromatic region does not change significantly. We can safely conclude that these observed effects are due to very specific solvent-substrate interactions. We therefore propose the following model for solvent effect observed in benzene solutions, and the model can be illustrated by the use of the Drieding models. Based on the X-ray crystal structure and assuming a true symmetry of the molecule, the model indicates that the benzene molecule (solvent) fits within the cavity between the two rings (ring A and B). This results in the benzene molecule being encapsulated in such a manner that its induced magnetic field (anisotropic effect) increases the electron density of the aliphatic protons. The most probable position of the solvent is such that the benzene ring is situated vertically or perpendicular to the vicinal protons, thus along the symmetry line of the molecule. This is made possible by the fact that benzene molecule has high symmetry and is rigid. Despite the fact that benzene ring produces induced magnetic field orientated in two different directions, one aligned to the applied magnetic field and the other against the applied, in this case they both counter the applied field to some extent, thus have the up-field shift effect.

It is generally accepted[60] that the effects that occur at intramolecular level also play a big role at intermolecular level. This effect is ascribed to

diamagnetic ring currents of benzene and its derivatives. A similar influence which, affect the chemical shifts of the neighbouring molecules associated with both shielding and dishielding can be expected from the effect of the magnetic anisotropy of multiple bonds or the electrical field effect of the molecules with large dipole moments. Solvent effects become even more important when intermolecular interactions in the solvents lead to the formation of weak complexes. On the bases of dipole-dipole or van der Waals interactions, certain steric orientations become favoured with respect to others and as a result, specific changes can be observed with the resonance frequencies of individual protons in the solute. This in turn can be used to obtain insight into the structure of such complexes.

CHAPTER 3

CONFORMATIONAL AND STRUCTURAL ANALYSIS OF SYSTEM 2

Compound **2** represents an intermediate with respect to systems **1** and **3** in the sense that it forms a stable non-symmetrical system with multiple spin systems, i.e. ABC, ABC_2, ABCD and ABCDX spin systems where X is phosphorus atom. These spin systems occur as a result of atomic arrangement of the aryl group, five-membered heterocyclic ring, seven-membered heterocyclic ring and a fused benzene ring (figure 3.1).

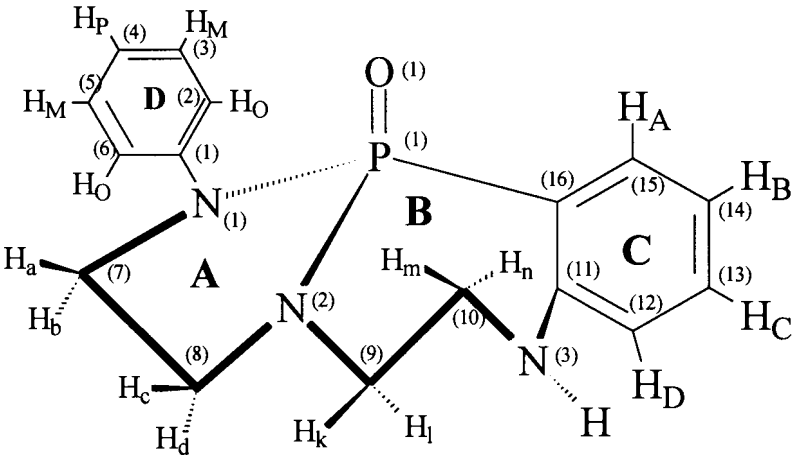

Figure 3.1. Molecular structure of **2.**

The presence of these multiple spin systems makes compound **3** to be the most complicated of the three systems analysed. These compounds have the same molecular weight as **1** except that there is a difference in atomic arrangement.

3.1 ^{1}H NMR ANALYSIS OF THE ALIPHATIC REGION OF COMPOUND 2.

^{1}H NMR analysis of **2** distinguishes approximately eight different aliphatic protons for both five and seven membered rings. Similar to **1**, there are six different hydrogens that are three bonds distance away from the phosphorus-31, whereas the seven-membered heterocyclic ring has additional two protons that are at least four bonds distance away from ^{31}P. Therefore we had to distinguish between three different spin systems, i.e. ABCDX, ABCD and ABC_2, for which their proton multiplicities appear within the chemical shift range of approximately 1ppm. The multiplicity of protons H_a, H_b, H_c, H_d, H_k and H_l is assumed to follow the typical coupling tree as for H_d in **1** because of the equivalent number of interacting nuclei. Theoretically, they are all supposed to produce 16 signals as for H_d in **1**. However, the degree of overlap in most of these protons in **2**, makes it difficult to resolve a single set

of multiplet independent of the corresponding coupling nuclei. In figure 3.2a, the methylene protons H_m and H_n resonate as broad multiplets at δ 3.9 ppm and δ 3.43 ppm respectively, instead of the expected triplet of triplet and multiplets (sixteen lines) due to additional, but unresolved coupling to the N-H proton (figure 3.2b). Figure 3.2b shows a recorded spectrum of **2** in which D_2O hydrogens exchanged with N-H protons and thus eliminating coupling due to N-H proton. Additionally, their proximity to the lone pair of electrons on the nitrogen and its planarity should reflect on the geometry of the ring. Proton H_n splits into triplet-triplet (following ABC_2) whereas H_m splits into sixteen signals (following ABCDX) at 600 MHz field. This difference can be explained in terms of the orientation of both protons with respect to the N-H bond and the lone pair electrons on the nitrogen atom. The ^{14}N nucleus has a spin quantum number, I=1 and in accordance with the formula 2I+1, should cause a proton attached to it and as well as adjacent protons to show three equally intense peaks. This nitrogen atom character is likely to be a temperature dependent factor, which can be confirmed by low temperature NMR experiment. However, there are two factors which complicate the picture: one being the rate of exchange of the proton on the nitrogen and the other being the electrical quadrupole moment of the ^{14}N nucleus due to its non-spherical charge distribution.

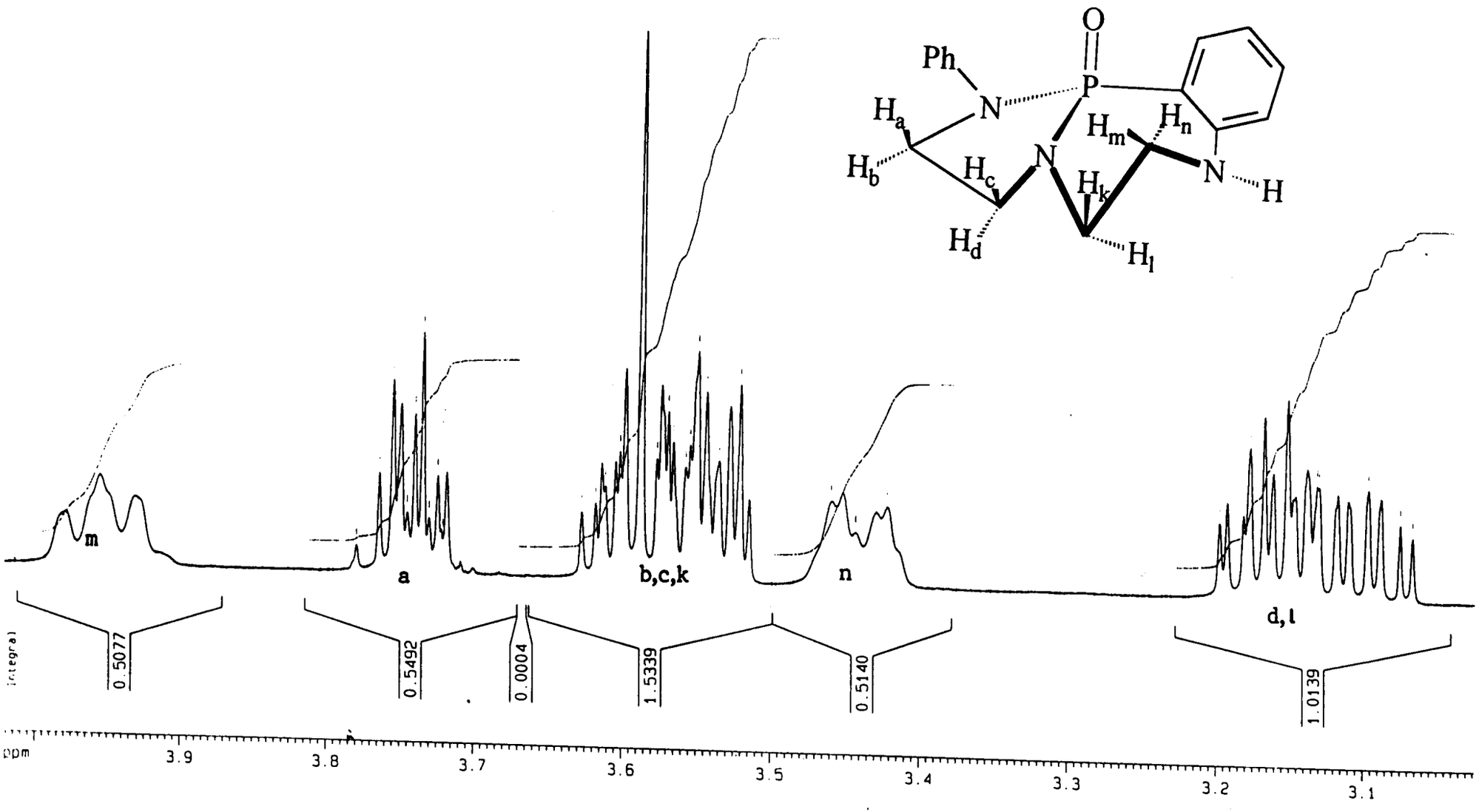

Figure 3.2a. ^{1}H NMR spectrum of aliphatic protons of **2** at 500 MHz field.

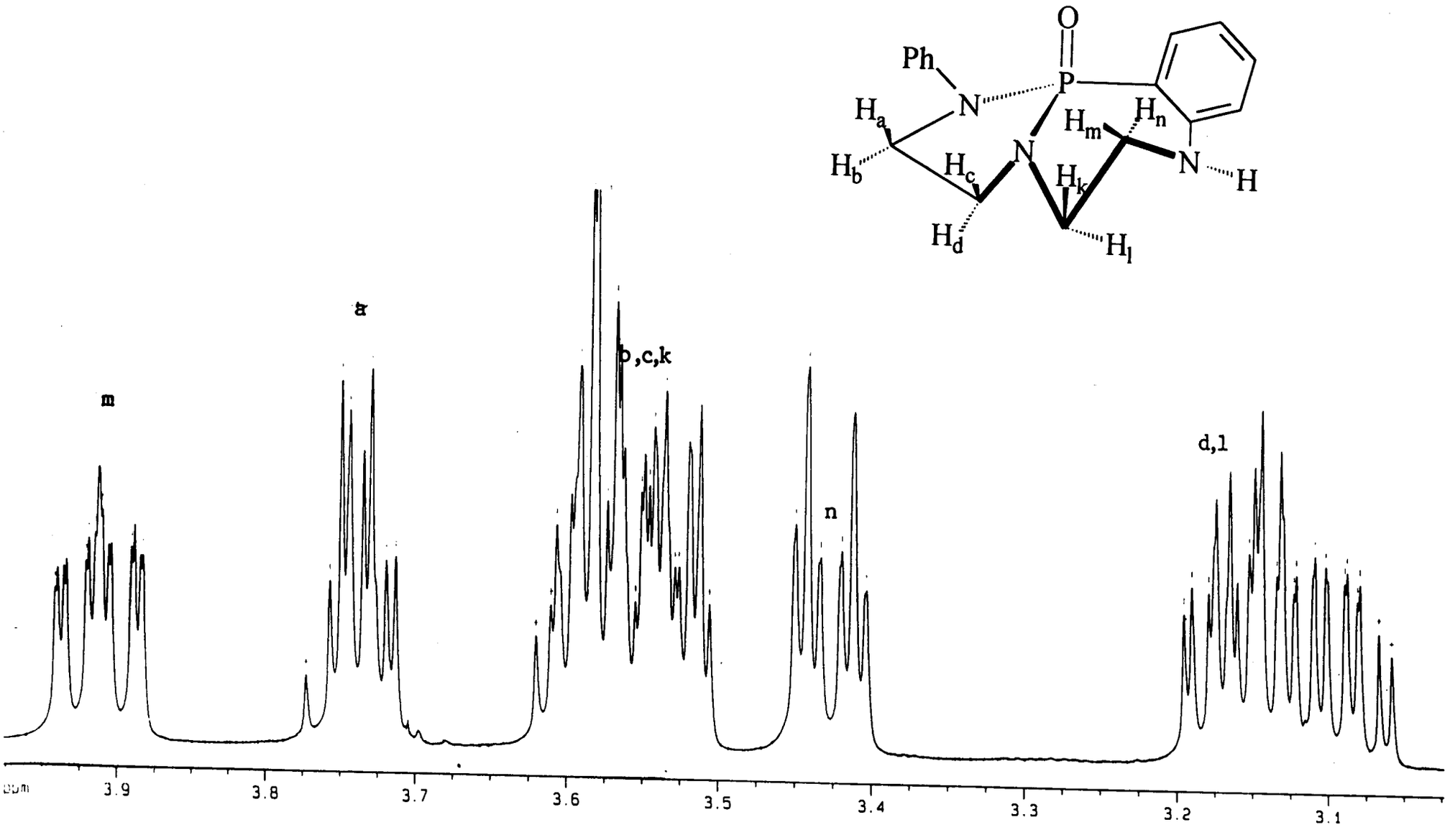

Figure 3.2b. ^{1}H NMR spectrum of **2** (D_2O washed) at 500 MHz field.

The proton on the nitrogen may undergo rapid, intermediate, or slow exchange. If the exchange is rapid, the N-H proton(s) will be decoupled from the nitrogen atom and from the protons on the adjacent carbon atoms. Therefore the N-H peak will be a sharp singlet and consequently the adjacent protons C-H are not split by N-H, as is the case with most aliphatic amines[61]. At intermediate rate exchange, the N-H proton would be partially decoupled, and a broad N-H peak results. The N-H proton does not split the adjacent C-H protons as is the case with N-methyl-nitroaniline and as is observed for system **3**. However if the N-H exchange is slow, the N-H will still be broad because the electrical quadrupole moment of the nitrogen nucleus induces a moderately efficient spin relaxation and thus an intermediate lifetime for the spin state of the ^{14}N (thus T_2 relaxation effect). The adjacent proton(s) thus sees three spin states of the nitrogen nucleus which are changing at a moderate rate, and the proton responds by giving a broad peak. In this case, N-H coupling to the adjacent protons is observed. Such is the case with pyrroles, indoles, secondary and primary amines, and carbamates[62]. Since the exchange process affects both protons in the same way, the difference in the patterns (triplet-triplet vs sixteen-signal multiplet) has to be the consequence of the different geometrical orientation of H_m and H_n. The spin-spin orientation of H_n results in a unique ABC spin system. The

coupling tree of H_n shows that it couples equally to both H_k and H_l by 4.0 Hz, thus producing a triplet-triplet. On the other hand H_m splits into sixteen signals which can easily be illustrated by its coupling tree. A significant observation is that H_m couples with ^{31}P nuclei through four bonds by 1.0 Hz, however this coupling was observed only at higher fields, e.g. 500 MHz and 600 MHz. Therefore, we can conclude that proton H_m has an ABCDX spin system where X is the phosphorus-31 at higher magnetic fields. A number of reasons can be advanced for the difference between H_n and H_m, one being their orientation to the lone pair of electrons on the N-H in which one experiences a stronger effect than the other. This can be expected if H_n is *trans*-coplanar, thus experiencing a strong electrical quadrupole moment effect and H_m being cis-coplanar to the lone pair of electrons. However this reasoning will only be applicable if N(3) has a planar geometry.

Figure 3.3. shows an aliphatic cosy spectrum of **2** illustrating a strong N-H interaction with H_n and a lesser interaction with H_m. Two carbon atoms of the fused benzene ring form a part of the seven membered ring and are expected to produce a low field chemical shift of H_m and H_n relative to other aliphatic protons. The most high field signal (δ 3.13 ppm), is therefore assigned to H_l and H_d, which are both positioned opposite to the P=O group

and that they are equally three-bond distance away from phosphorus atom. The assignment of atoms H_a, H_b, H_c and H_d is in complete agreement with that of **1**.

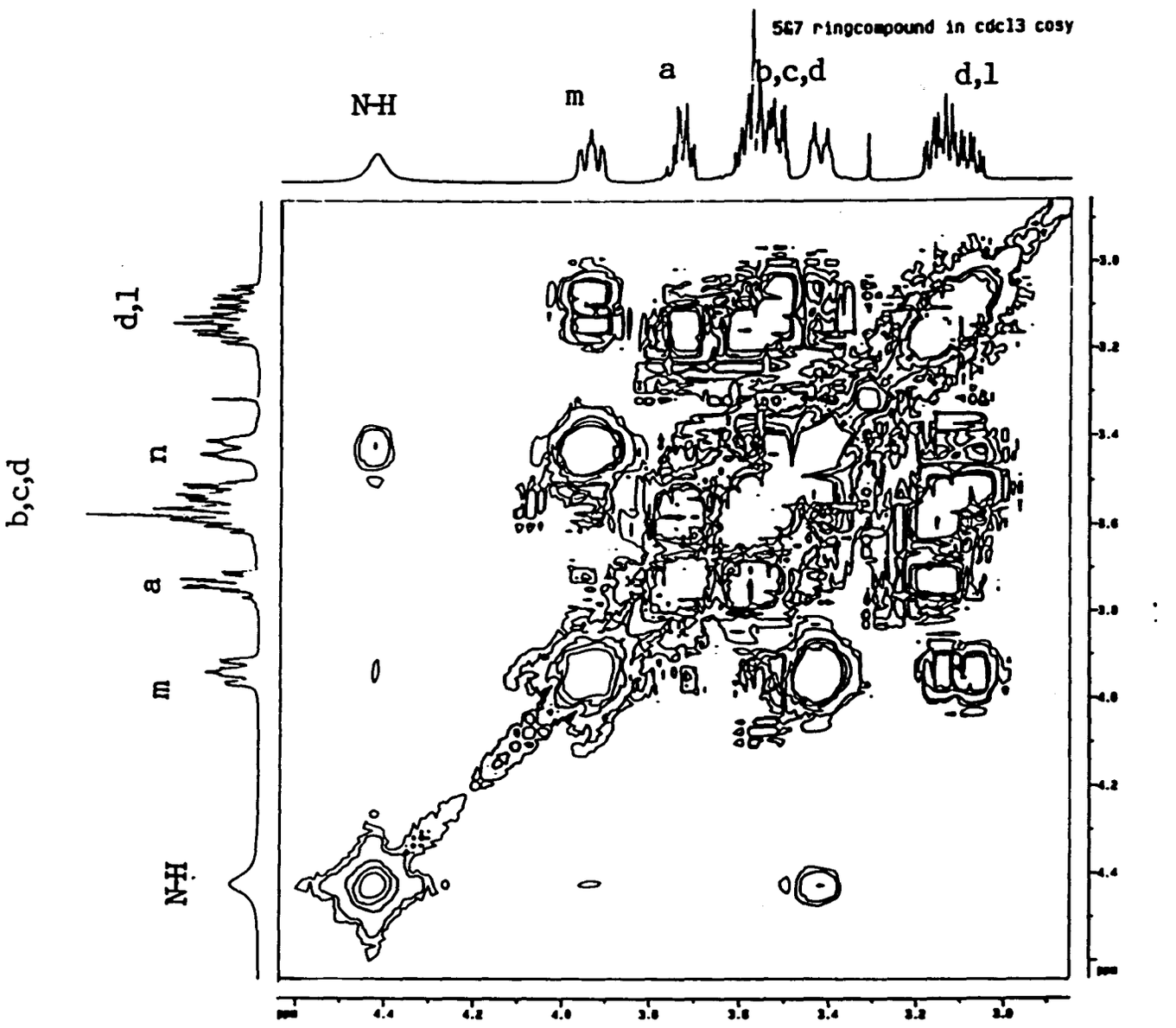

Figure 3.3. The cosy spectrum of the aliphatic region of **2** at 500 MHz field.

Table 3.1. The aliphatic ^{1}H NMR chemical shifts of **2** in dueterated chloroform.

Five-membered ring		Seven-membered ring	
Proton	δ (ppm)	Proton	δ (ppm)
H_a	3.74	H_m	3.91
H_b	3.56	H_n	3.43
H_c	3.56	H_k	3.56
H_d	3.13	H_l	3.13

The ^{1}H NMR spectrum of **2** shows a great deal overlap of signals, as illustrated in table 3.1. It was difficult to assign protons H_c, H_b and H_k to a proper sequence for the multiplet at 3.56 ppm. But, since all hydrogens show specific coupling interactions (i.e. geminal, *cis*- and *trans*-) relative to their neighbouring protons, it was possible to correlate their coupling constants with their molecular positions. It is interesting to note that the coupling interactions involving the protons of the five-membered ring of compound **2** are greater than those of compound **1** in terms of geminal and phosphorus-31 couplings, with the highest value for the $^3J_{PH(b)}$ = 16.7 Hz. The determined coupling constants of the ethylene groups in **2** are given in table 3.2.

Table 3.2. The aliphatic ^{1}HNMR coupling constants for **2** as in figure 3.1.

Five-membered ring		Seven-membered ring		Orientation
Coupling interaction	J (Hz)	Coupling interaction	J (Hz)	
$^{2}J_{H(a)H(b)}$	8.0	$^{2}J_{H(m)H(n)}$	15.0	Geminal
$^{2}J_{H(c)H(d)}$	8.3	$^{2}J_{H(k)H(l)}$	14.6	Geminal
$^{3}J_{H(a)H(d)}$	2.9	$^{3}J_{H(m)H(l)}$	10.6	*Trans/Gauche*
$^{3}J_{H(b)H(c)}$	2.3	$^{3}J_{H(k)H(n)}$	4.0	*Trans/Gauche*
$^{3}J_{H(a)H(c)}$	7.3	$^{3}J_{H(k)H(m)}$	3.0	*Cis/Gauche*
$^{3}J_{H(b)H(d)}$	7.2	$^{3}J_{H(l)H(n)}$	4.0	*Cis/Gauche*
$^{3}J_{PH(a)}$	16.5	$^{3}J_{PH(m)}$	1.0	-
$^{3}J_{PH(b)}$	16.7	$^{3}J_{PH(n)}$	-	-
$^{3}J_{PH(c)}$	14.6	$^{3}J_{PH(k)}$	11.4	-
$^{3}J_{PH(d)}$	15.5	$^{3}J_{PH(l)}$	10.5	-

The aliphatic protons of **2,** as in the case of **1** and **3** can be referred to as being *cis* or *trans* orientated with respect to the P=O group. Following an ABC_2 spin system for H_n, it was found that H_n couples equally to both H_k and H_l, i.e. $^{3}J_{H(k)H(n)} = {}^{3}J_{H(l)H(n)} = 4.0$ Hz.

3.2 X-RAY DIFFRACTION ANALYSIS OF 2.

It is important to note that compound **2** represents an intermediate structure between a more rigid, molecule of **1** and a more flexible **3**. Compound **2** is non-symmetrical by virtue of having two heterocyclic rings of different sizes, i.e. five- and seven- membered rings. A significant observation to note is that all nitrogens in **2** are planar (figure 3.4).

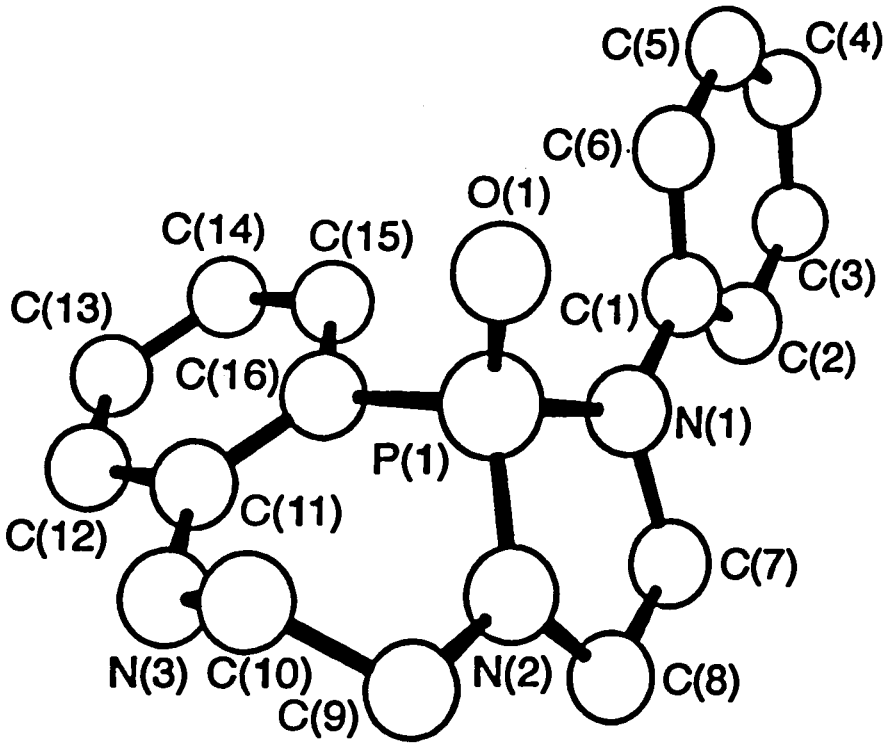

Figure 3.4. ORTEP[55] plot of the molecular structure of **2**.

Table 3.3 shows the selected bond lengths and angles of **2**. The observed P-N bond-lengths are typical for the amides of P^{IV} acids[63]. However, a relatively significant differences in P=O bond-length were observed for **2** compared to **1** and **3**[54].

Table 3.3. Selected bond-lengths [A] and angles [deg] for **2**.

Bonded atoms	Length [A]	Bonded atoms	Angle [deg]
P(1)-N(2)	1.631	C(1)-N(1)-C(7)	119.8
P(1)-N(1)	1.667	C(1)-N(1)-P(1)	127.5
P(1)-C(16)	1.806	C(7)-N(1)-P(1)	112.5
N(1)-C(1)	1.408	C(8)-N(2)-C(9)	120.3
N(1)-C(7)	1.473	C(8)-N(2)-P(1)	115.6
C(7)-C(8)	1.497	C(9)-N(2)-P(1)	123.6
C(9)-C(10)	1.505	C(11)-N(3)-C(10)	125.1
N(3)-C(11)	1.377	N(3)-C(10)-C(9)	112.8
N(2)-C(9)	1.445	C(10)-C(9)-N(2)	111.4
C(8)-N(2)	1.416	N(2)-C(8)-C(7)	109.2
N(1)-C(7)	1.473	N(1)-C(7)-C(8)	107.0

Significant observation is about the increment in the endocyclic bond angle around the heterocyclic carbons of the five and seven membered rings, with the angle increasing in the order: C(7)<C(8)<C(9)<C(10). This pattern shows that the five-membered ring experiences more angular strain than the seven-membered rings which leads to a limited flexibility of the five-membered ring. From the dihedral angles of **2,** determined by the X-ray diffraction, the following selected values are of importance:

N(1)-C(7)-C(8)-N(2) $= 8.4^0$.....[A]

N(2)-C(9)-C(10)-N(3) $= 63.2^0$.....[B]

P(1)-N(2)-C(9)-C(10) $= 22.7^0$.....[C]

The dihedral values, [A] and [B] were used to extrapolate the relative dihedral angles of all aliphatic vicinal protons by applying Newman projection method. A dramatic observation was made in terms of the geometry of the two different heterocyclic rings of **2** to the effect that, the projection along the C(7)-C(8) bond reveals an almost eclipsed conformation [A] whilst that for system [B] shows a staggered conformation (figure 3.5). The eclipsed conformation represents the geometry of vicinal protons of the five-membered ring whilst the staggered conformation represents the geometry of protons on the seven-membered ring.

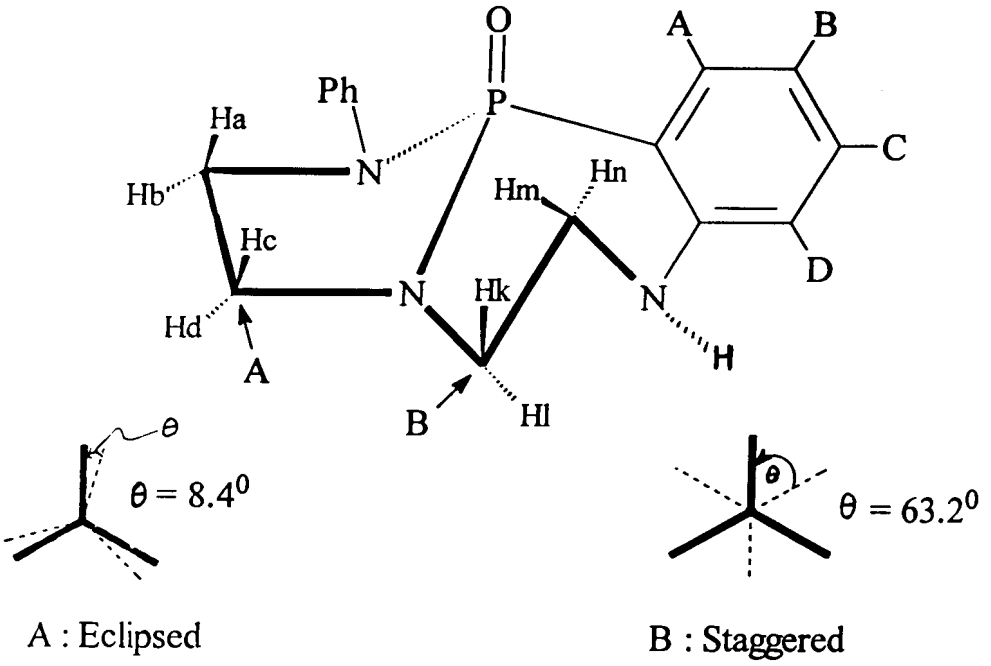

Figure 3.5. Representative molecular geometry of **2** as determined by X-ray diffraction method.

3.3 A COMPARISON OF DIHEDRAL ANGLES DETERMINED BY ^{1}H NMR AND X-RAY DIFFRACTION METHODS.

Contrary to the accepted trend, in which the *trans*-coupling constants are generally bigger than the *cis*-couplings, e.g. in cyclohexane systems ring, in which the hydrogens are either axial or equatorial, forming with their neighbours dihedral angles of 60^0 or 180^0, the opposite scenario was observed for **2**. The NMR calculated results are based on the coupling constants given in table 3.2. The observed *trans*-couplings of the five-

membered ring protons are smaller than the *cis*-coupling constants. These values are in full agreement with the literature values given for substituted cyclopentanes[58]. The dihedral angles shown in table 3.4 agree reasonably with the Karplus curve[13], where the vicinal couplings for *cis*-coplanar protons could also be as large ($\theta = 0^0$).

Table 3.4 A comparison of dihedral angles of **2** obtained from the NMR and X-ray diffraction.

Connection	NMR determined angle [deg]	X-ray determined angle [deg]
H(a)-C(7)-C(8)-H(c)	19.2	8.4
H(b)-C(7)-C(8)-H(d)	20.3	8.4
H(b)-C(7)-C(8)-H(c)	121.0	111.6
H(a)-C(7)-C(8)-H(d)	125.0	128.4
H(k)-C(9)-C(10)-H(m)	51.6	63.2
H(l)-C(9)-C(10)-H(n)	45.0	63.2
H(k)-C(9)-C(10)-H(n)	45.0	56.8
H(l)-C(9)-C(10)-H(m)	177.9	183.2

3.4 CONFORMATIONAL ANALYSIS OF HETEROCYCLIC RINGS OF 2.

The X-ray crystal structure of **2** shows one stable molecular structure. It must be remembered that compound **2** has four rings which differ fundamentally from each other and thus represents the most complicated molecular structure within our scope of research. The Drieding model shows only one possible conformation whereby the phenyl, aryl and the five membered rings are rigid. However, the phenyl ring enjoys a free rotation around N(1)-C(1) bond. The seven-membered heterocyclic ring shows a twist half-chair to a half-chair conformation, where a twist half-chair is the most stable conformation with bond-angles as large as 112^0. A staggered geometry of vicinal hydrogens of the seven-member ring results in such position of H_m that it becomes the proton most exposed to the P=O group, this conclusion is also supported by the ^1H NMR data. The only possible conformation shown by the Drieding models is an alternative half-chair system in which the dihedral angle: N(2)-C(9)-C(10)-N(3) approaches zero degrees. However, this possibility, orientates the position of H_k to be the most exposed proton to the P=O group of the seven-member heterocyclic ring. Remarkably, this re-orientation does not affect the five-member ring at

all. The non-existence of this possible conformation suggests the presence of other factors limiting this re-orientation. Neither the X-ray diffraction, nor the ^{1}H NMR experiment supports this possibility. In either case, the conformation of ring **B** (see figure 3.1) is of the half-chair structure. Therefore, it may be concluded that the conformational changes in the heterocyclo-heptanes are accompanied by only slight flexing of bond-angles.

3.5 ^{1}H NMR ANALYSIS OF THE AROMATIC PART OF 2.

Apart from two heterocyclic rings of different sizes, compound **2** has two aromatic rings, which display different ^{1}H NMR coupling interactions transmitted through three and four bonds. The N-phenyl ring, however does not display any proton-phosphorus-31 coupling interactions. Since the phenyl ring enjoys a free rotation about N(1)-C(1) bond, three typical signals due to the ortho-, meta-, and para- positioned protons are observed (Table 3.5). Their splitting pattern follows an ABC spin system. The fused aryl group on the other hand, displays a very interesting coupling interaction following the ABCDX spin system where X is again the phosphorus-31 nucleus. Being a ring fused with the seven-membered ring, conjugation becomes a very significant factor in the respective coupling interactions. An

interesting pattern was observed for these aryl protons of **2**. The chemical shifts follow the deshielding of the order: $H_A > H_C > H_B > H_D$, which is in complete agreement with that observed for a reasonably related compound, aspirin[25].

Table 3.5 ^{1}H NMR chemical shifts data for the aromatic protons in **2**.

N-Phenyl chemical shifts (ppm)		Aryl chemical shifts (ppm)	
H_o	7.43	H_A	7.08
H_m	7.29	H_B	6.61
H_P	7.29	H_C	6.99
		H_D	6.56

The span of resonance for both the phenyl and the aryl protons is within the literature range[65] and they show typical vicinal coupling constants within the range of 7.2-8.2 Hz, where $^3J_{H(o)H(m)}$ = 8.3 Hz. There are two $^4J_{HH}$ = 1.1 Hz values observed which are in accordance with the "W" pattern of coupling interaction. A very significant increment was noticed for the $^4J_{PH(D)}$ = 2.8 Hz for **2** to the value of $^4J_{PH(D)}$ = 6.7 Hz for **2a**, which was in accordance with the "W" coupling interaction. As expected, this coupling is not observed for

$^4J_{PH(O)}$ in the freely rotating phenyl ring **D**. This coupling interaction was confirmed by recording the ^{31}P-decoupled ^1H NMR spectrum of the methoxy substituted analogue **2a** (the structure given in figure 3.6). The proton couplings in the aromatic ring **C** are given in table 3.6. A remarkable and unexpected increment of $^3J_{PH(A)}$= 8.2 Hz for **2** to $^3J_{PH(A)}$= 15.6 Hz for **2a** was observed. A ^1H NMR spectrum of compound **2a** produced an ABCX spin system whilst the ^{31}P-decoupled spectrum produced an ABC spin system.

Table 3.6. The aromatic ^1H NMR coupling interactions for **2**, and **2a**.

J (Hz) for aryl ring of **2** (^1H-^{31}P coupled)		J (Hz) for aryl ring of **2a** (^1H-^{31}P coupled)		J (Hz) for aryl ring of **2a** (^{31}P-decoupled)	
$^3J_{H(A)H(B)}$	7.7	$^3J_{PH(A)}$	15.6	$^3J_{PH(A)}$	-
$^3J_{H(B)H(C)}$	7.4	$^3J_{H(C)H(D)}$	8.7	$^3J_{H(C)H(D)}$	8.7
$^3J_{H(C)H(D)}$	7.8	$^4J_{H(A)H(C)}$	2.7	$^4J_{H(A)H(C)}$	2.4
$^4J_{H(A)H(C)} = {}^4J_{H(B)H(D)}$	1.1	$^4J_{PH(D)}$	6.7	$^4J_{PH(D)}$	-
$^3J_{PH(A)}$	8.2				
$^4J_{PH(D)}$	2.8				

It was interesting not to observe the similar incremental effect on the proton-proton vicinal coupling interaction when going from **2** to **2a**, and only a slight effect on the four-bond coupling interaction for $^{4}J_{H(A)H(C)}$.

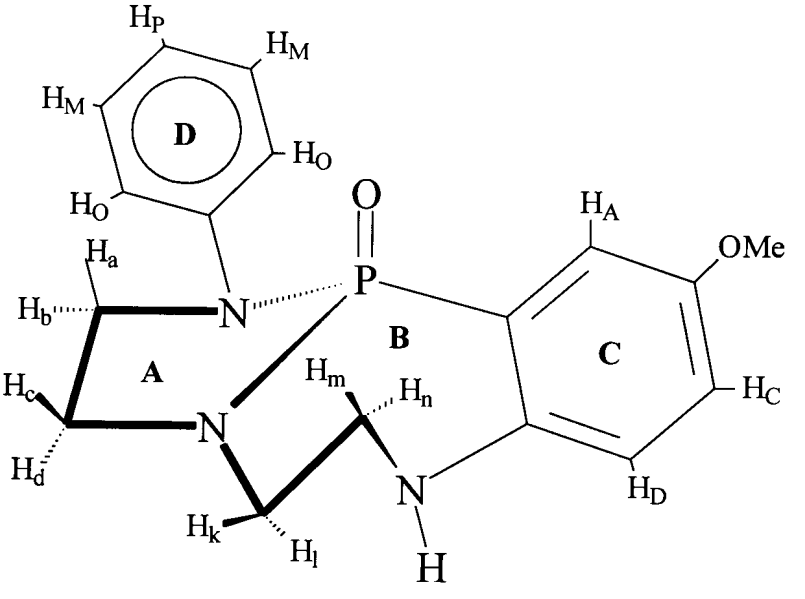

Figure 3.6 Molecular structure of **2a**.

3.6 ^{13}C NMR ANALYSIS OF 2.

The ^{13}C NMR spectrum of **2** was complicated by the coupling interactions with phosphorus-31, where nearly all carbons-13 nuclei are coupled. An interesting observation was made about an unusually high one-bond coupling, i.e. $^{1}J_{PC(16)}$ = 170,9 Hz. Table 3.7 shows the chemical shifts of

carbons atoms in compound **2** and their coupling constants to phosphorus-31.

Table 3.7 ^{13}C NMR data of **2** (see the adjacent figure).

Carbon-13 nucleus	δ_C (ppm)	J_{PC} (Hz)
C(1)	143.7	6.9
C(2)	117.7	4.0
C(3)	129.2	-
C(4)	121.8	-
C(7)	47.2	10.0
C(8)	46.1	8.1
C(9)	50.5	6.9
C(10)	45.5	1.5
C(11)	149.9	6.5
C(12)	118.1	11.5
C(13)	131.1	2.4
C(14)	118.9	13.3
C(15)	131.2	7.6
C(16)	119.4	170.9

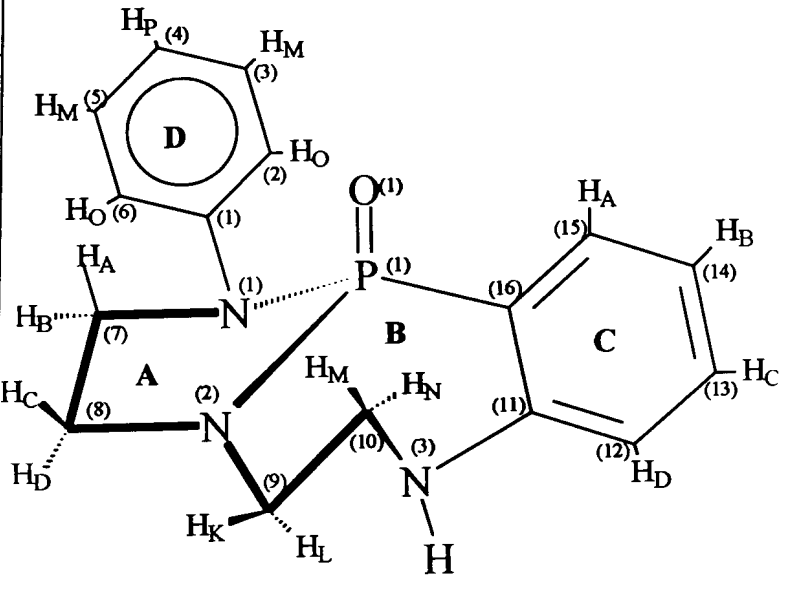

A comparison of similarly positioned carbons in the five-membered rings of **1** and **2** revealed different coupling constant values. For **1**, $^{2}J_{PC(7)}$ = 19.5 Hz compared to 10.0 Hz for **2**, whereas, $^{2}J_{PC(8)}$ = 6.7 Hz for **1**, and 8.5 Hz for **2**.

3.7 SOLVENT EFFECT FOR 2.

The recorded spectra of ^{1}H NMR of **2** in acetone-d_6 and bezene-d_6 showed the same chemical-shifts pattern as observed for compound **1**. However, the protons due to the aromatic region were better resolved in acetone-d_6 than in benzene-d_6 and chloroform-d_1 and that the improvement in the splitting patterns simplified proton assignments (figure 3.7). The ^{1}H NMR spectrum of **2** showed in benzene-d_6 a collective up-field shift by all the aliphatic protons of the seven and five membered rings. A more first-order pattern could be achieved at higher fields. We can expect similar solvent-substrate interaction for **2** as we observed for **1**, and which are discussed in chapter 2. We have demonstrated that while the vicinal protons at the five-membered ring in **2** have the same geometry as those in **1** (eclipsed), the vicinal protons of the seven-membered ring in **2** adopt a staggered conformation. Since the effect of substituting chloroform-d_1 (or acetone-d_6) for benzene-d_6 has a similar effect on the aliphatic protons of both

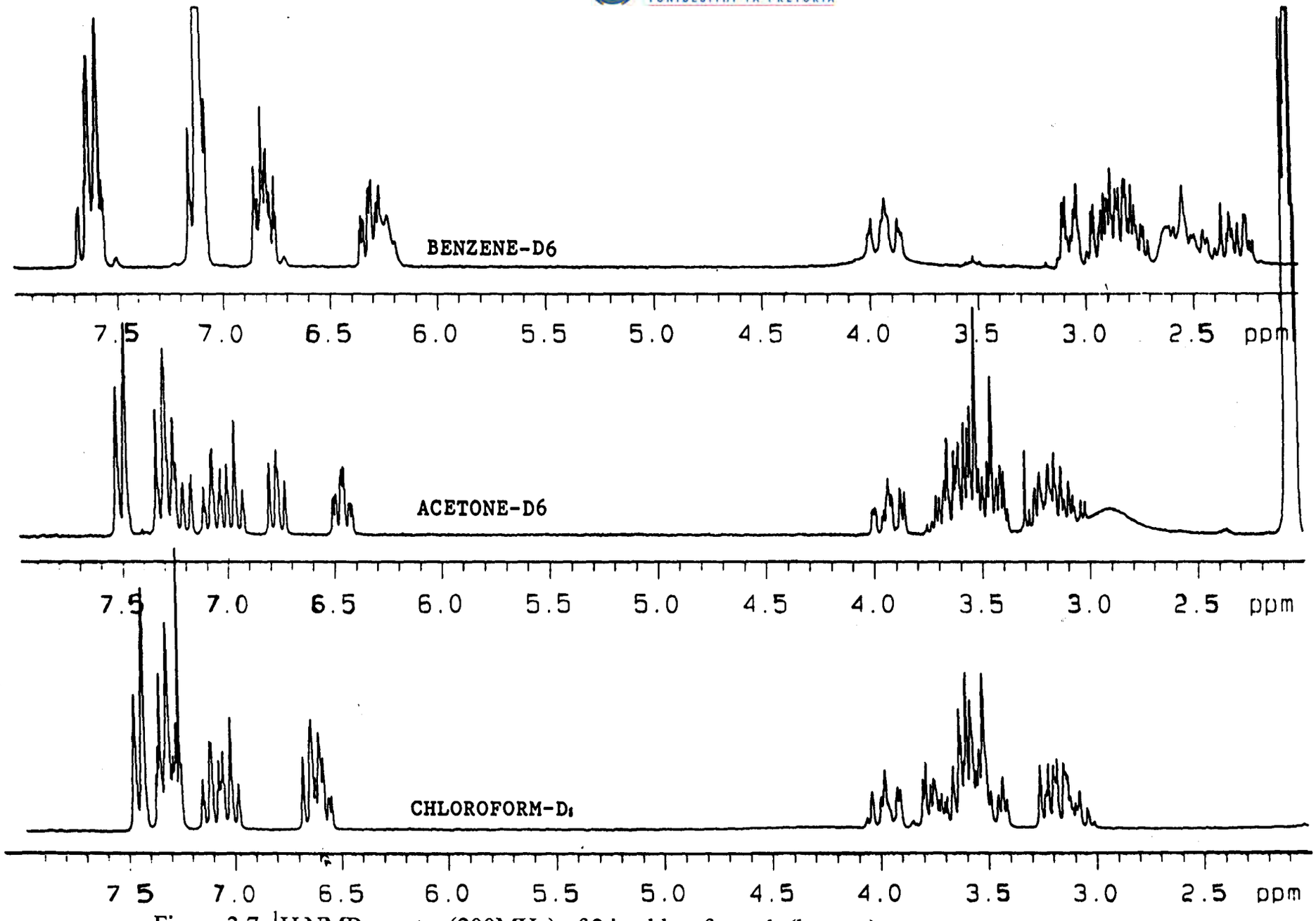

Figure 3.7. ^{1}H NMR spectra (200MHz) of 2 in chloroform-d_1 (bottom), acetone-d_6 (middle) and benzene-d_6 (top).

compounds, the specific solvent effect by benzene-d_6 should be in both cases similar. We propose therefore that benzene molecule align similarly around the aliphatic protons of the molecule of **1**, as well as of **2**, and affect the chemical shift of protons in the compounds via the magnetic anisotropic effect.

CHAPTER 4

CONFORMATIONAL AND STRUCTURAL ANALYSIS OF COMPOUND 3.

As another isomer of **1** and **2**, compound **3** also has a molecular weight of approximately 300 g/mol. Compound **3** consists of two fused heterocyclic seven-member rings. Each of those rings is additionally fused to aromatic ring. System **3**, similar to **1** has a plane of symmetry (figure 4.1) with an appreciable conformationally rigid structure on the NMR time scale. However, the N-CH_2-CH_2-N moiety in **3** exhibits two spin systems, which are different because of different hydrogen-phosphorus bond distances. Spin system of ABCD is observed as a result of the absence of the interactions of protons with phosphorus due to the separation by the aromatic carbons, Whereas the ABCDX spin system results from the protons attached to C(8) and C(9), coupling with ^{31}P (figure 4.1). Another ABCDX spin system was observed for protons of the fused aromatic rings where X is again the ^{31}P nucleus. System **3** differs fundamentally from system **1**, both in terms of the size of the heterocyclic rings, and the bonds around phosphorus (two P-C bonds; a phosphinic derivative).

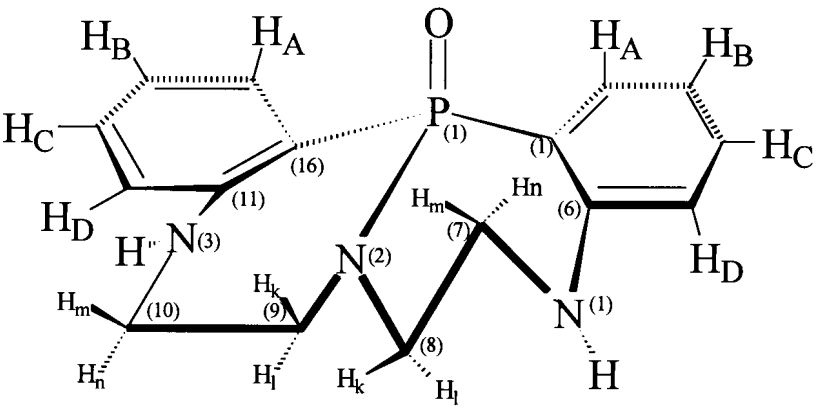

Figure 4.1. Molecular structure of compound **3**.

4.1 ^{1}H NMR ASSIGNMENT OF HETEROCYCLIC PROTONS OF 3.

The ^{1}H NMR assignment of hydrogens due the aliphatic vicinal moiety is based on the first order interaction with phosphorus atom, depending on the number of bonds between them. Carbons at position 8(C-8) and 9(C-9) are both two-bond distance from phosphorus atom and thus their protons are strongly coupled to it through ABCDX spin system. This coupling interaction results in sixteen signals where the overlap of three signals is observed. Figure 4.2 gives a clear first order splitting pattern of the vicinal hydrogens, where protons H_k and H_l each produces an ABCDX spin system.

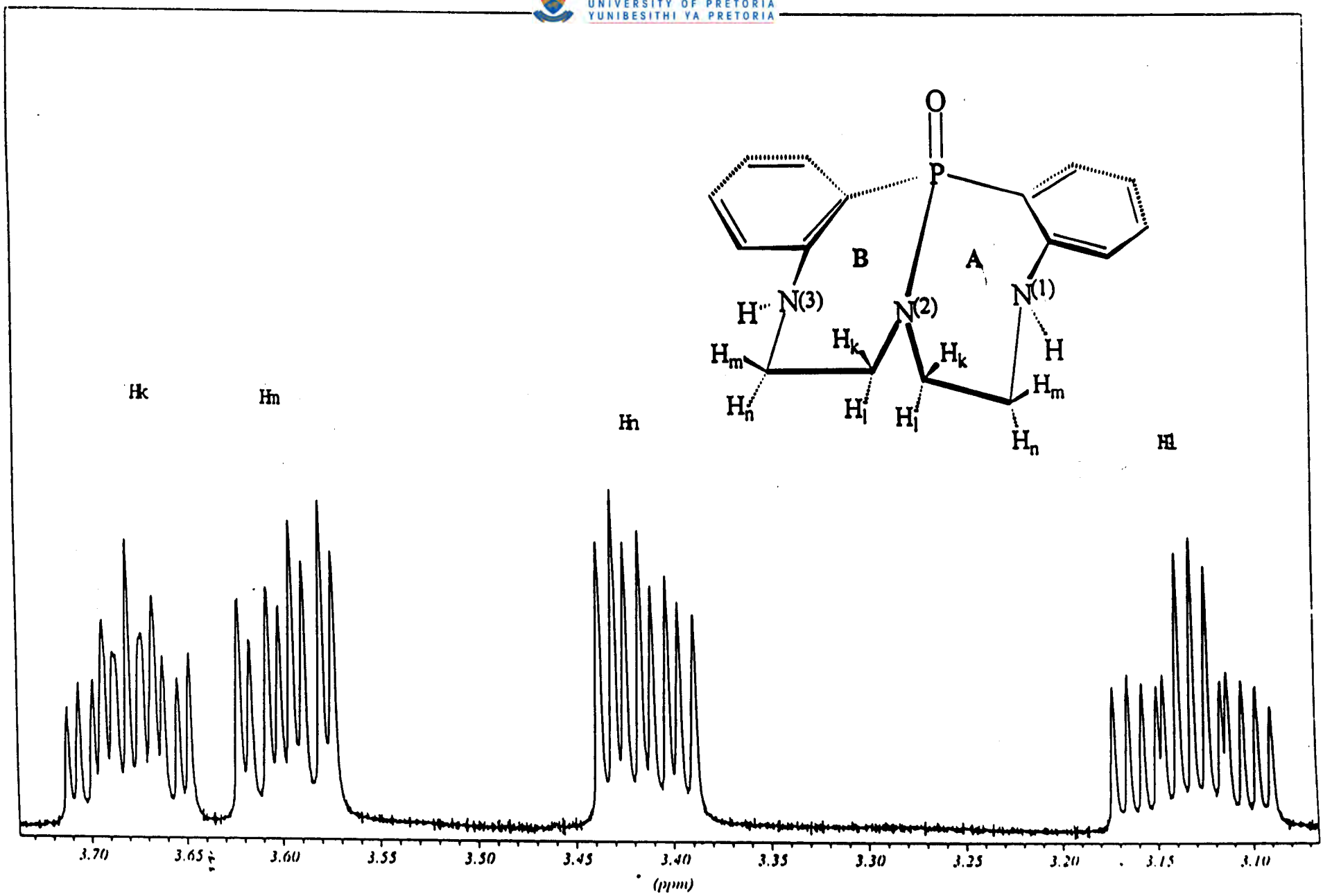

Figure 4.2. ^{1}H NMR spectrum of the aliphatic region of **3** at 500 MHz field.

Protons H_m and H_n are both at least four bonds away from the phosphorus atom and thus experience little if no effect at all from it. Protons H_m and H_n produce eight signals each corresponding to their spin system ABCD. The possible four-bond coupling would be observed if it had been transmitted through a 'W' pattern which, is known to enhance the coupling interaction, but is not allowed by the geometry of the molecule. Proton NMR spectral data of **3** produced a first order coupling interaction from which it was possible to relate each proton of the vicinal system to its neighbouring protons. Due to a clear plane of the molecular symmetry on the NMR time scale, only four set of multiplets at high field region were observed.

4.1.1 Comparison of aliphatic protons of system 2 and 3.

A very significant observation is noted in **3** as compared to **2** (at 500 MHz), in the sense that signals at both heterocyclic vicinal protons next to the N-H group were influenced in their shape by that group in **2,** whereas no such effect is observed in **3**. For **2,** at 600 MHz, H_n splits into a triplet-triplet while H_m gives eight signals. Table 4.1 gives the chemical shifts comparison of seven-membered heterocyclic rings of **2** and **3**.

Table 4.1 ^{1}H NMR chemical shifts of seven-membered rings of **2** and **3** in dueterated chloroform.

δ_H/ (ppm) of system **2**		δ_H/ (ppm) of system **3**	
H_k	3.56	H_k	3.68
H_l	3.13	H_l	3.13
H_m	3.91	H_m	3.60
H_n	3.40	H_n	3.41

It can be noted from figure 4.2 that the splitting pattern of H_m and H_n observed for **2** improved from a second order pattern to first order splitting pattern in system **3**. While the chemical shifts of H_n are similar in both compounds, δ_H of H_m differs by a factor of about 0.3 ppm. A significant chemical shift difference was observed for proton H_m in **3**, which showed an upfield shift of 0.31 ppm. We therefore conclude that on average, H_l, H_k and H_n showed only a minor chemical shift difference whereas H_m showed much larger shift on moving from system **2** to **3**. One of the reasons for this difference could be the plane of symmetry in **3**. It can be noted from figure 4.2 and table 4.1 that protons H_m and H_n in **3** resonate within the span of frequencies of resonance of H_k and H_l.

4.2 COUPLING INTEREACTIONS OF ALIPHATIC PROTONS OF 3.

Table 4.2 shows a number of interesting observations, which can help in visualising the molecular structure of **3** in three dimensional projection. These coupling constant were measured assuming that the molecule is symmetrical in solution state (i.e. that the two halves of the molecule are equivalent).

Table 4.2. ^{1}H NMR coupling constants of system for the **3** N-CH_2-CH_2-N moiety.

Proton	δ_H (ppm)	Multiplicity	$^{2}J_{HH}$ (Hz)	$^{3}J_{HP}$ (Hz)	$^{3}J_{HH}$ (*trans*)	$^{3}J_{HH}$ (*cis*)
H_l	3.13	16 lines	13.1	16.8	7.6	3.8
H_n	3.41	8 lines	13.7	-	6.8	3.8
H_m	3.60	8 lines	13.7	-	7.6	2.9
H_k	3.68	16 lines	13.1	9.4	6.8	2.9

There are two prominent $^{3}J_{PH}$ relationships observed for **3** that are strong relative to the analogous *cis*- and *trans*- coupling constants for an also

symmetrical system **1**. The strong three bond coupling system in **3** is even more distinctive given the fact that the Drieding models show more than one possible conformational structure for this molecule. This strong proton-phosphorus coupling interaction is emphasised by the additional multiplicity of the signals due to H_k and H_l, where H_l can be regarded as *trans*-coplanar to P=O group while H_k is *cis*-coplanar to it. Another significant observation is that the *cis*, as well as *trans* proton-proton coupling interactions are different for each pair, i.e. $^3J_{H(k)H(m)} \neq {}^3J_{H(l)H(n)}$ and $^3J_{H(k)H(n)} \neq {}^3J_{H(l)H(m)}$. Apart from the mentioned dissimilarities, $^2J_{HH}$ (geminal couplings) are similar. A simulated spectrum of the aliphatic region confirmed the ^1H NMR assignments.

4.3 X-RAY DIFFRACTION ANALYSIS OF SYSTEM 3.

Figure 4.3 (the X-ray crystal structure of **3**) shows the solid state molecular geometry of compound **3**. Since X-ray structure does not show the related positions of hydrogen atoms, a Newman-projection method was used to extrapolate the orientation of all protons. By using the Newman-projection method it was also possible to deduce the torsion angles around all aliphatic protons of the seven-memberd heterocyclic system. The X-ray diffraction

data differentiated the two heterocyclic rings (i.e. ring A and ring B) as if the molecule had no plane of symmetry. Therefore, the existence of two conformations in rapid exchange is possible.

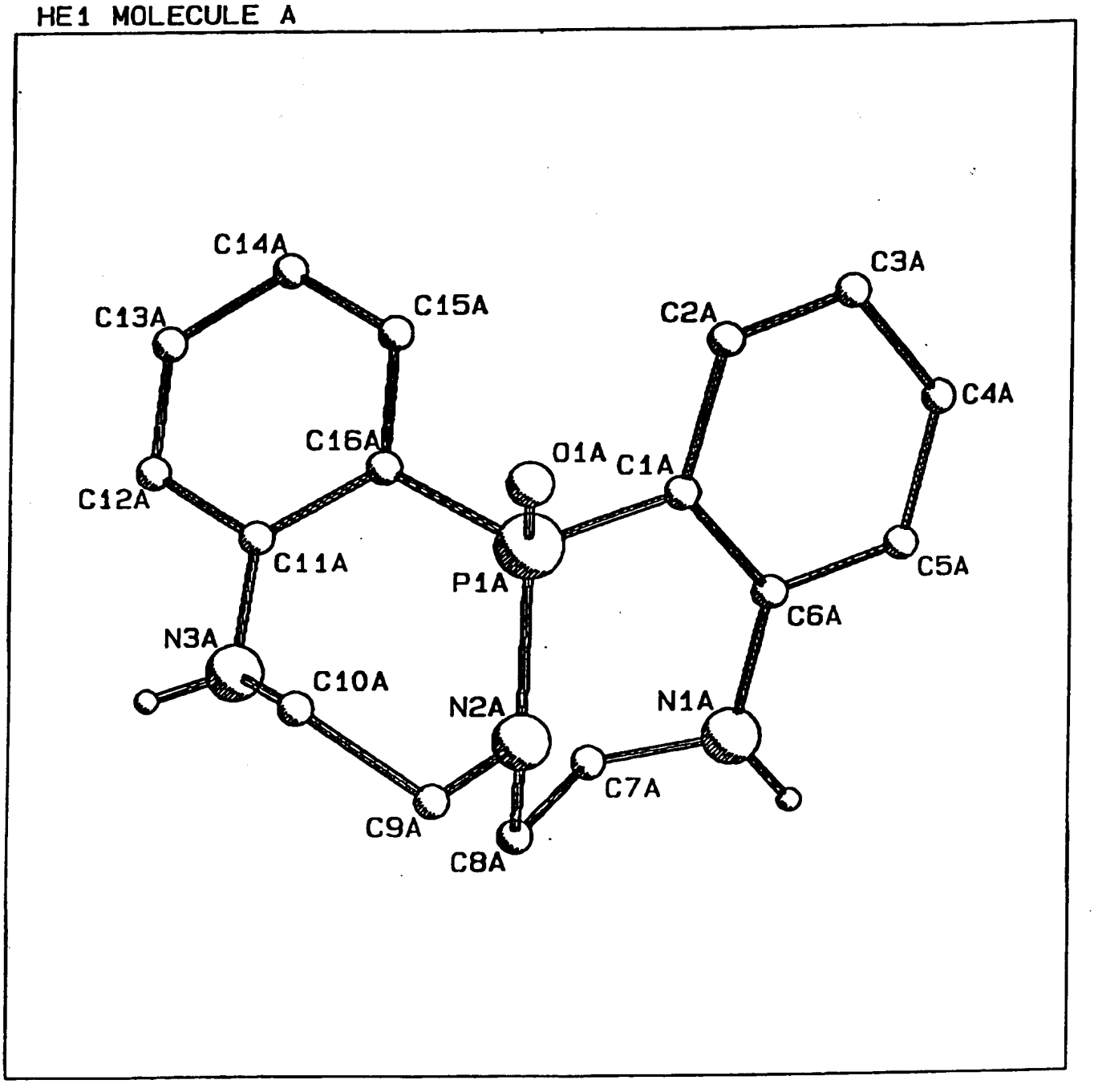

Figure 4.3a. X-ray crystal structure of **3**.

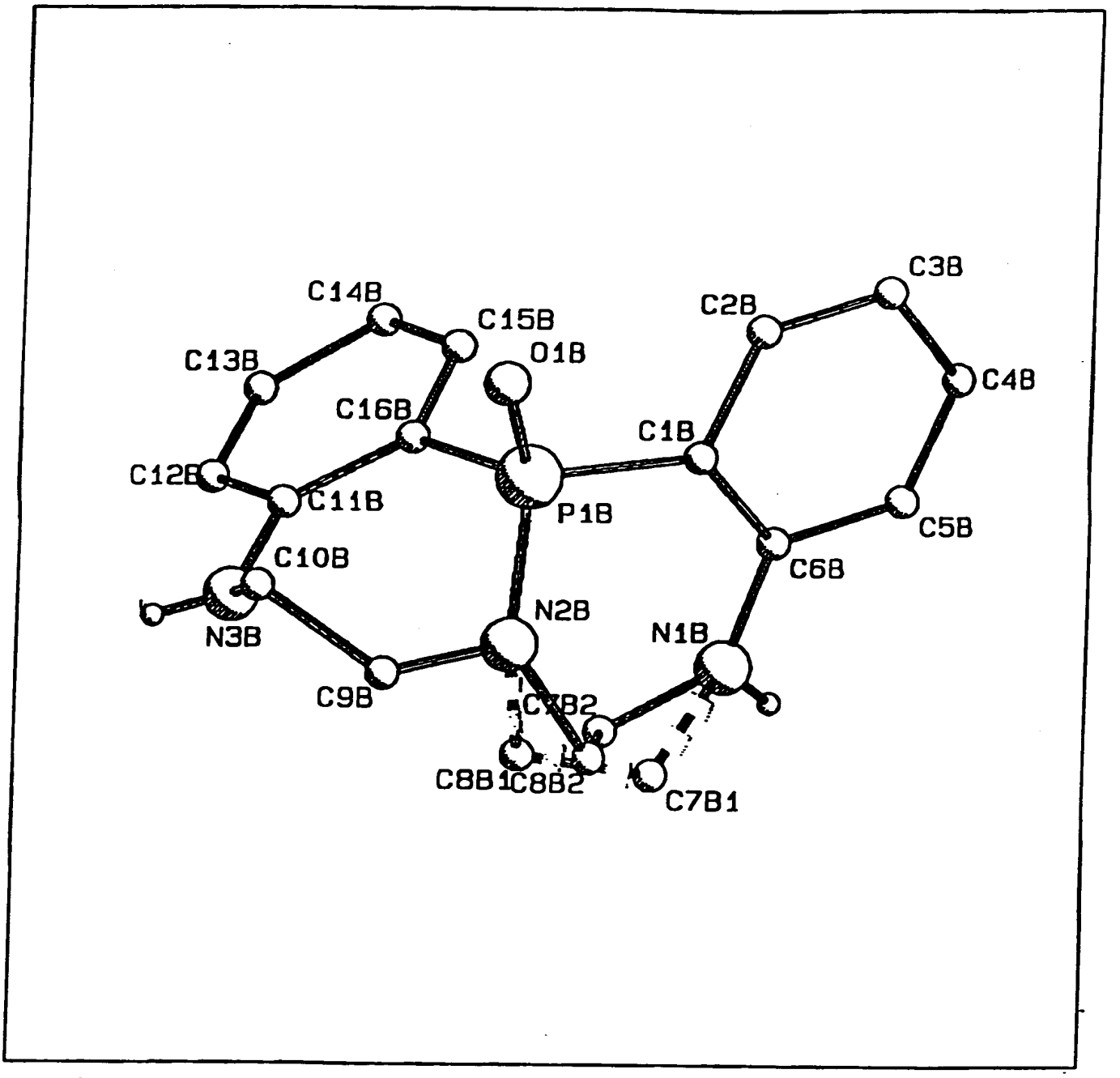

Figure 4.3b. X-ray crystal structure of **3**

A comparison of bond lengths and angles in molecule A (figure 4.3a) and B (figure 4.3b) show some small differences. Figure 4.3b helps to illustrate the extend of flexibility through N(2B)-C(7B)-C(8B)-N(1B). The major reason for the two independent molecules appears to arise from the way in which

they pack. The existence of these two different molecules suggests a flexible nature of system **3**, in particular around the common, N (2) - P (1) bond.

Table 4.3. Selected bond lengths [A] and angles [deg] for X-ray diffraction molecular structures of **3** from figure 4.3a and 4.3b.

Figure 4.3a		Figure 4.3b	
Connection	Bond length [A]	Connection	Bond length [A]
P(1A)-C(16A)	1.608	P(1B)-C(16B)	1.607
P(1A)-O(1A)	1.641	P(1B)-O(1B)	1.578
P(1A)-C(1A)	1.750	P(1B)-C(1B)	1.959
P(1A)-N(2A)	1.785	P(1B)-N(2B)	1.664
N(1A)-C(7A)	1.246	N(1B)-C(7B2)	1.416
		N(1B)-C(7B1)	1.61
N(1A)-C(6A)	1.482	N(1B)-C(6B)	1.312
N(2A)-C(9A)	1.495	N(2B)-C(9B)	1.678
N(2A)-C(8A)	1.655	N(2B)-C(8B1)	1.552
		N(2B)-C(8B2)	1.605
N(3A)-C(10A)	1.387	N(3B)-C(10B)	1.463

Connection	Bond length [A]	Connection	Bond length [A]
N(3A)-C(11A)	1.406	N(3B)-C(11B)	1.504
C(7A)-C(8A)	1.511	C(7B1)-C(8B1)	1.580
		C(7B2)-C(8B2)	1.670
C(9A)-C(10A)	1.505	C(9B)-C(10B)	1.434

Angle description	Angle[deg.]	Angle description	Angle[deg.]
C(7A)-N(1A)-C(6A)	113.8	C(6B)-N(1B)-C(7B2)	120.0
		C(6B)-N(1B)-C(7B1)	119.0
C(9A)-N(2A)-C(8A)	118.7	C(8B1)-N(2B)-C(9B0	118.2
		C(8B2)-N(2B)-C(9B)	129.2
C(9A)-N(2A)-P(1A)	105.8	P(1B)-N(2B)-C(9B)	115.2
C(8A)-N(2A)-P(1A)	127.2	C(8B1)-N(2B)-P(1B)	114.2
		C(8B2)-N(2B)-P(1B)	114.6
C(10A)-N(3A)-C(11A)	124.5	C(10B)-N(3B)-C(11B)	130.6
C(7A)-C(8A)-N(2A)	117.1	N(2B)-C(8B1)-C(7B1)	126.0
		N(2B)-C(8B2)-C(7B2)	120.5
N(2A)-C(9A)-C(10A)	115.3	C(10B)-C(9B)-N(2B)	114.0
N(3A)-C(10A)-C(9A)	101.0	C(9B)-C(10B)-N(3B)	99.5

The following torsion angles, selected from the X-ray data, were then used to apply Newman projection procedures to extrapolate all angles involving the aliphatic vicinal hydrogens.

1. N(2A)-C(9A)-C(10A)-N(3A) = 42.4°..... [A]

2. N(1A)-C(7A)-C(8A)-N(2A) = 61.5°..... [B]

3. N(2B)-C(9A)-C(10B)-N(3B) = 42.4°..... [C]

4. N(1B)-C(7B1)-C(8B1)-N(2B) = -64.0°..... [D]

5. N(1B)-C(7B2)-C(8B2)-N(2B) = 96.0°..... [E]

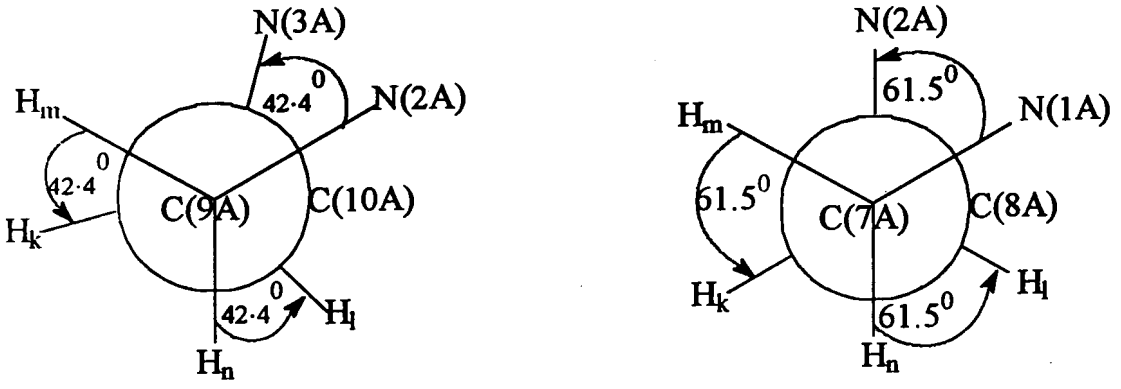

Figure 4.4. Newman projections showing the dihedral angles of the aliphatic vicinal protons of **3** following the molecular structure given in figure 4.3a.

Figure 4.4 gives a typical illustration of the Newman projection of the dihedral angles around the aliphatic vicinal protons. Torsion angles 1 and 2 were measured from the molecular structure given in figure 4.3a, whereas 3, 4 and 5 were measured from the molecular structure given in figure 4.3b. A dihedral relationships shown in figure 4.3a follow an X-ray determined torsion angle N(1A)-C(7A)-C(8A)-N(2A) and gives a value of 61.5° whilst a figure 4.3b following X-ray torsion angle N (2A)-C(9A)-C(10A)-N(3A) gives a value of 42.4°. It then follows from figure 4.3a and b that these dihedral angles are most appropriate as compared to those measured from ^{1}H NMR, though the NMR spectrum gives an average of the two equal halves of the molecule. The two X-ray molecular structures, i.e. figure 4.3a and b exhibit a set of *cis*- and *trans*- coplanar atomic relationships complicating the comparison with NMR calculated values. It comes as no surprise that the ^{1}H NMR coupling (coupling constants different for different pairs of protons; the situation different from that observed for **1**) also suggest to some extent an existence of two different aliphatic vicinal systems, thereby indicating a possibility of two conformationally different seven-membered heterocyclic rings. A good illustration of the three dimensional molecular structure of **3** which fitted the results as recorded both by NMR and X-ray, can easily be represented by Drieding models.

Table 4.4. Comparison of dihedral angles obtained for **3** from the NMR data and from the X-ray diffraction data as in figure 4.1 and 4.3a,b respectively.

NMR dihedral angles [deg]		X-ray diffraction torsion angles [deg]		Orientation
Connection	Angle	Connection**	Angle*	
H_l-C_8-C_7-H_m	155.6°	H(m)-C(7A)-C(8A)-H(l)	181.5°	*Trans*
H_k-C_8-C_7-H_n	155.9°	H(k)-C(9A)-C(10A)-H(n)	162.4°	*Trans*
H_k-C_8-C_7-H_m	52.2°	H(m)-C(7A)-C(8A)-H(k)	61.5°	*Cis*
H_l-C_8-C_7-H_n	46.0°	H(l)-C(9A)-C(10A)-H(n)	42.4°	*Cis*

** Arbitrary assignments of hydrogens from figure 4.3a.

*Averaged calculation of torsion angles from figure 4.3a and 4.3b.

4.4 CONFORMATIONAL ANALYSIS OF HETEROCYCLIC RINGS FOR SYSTEM 3.

Similar as with system **1**, the conformation of **3** can be derived from the information collected from the NMR data as well as X-ray diffraction studies. ^{1}H NMR spectrum of system **3** indicates an averaged time-scale data whereby the symmetry of the molecule plays an important role. Unlike

system **2** where all eight aliphatic protons are practically and theoretically different, there are only four chemically and magnetically different protons in system **3**. This outcome suggests a relatively rigid molecular structure in which there is a similar chemical environment in either symmetrical part of the molecule. The X-ray crystal (figure 4.3a and b) structure on the other hand suggests a rather more distorted molecular structure, which lacks a clear plane of symmetry. Both the X-ray and Drieding model structures predicts a half-chair conformation for one ring and a boat conformation for another. Obviously, the two rings can interchange their conformations depending on the relative dihedral angle around N(2A) to either N(3A) or N(1A).

Hendrickson's molecular mechanics calculations[39] support both conformations. The co-existence of these two conformations is also supported by energy equilibrium between them. X-ray structure for system **1** showed a relatively consistent plane of symmetry in relation to ring A and B. However, the X-ray structure for system **3** shows two rings with different geometry. For system **3**, C(9A) and C(8A) carbons are positioned opposite relative to the P=O group and obviously this feature has a profound impact on the orientation of aliphatic vicinal protons. This geometrical dissimilarity

(relative to the molecule of **1**) can be attributed to nitrogen N(2A) geometry, which is more planar compared to the pyramidal configuration of the analogous N(2) atom in **1**. Nitrogen N(2A) in **3** is planar, opposite to the pyramidal derivative in **1**. This difference results in different conformations of the seven- and five- membered rings in **3** and **1**. This difference, in turn, as tested by Dreiding models, makes it possible for the molecule of **3** to have distinct seven-membered heterocyclic rings, as demonstrated by the X-ray diffraction molecular structure.

4.5 ^{1}H NMR OF AROMATIC REGION FOR 3.

The resonance frequency of the aromatic protons for both fused rings of **3** shows that the corresponding protons are both magnetically and chemically equivalent. This behaviour is supported by the fact that the aromatic systems are relatively rigid and therefore protons, which are similar in terms of chemical environment, will resonate equally on the NMR time scale. A fully coupled ^{1}H NMR spectrum reveals a similar spin interaction as found for protons H_k and H_l, thus the ABCDX spin system. The fused aromatic ring has two highly polar substituents, i.e. the. P=O and N-H groups. The bond distance from these groups has a direct bearing on the chemical shift of

aromatic protons. Table 4.5 shows an interesting magnetic interactions of different aromatic protons following a unique pattern as seen in figure 4.5. The aromatic section of the ^{1}H NMR spectrum of **3** was also simulated in the same manner as the aliphatic region.

Table 4.5. ^{1}H NMR data for aromatic protons of **3**.

Proton	δ (ppm)	**Coupling constant (Hz)**
H_A	7.44	$^3J_{H(A)H(B)} = 7.6$
		$^3J_{PH(A)} = 14.4$
H_B	6.86	$^3J_{H(B)H(C)} = 7.6$
		$^4J_{PH(B)} = 2.2$
H_C	7.26	$^3J_{H(C)H(D)} = 8.0$
		$^4J_{H(A)H(C)} = 1.6$
H_D	6.72	$^4J_{PH(D)} = 5.4$
		$^4J_{H(B)H(D)} = 1.1$

The manner in which these aromatic protons resonate follows a characteristic pattern: $\delta_{H(A)} > \delta_{H(C)} >> \delta_{H(B)} > \delta_{H(D)}$.

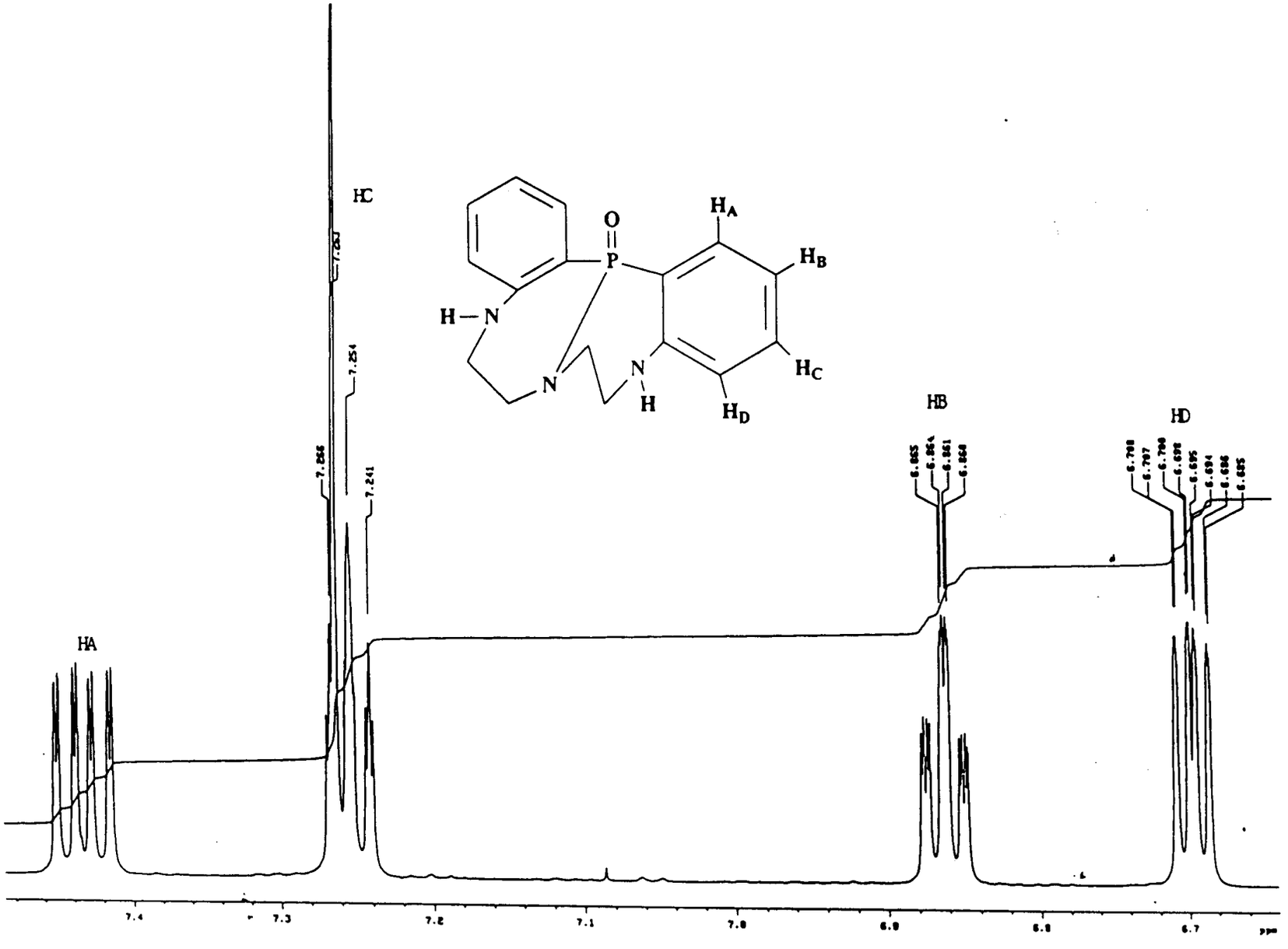

Figure 4.5 Aromatic ^{1}H NMR spectrum of **3**.

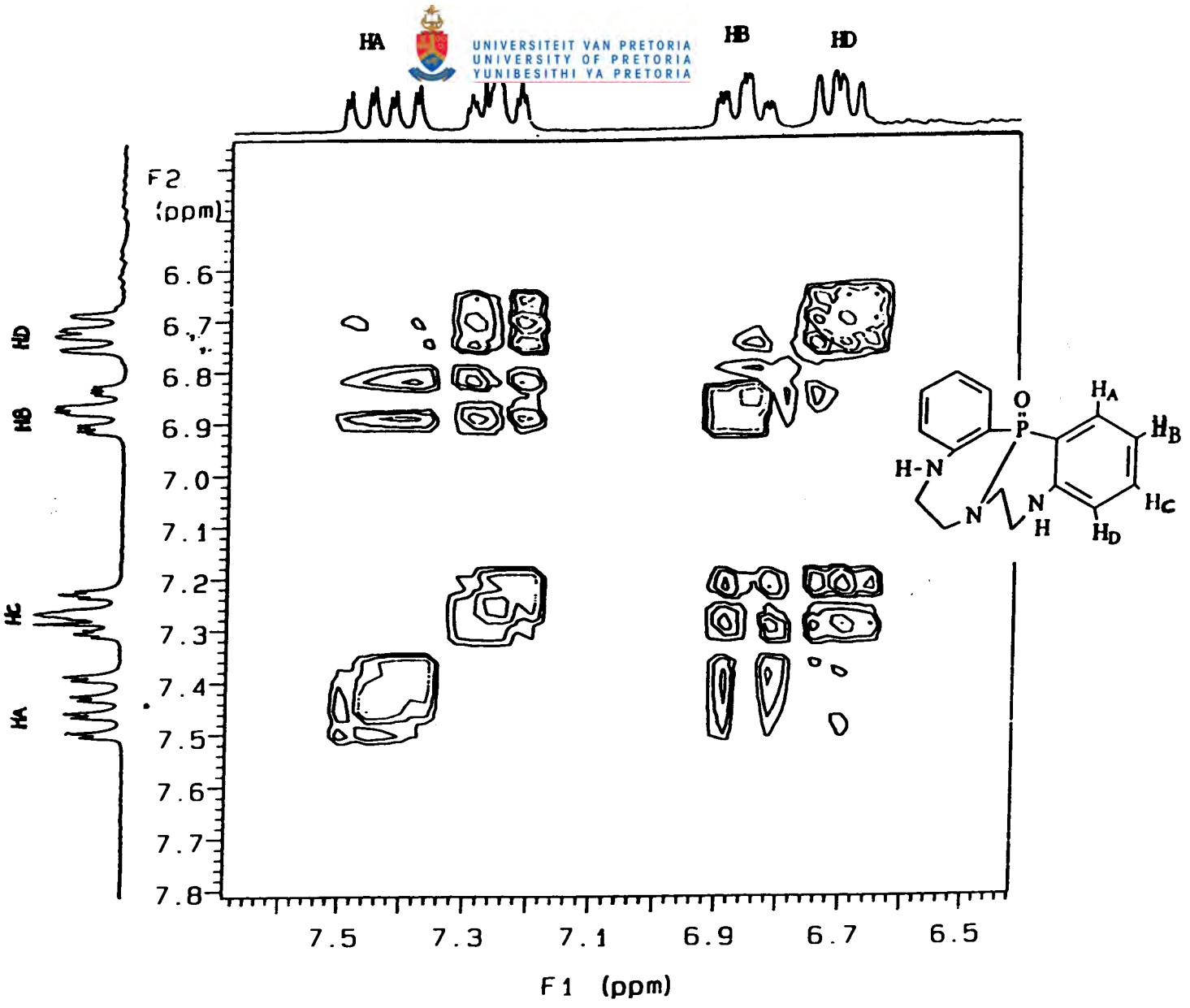

Figure 4.6. A cosy spectrum of aromatic protons of **3** at 200 MHz field.

The pattern observed for **3** has been observed earlier with different ortho disubstituted benzene rings though the examples were resolving into an ABCD spin system.[25]. A cosy spectrum of the aromatic section of **3** (figure 4.6), gives a convincing information about aromatic proton resonance relative to their scalar couplings. The aromatic system of **3** shows a good

illustration of strong "W" coupling interaction over four bonds, where $^4J_{PH(D)}$ = 5.4 Hz is evident. With an increase in magnetic field, a similar scalar coupling is involving all aromatic protons. Another significant observation from aromatic system of **3** is that the proximity of N-H moiety was made evident by a D_2O wash experiment, whereby the broad multiplet due to improved to H_D after washing. To further confirm the unusual coupling interaction of the fused aromatic ring of **3**, the ^1H NMR spectrum of derivative system (**3a**) was recorded (figure 4.6).

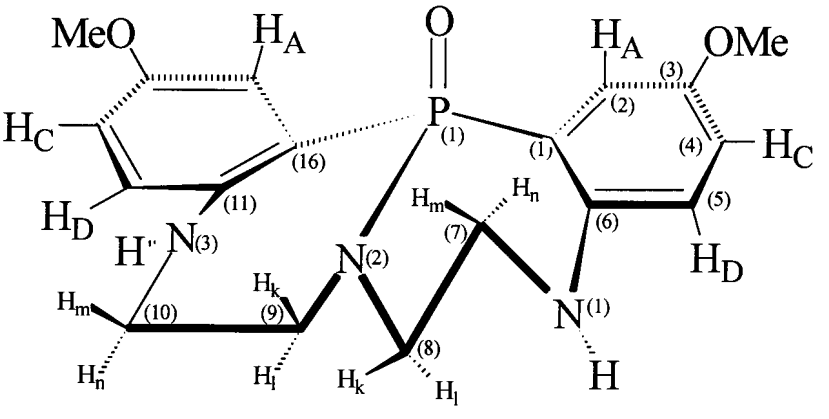

Figure 4.7. Molecular structure of system analogue of **3, 3a**.

The ^1H NMR spectrum of aliphatic region of **3a** produced a similar spin system as for the aliphatic moiety of **3**. The biggest difference comes from the aromatic region of **3a** since both benzene rings are additionally *meta*

substituted with respect to the P=O group. Figure 4.8 gives the aromatic phosphorus decoupled and coupled ^{1}H NMR spectrum of **3a**. However, due the additional substitution in the aryl group, a decoupled spectrum produces an ABC spin system. A similar strong "W" coupling interaction between phosphorus-31 and H_D is also observed. A significant chemical shift of 0.31 ppm by H_A, relative to **3** is observed. This is due to the resonance effect of the OMe group. Figure 4.7 confirmed without doubt the assignment of the signal at position 6.86 ppm observed for **3** which then correlates with protons H_C (δ_H 7.26 ppm) and H_A (δ_H 7.44 ppm) and which disappeared in the spectrum of **3a**. For **3**, there is also a clear correlation between H_C (δ 7.26 ppm) and H_D (δ 6.71 ppm) with a coupling constant of 8.6 Hz. Figure 4.5 shows a multiplet at δ_H 6.88 ppm (H_B), but in the case of **3a** (figure 4.7) it is proton H_C, which resonates at this position. This observations show that proton H_C has moved upfield from δ_H 7.26 ppm (figure 4.5) to δ_H 6.88 ppm (figure 4.8). This shows an upfield shift of about 0.38 ppm upon substitution of H_B (figure 4.5) by methoxy group (system **3a**).

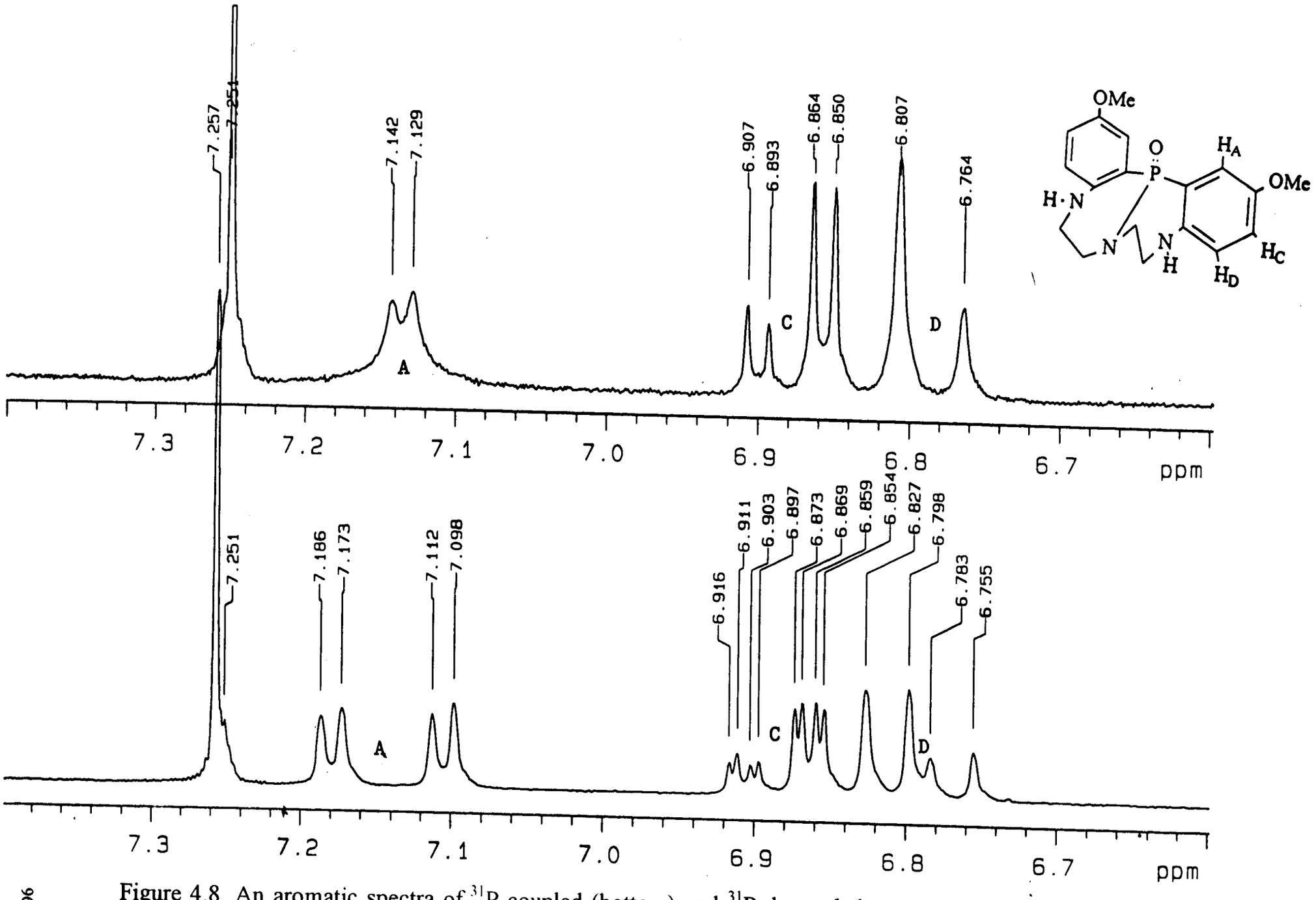

Figure 4.8. An aromatic spectra of ^{31}P coupled (bottom) and ^{31}P decoupled (top) of **3a** at 200 MHz field.

4.6 ^{13}C NMR ANALYSIS OF COMPOUND 3.

Carbon-13 chemical shifts and J_{PC} values for both aromatic and aliphatic regions in **3** were also determined. Carbon-13 spectrum does not give clear indication about the symmetry of the molecule compared to what ^{1}H NMR and X-ray diffraction do.

Table 4.6. ^{13}C chemical shifts and J_{PC} coupling constants of **3** (see the adjacent figure for numbering).

Carbon	δ_C (ppm)	J_{PC} (Hz)
C(5)	47.8	-
C(6)	52.7	3.8
C(9)	119.4	9.5
C(8)	120.4	12.6
C(2)	120.8	126.1
C(10)	132.4	2.3
C(11)	133.9	9.1
C(3)	149.9	5.3

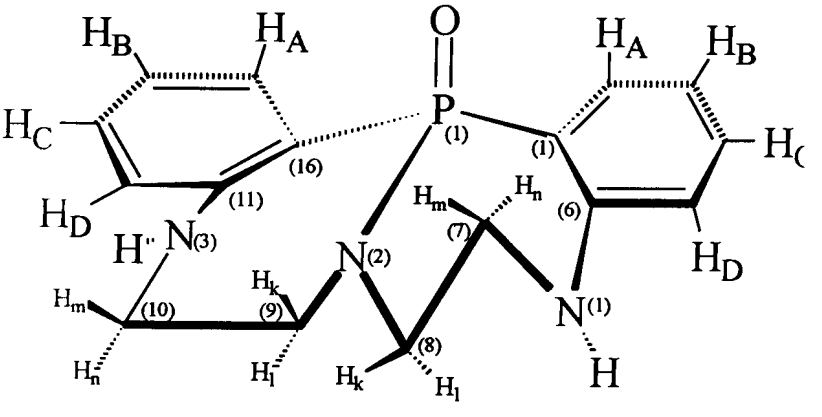

SYSTEM **3**

Carbon-phosphorus interaction extends from $^{1}J_{PC}$ to $^{3}J_{PC}$, with $^{3}J_{PC}$ being more effective in the aromatic system. Table 4.6 shows chemical shifts of phosphorus-coupled ^{13}C NMR spectrum and their respective coupling constants. It is interesting to note the $^{1}J_{PC(2)}$ = 126.06 Hz significantly smaller than^{1} $J_{PC(2)}$ =170.9 Hz observed for system **2** although C(2) is *ipso* carbon in both cases. This observation should come as no surprise as $^{1}J_{PC}$ increases with percent *s* character in the P-C bonding orbitals[27]. This relatively strong carbon-phosphorus interaction is also enhanced by the conjugation system extending from P=O to the whole aromatic ring. The effectiveness of aromatic system in enhancing scalar coupling is clearly illustrated by $^{3}J_{PC}$ which is observed for aromatic systems whilst it is not observed for the same coupling interaction for aliphatic region. This is despite the relatively significant population transfer phenomenon experienced by C(5) of the heterocyclic ring. This lack of ^{31}P-^{13}C spin-spin coupling interaction is observed despite the nitrogen atoms serving as bridges, where they are regarded as effective in transmitting spin-spin interaction due to the presence of the lone pair of electrons[60] on both N(1) and N(3) atoms of **3**. $^{3}J_{PC(8)}$ and $^{3}J_{PC(9)}$ are almost equal and that they all conform to "W" bond arrangement which promotes spin-spin interactions more effectively.

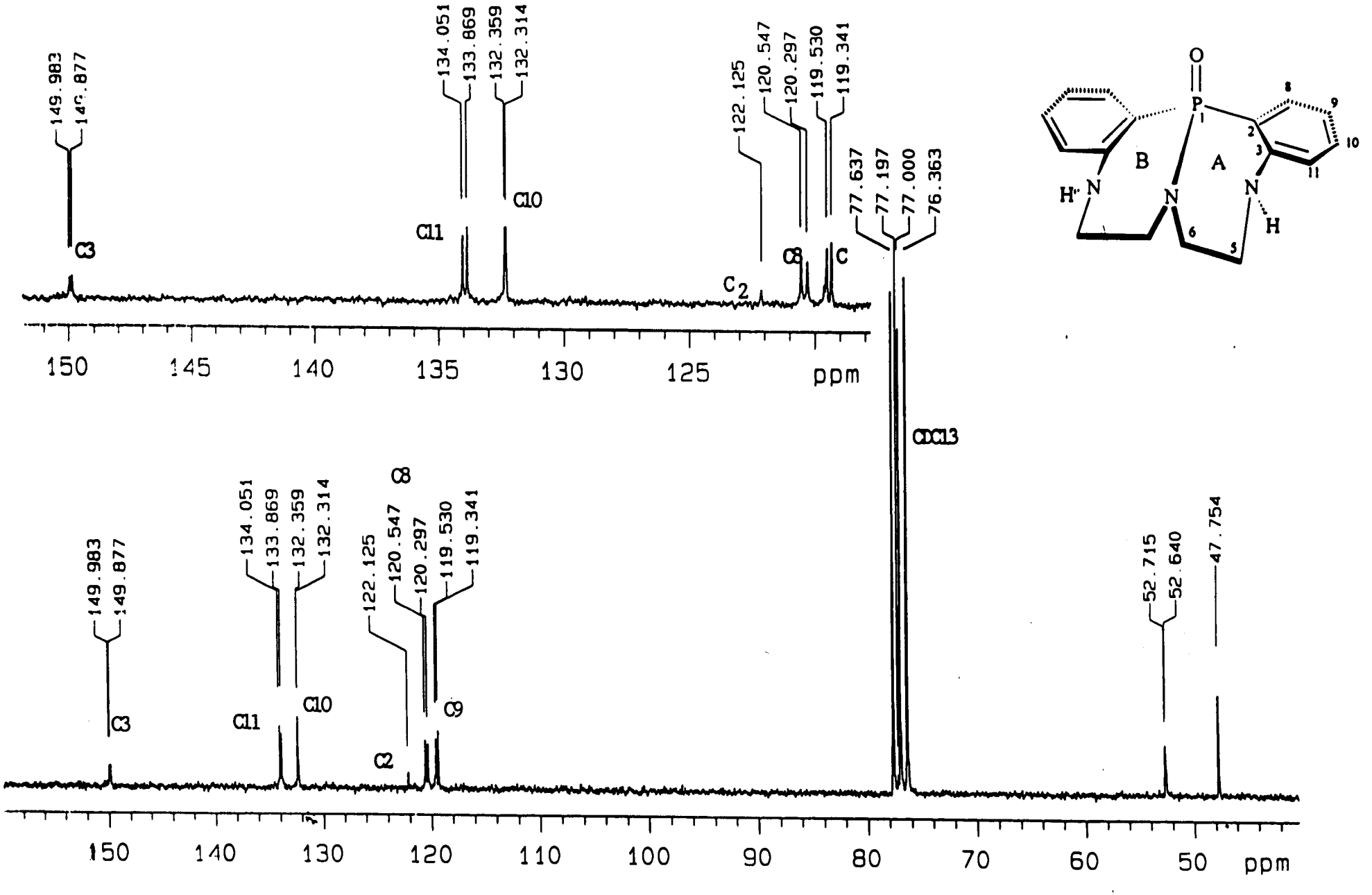

Figure 4.9 ^{13}C NMR spectrum of **3** at 50MHz.

A small $^{4}J_{PC(10)} = 2.2$ Hz, which emphasises the effect of conjugation in spin-spin interactions, is observed.

4.7 SOLVENT EFFECTS FOR SYSTEM 3.

A similar solvation mode as for **1** was expected for **3** for a number of reasons. One of the reasons being the existence of plane of symmetry on the NMR time scale. Compound **3** seems to interact with acetone-d_6 as in chloroform-d except that the N-H (δ_H = 5.87 ppm) signal is even more expressed in acetone-d_6 than in chloroform-d. A significant chemical shift is observed for **3** in benzene-d_6 where there is a general up-field chemical shift (about 0.5 ppm) of aliphatic protons (figure 4.8). It should be remembered that whilst the ^{1}H NMR data suggest a planar molecular structure for **3**, the X-ray crystal diffraction data suggest otherwise. It is however interesting not to observe the effect of the existence of two flexible seven-membered heterocyclic rings as noted from X-ray data. Therefore it can be concluded that the two exist in rapid exchange such that this exchange is not observable on the NMR time scale. The same reasons advanced for upfield ^{1}H NMR chemical shift for **1** are still applicable for **3**.

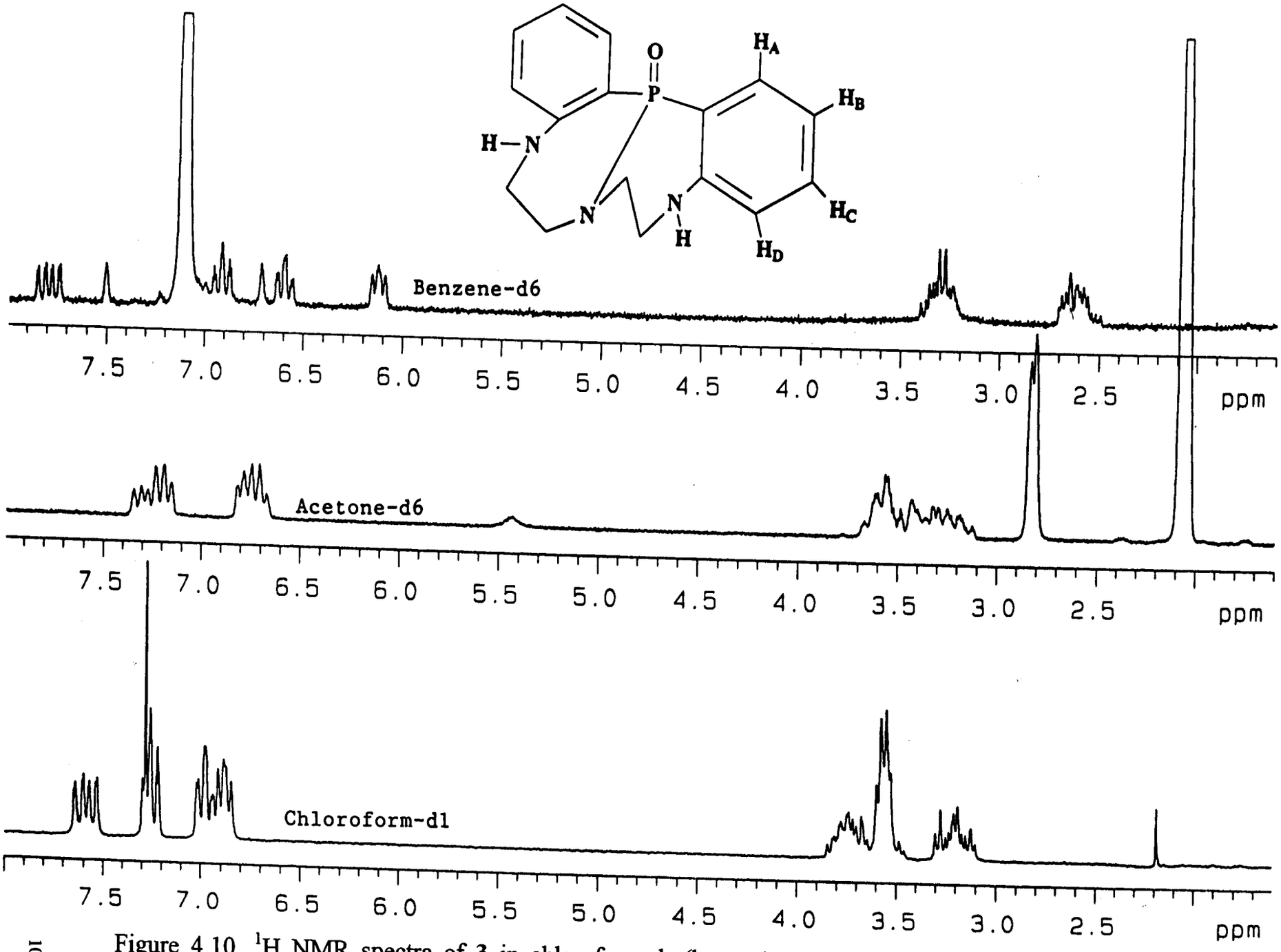

Figure 4.10. ^{1}H NMR spectra of **3** in chloroform-d_1 (bottom), acetone-d_6 (middle) and benzene-d_6 (top) 200 MHz field.

CHAPTER 5: EXPERIMENTAL.

Materials.

NMR spectra were recorded at different magnetic fields at different operating frequencies. The following spectrometers, as mentioned elsewhere (chapter 1), were used at different stages: 200 MHz, 400 MHz, 500 MHz and 600 MHz instruments. All deuterated solvents were of 99.9% purity and all were Sigma-Aldrich products. Chloroform-d_1 (δ_H 7.25 ppm, δ_C 77,0 ppm) was used for all spectral analysis whereas acetone-d_6 (δ_H 2.05 ppm) and benzene-d_6 (δ_H 7.30 ppm) were used for solvent effect analysis. Tetramethylsilane (TMS: δ_H 0.0 ppm) was used as internal reference. All samples were prepared in a 5 mm NMR tube size. Unless specified, all experiments were recorded at the temperature of 298 K (25^{0}C).

Compound 1: 1-oxo-2,8-diphenyl-2,5,8-triaza-1-phosphabicyclo [3.3.0] octane

(a) Solvent effect.

Phosphoric triamide **1** was prepared in our laboratory as described before[51]. Different experiments were conducted for **1** at different magnetic fields and

different deuterated solvents. The solvent effect spectra were recorded on the 200 MHz NMR instrument operating at proton frequency of 199.976 MHz. Similar experimental parameters were employed for ^{1}H NMR experiments in chloroform-d_1, acetone-d_6 and benzene-d_6 at room temperature (25^0C). Approximately 5 mg of **1** was dissolved in 0.5 ml of each deutereted solvent. The following selected acquisition parameters were employed: acquisition time, 3.744 s; spectral width, 3000.3 Hz; transmitter power, 52 dB; pulse width, 6.1 μs; data points, 22464; transients/scans, 100.

(b) ^{1}H NMR spectra for proton assignments.

The ^{1}H NMR spectrum for proton assignments and the determination of coupling constants of **1** was recorded on the 400 MHz spectrometer operating at proton frequency of 399.951 MHz. Five (5) mg of **1** was dissolved in 0.5 ml of chloroform-d. The following selected acquisition parameters were employed: acquisition time, 3.74 1 s; pulse width, 6.2 μs; data points, 38912; d_1 (time delay), 0.0 s. Before acquisition, the following pre-saturation procedure was set: pre-saturation power, 5.0 dB; pre-saturation frequency, -1157.100 Hz; pre-saturation delay, 1.50 s. The spectrum was later simulated using the calculated coupling constants and

iterated by the application of LAOCOON principle[66,67,68] on the VNMR software platform.

(c) ^{31}P-decoupled ^{1}H NMR experiment.

The ^{31}P-decoupled spectrum of **1** was recorded on the 400 MHz NMR instrument operating at proton frequency of 399.951 MHz. The same sample used for ^{1}H NMR spectrum (b) was used for this purpose. The following selected experimental conditions were employed: acquisition time, 3.734 s; data points, 17152; spectral width, 2296.7 Hz; pulse width, 6.2 μs; delay time (d1), 2.00 s; transmitter frequency offset, -361.9 Hz; transients, 32; decoupling nucleus, ^{31}P; decoupler mode, 'nny'; decoupler modulation mode, 'w'; decoupler modulation frequency, 8000 Hz; decoupler power, 45 dB; temperature, 25 ^{0}C. TMS was used as internal reference.

(d) Selective ^{1}H decoupling.

The same sample as in (b) was used for this purpose. The following selected experimental conditions were employed: acquisition time, 1.799 s; data points, 13184, spectral width, 3664.0 Hz; transmitter power, 60 dB, pulse width, 11.0 μs; delay time (d1), 0.0 s; transmitter frequency offset, 4635.7 Hz; transients, 128. Before acquisition, pre-saturation mode was set as

follows: pre-saturation delay time, 1.500 s; pre-saturation mode, 'ynn'. The following selective decoupling parameters were set: decoupler frequency offset (dof), -915.7 Hz, decoupler modulation mode, 'c'; decoupler power, 26 dB; decoupler modulation frequency, 8589 Hz; decoupler mode, 'nny'. The experiment was carried out at 25 ^{0}C and the ^{31}P chemical shift are relative to 85% orthophosphoric acid (δ_P 0.00 ppm).

(e) ^{13}C NMR spectrum.

The spectrum was recorded on the 200 MHz NMR instrument operating at the ^{13}C frequency of 50.289 MHz. A 10mg sample of **1** was dissolved in 0.5 ml chloroform-d_1. The following selected acquisition parameters were employed: acquisition time, 1.498 s; data points, 37440; spectral width, 12500.0 Hz; pulse width, 3.2μs; transients, 2048. The chemical shifts values are relative to chloroform-d_1 signal (δ_C 77.00 pm).

(f) X-ray diffraction data.

Sample preparation and data collection of **1** have been described previously[52]. Structure of **1**, was solved by the direct methods using SHELX-86[69] and refined by full matrix least squares of F^2 using the SHELXL-93[70] and other additional parameters[52]. Molecular and crystal

structures of **1** have been deposited at the Cambridge Crystallographic Data centre (CCDC)[52].

Compound 2: 1-oxo-10-phenyl-4,7,10-triaza-2,3-benzo-1-phosphabicyclo [5.3.0]decane.

(a) Preparation and characterisation of **2**.

Compound **2** was prepared and characterised as described previously[54].

(b) Solvent effect experiments.

Similar to **1**, the ^{1}H NMR spectra of **2** were recorded on the 200 MHz NMR instrument operating at proton frequency of 199.976 MHz. Where possible, similar experimental parameters to those used for compound **1** were also employed for compound **2**. The solvent effect spectra were recorded in chloroform-d_1, acetone-d_6 and benzene-d_6 at room temperature (25^0C). Similar to **1**, 5 mg of compound was dissolved in 0.5 ml of each deuterated solvent and warmed to facilitate dissolution. The following important parameters were uniformly employed: acquisition time, 3.744 s; data points, 22464; pulse width, 6.1μs; transmitter power (tpwr), 52 dB and 400 transients.

(c) ^{1}H NMR spectrum for proton assignments.

The ^{1}H NMR spectrum of **2** was recorded on the 600 MHz instrument operating at proton frequency of 599.983. MHz at room temperature. Approximately 5mg of **2** was dissolved in 0.5 ml of chloroform-d_1. TMS was used as internal reference as for all ^{1}H NMR spectra. The following selected acquisition parameters were employed: acquisition time, 4.096 s; data points, 65536; spectral width, 8000.0 Hz; transmitter power, 58 dB; pulse width, 1.4 μs; delay time (d1), 0.012 s; transients, 64.

(c) 'D_2O wash' experiment.

Approximately 5mg of **2** was dissolved in 0.5ml of cloroform-d_1 and the ^{1}H NMR spectrum was recorded on the Bruker 500 MHz NMR instrument operating at proton frequency of 500.1321 MHz before and after D_2O wash. Two drops of D_2O were added to the already prepared sample and vigorously shaken at intervals to facilitate proton exchange. The improvement on the 'non-D_2O' washed spectrum was monitored until no physical changes could be observed. It was then that the final spectrum was recorded. Similar acquisition parameters were used for both experiments as follows: acquisition time, 7.707 s; delay time (d1), 1.00 s; data points, 65536; spectral width, 4251.70 Hz; transients, 256.

(d) ^{1}H NMR and ^{31}P –decoupled ^{1}H NMR spectra of **2a**.

Approximately 5mg of **2a** was dissolved in 0.5 ml of chloroform-d_1 and the spectra recorded at the operating proton frequency of 199.976 MHz. Similar experimental conditions as applied for solvent effect experiment for **2** were also employed for initial ^{1}H NMR spectrum before decoupling. The following selected decoupling parameters for ^{31}P-decoupling were employed: decoupling nucleus, ^{31}P; decoupler frequency, 80.95 MHz; de-coupler power, 17 dB; decoupler offset (dof), 1863.8 Hz; decoupler mode, 'nny'; decoupler modulation mode, 'w'; decoupler modulation frequency, 200M Hz. The same acquisition parameters for ^{1}H NMR spectrum were employed for ^{31}P-decoupled spectrum.

(e) Cosy spectrum of **2**.

The same solution used for 'D_2O wash' experiment was also used to acquire the cosy spectrum of **2** before the introduction of D_2O. The cosy spectrum was recorded on the 500 MHz NMR instrument operating at proton frequency of 500.13 MHz. This homo-nuclear ^{1}H-^{1}H two-dimensionally correlated spectrum was obtained using the cosygs pulse sequence (i.e. a program in the Bruker software). The following important conditions were set before the actual acquisition: transients, 8; spectral width, 4251.70;

acquisition time, 0.240 s; receiver gain, 64; delay time (d0), 0.00 s; first delay time (d1), 1.486 s, temperature, 25 ^{0}C.

(f) ^{13}C NMR spectrum of **2**.

Additional 5mg of **2** was added to the solvent effect sample (b) in chloroform-d_1 to increase the sensitivity and warmed to facilitate dissolution. This experiment was recorded on the 200 MHz instrument operating at carbon-13 frequency of 50.289 MHz. The following selected parameters were employed: acquisition time, 1.498 s; data points, 37440; spectral width, 12500.0 Hz; transmitter power, 50 dB; pulse width, 3.2 μs; transients, 10 240.

(g) X-ray diffraction data for **2**.

Crystallographic data of **2** has been reported elsewhere[54]. The molecular structure was resolved by different methods and refinement, based on F^2, was by full-matrix least square method[55,71]. Additional crystallographic data not included in the text is available in .cif format from the RSC website (http://www.rsc.org/suppdata/cc/1999/853/).

Compounds 3: 1-oxo-4,7,10-triaza-2,3,11,12-dibenzo-1-phophabicyaclo [5.5.0]dodecane.

(a) Preparation and characterisation of **3**.

Compound **3** was prepared and characterised previously[54] through lithiation-induced rearrangement of **2** by single N→P migration or double N→P migration from **1**.

(b) Solvent effect experiments for **3**.

Approximately 5mg of **3** were prepared in 0.5 ml of each deuterated solvent, i.e. chloroform-d_1, acetone-d_6 and benzene-d_6. Exactly similar experimental conditions for ^{1}H NMR spectral recordings as for **1** and **2** were employed. However, the solution was warmed to facilitate dissolution in benzene-d_6 and acetone-d_6. The following selected acquisition parameters were uniformly applied for all solvents at the operating proton frequency of 199.977 MHz: acquisition time, 3.744 s; data points, 22564; spectral width, 3000.3 Hz; filter bandwidth, 1600.0 Hz; transmitter power, 52 dB, pulse width, 6.1 μs; 400, transients.

(c) ^{1}H NMR spectrum for proton assignments of **3**.

Approximately 5 mg of **3** was dissolved in 0.5 ml of chloroform-d_1 and warmed to enhance dissolution. The following selected experimental parameters were set on the 500 MHz in NMR instrument operating at proton frequency of 500.132 MHz: data points, 65536 Hz; transients; spectral width, 4251.701 Hz; acquisition time, 7.707 s, delay time (d1); temperature, 25^{0}C. The Fourier transformed spectrum was processed by 1D-WINNMR program software. The spectrum was also later simulated using the same program based on LAOCOON [66,67,68] principle.

(d) Aromatic cosy spectrum of **3**.

An already prepared sample solution of **3** in chloroform-d_1 was used for this purpose. The homonuclear ^{1}H-^{1}H two-dimensional correlated spectrum was obtained using the relay cosy 90-90 pulse sequence (program on the Varian VNMR software). The following selected acquisition parameters were employed: acquisition time, 0.213 s; spectral width, 600 Hz; sixteen repetitions; increments, 25; operating proton frequency, 199.975 MHz. Some of the processing parameters used were as follows: sine bell, 0.052 s; Fourier transform size (FT), 256 x 256, at 25^{0}C.

(e) ^{1}H NMR and ^{31}P-decoupled ^{1}H NMR spectra of **3a**.

A fresh solution of approximately 5 mg of **3a** in 0.5 ml of chloroform-d_1 was prepared for the experiment. Normal acquisition parameters as for solvent effect experiment of **3** in chloroform-d_1 at operating proton frequency of 199.976 MHz were employed to acquire the ^{1}H NMR spectrum of **3a**. However, for ^{31}P-decoupled spectrum of **3a**, calibrated decoupling power level with the correct pulse sequence were employed as follows: transmitter frequency of first decoupler, 80.954 MHz, decoupler nucleus, ^{31}P; decoupler power, 16 dB; decoupler mode, 'nny'; decoupler modulation mode, 'w'; decoupler modulation frequency, 200 Hz. The experiment was carried out at 25^{0}C.

(f) The ^{13}C NMR spectrum of **3**.

A representative ^{13}C NMR was recorded for **3** at 200 MHz instrument operating at carbon-13 frequency of 50.289 MHz. Approximately 10 mg of **3** was dissolved in 0.5 ml of chloroform-d with little warming to achieve complete dissolution. The following selected acquisition parameters were employed: acquisition time, 1.498 s; data points, 37440; spectral width, 12500.0 kHz; transmitter power, 50 dB; pulse width, 3.2 μs; transients, 30 000.

(g) X-ray diffraction of **3**.

Crystallographic data acquisition and processing of **3** have been described elsewhere[54]. A single crystal was mounted on a glass fibre. X-ray intensity data were collected on a Nonius CAD4 diffractometer using graphite-monochromated Mo-Kα radiation (λ = 0.7107A^0) and ω-2θ method. The unit cell was then refined by setting angles of 24 reflections in the range 16-17^0 in 2θ. Reference reflections were monitored periodically for intensity and orientation control. A Lorentz-polarization correction was applied to the data. The non-hydrogen atoms were located with direct method using SHELXL-86[72] and refinement was completed using SHELXL-97[71]. The two independent molecules in the symmetric unit (included in the text) gave rise to eight (8) molecules in space group $P2_{1/C}$. Similar to **2**, the crystallographic data of **3** are available in the .cif format from the RSC website (http://www.rsc.org/suppdata/cc/1999/853/).

CONCLUSIONS

NMR spectroscopy is without doubt the most powerful technique in structural and spectroscopic studies. Several aspects of its application to those subjects form a content of an excellent series "Methods in Stereochemical Analysis" [72]. Volume 8 of this series is dedicated to stereochemical analysis of organophosphorus compounds[24]. In the 10th volume, a specific topic of conformation and stereochemistry of cyclic compounds is discussed[73]. It is surprising to find out that in a section concerning the five membered rings, only one system containing a nitrogen atom incorporated into the heterophospholane ring is discussed in some detail.

In this work we attempted to interpret the NMR spectra of a selected series of new heterocyclic systems containing atoms of carbon, nitrogen and phosphorus in cyclic skeletons of a very defined structure. Since the X-ray diffraction data of our model compounds were available, we were particularly interested in the correlation between the molecular structure and the NMR spectroscopic characteristics. Since the three-bond proton-proton coupling ("vicinal") interactions are related to the corresponding H-C-C-H

torsion angle via the Karplus equation, we identified an opportunity of correlating the structural data obtained from the X-ray diffraction measurements (solid state phase) with the time averaged stereochemical relationships operating in the same molecule, but in a solution. Our selected models of the bicyclic compounds are all of a relatively rigid structure; hence the conformational variations of the heterocyclic rings (five- and seven-membered) are seriously limited. Still, the agreement between the values of the H-C-C-H torsion angles calculated from the experimental $^{3}J_{HH}$ value, and those determined from the molecular parameters obtained in the solid state, is in some cases fair. Obviously, additional spectroscopic determinations, preferably at low temperature, should provide us with more information about the conformational flexibility of our systems.

The chemical assignments of the individual atoms (^{1}H and ^{13}C) in our molecules were not always easy. We are, however, confident that our assignments are correct, as they reflect the usual effect of the molecular environment (transmitted through the chemical bonds, as well as through space) on the shielding parameters of individual nuclei. Since the commencement of the work, a new heterocyclic system, the thio-analogue (P=S bond instead of the P=O bond) of our model **1** has been prepared in our

laboratory, and its X-ray diffraction structure has been determined[75]. It should be of particular interest to prepare the analogue series of the thio-derivatives of the systems **1**, **2** and **3**, and to parallel the study reported in this work with a similar research carried out for the thio-derivatives. The results of such research should yield some information on the relative properties and the effect of the phosphoryl (P=O) and the thio-phosphoryl (P=S) functional groups.

Another extensions of our project should be directed towards solvent effects on the NMR spectra.

REFERENCES

1. Roberts, J.D.; *Chemical Reviews*, 1991, **91**, 7.

2. Becker, E.D.; in *High Resolution NMR, Academic Press, New York,* 2nd ed., 1980, 94.

3. Harries, R.K.; in *Nuclear Magnetic Resonance Spectroscopy*, Longman Scientific and Technical, John Wiley and Sons, New York, 1986, 221-224.

4. Kemp, W.; in *Organic Spectroscopy*, Macmillan, Hong Kong, 3rd ed., 1997, 137.

5. Macomber, R.S., in *Modern NMR Spectroscopy*, John Wliey and Sons, INC, New York, 1st ed., 1998, 135, 139, 155, 226.

6. Jackman, L.M.; Sternhell, S.; in *Application of Nuclear Magnetic Resonance Spectroscopy in Organic Chemistry*, 2nd ed., Pergamon Press, Elmsford, New York, 1969, 270-277.

7. Friebolin, H.; in *Basic One and Two Dimensional NMR Spectroscopy*, Wiley-VCH, Weinhiem, 3rd ed. 1998, 103.

8. Atta-ur-Rahman, in *Nuclear Magnetic Resonance*, Springer-Verlag, New York, 1986, 82-85.

9. Becker, E.O.; in *High Resolution NMR*, Academic Press, New York, 2nd ed., 1980, **93**, 103.

10. Karplus, M.J.; *Am. Chem.* Soc., 1963, **85**, 2870.

11. Haasnoot, C.A.G,; de Leeuw, F.A.M.; Altona, C.; *Tetrahedron*, 1980, **36**, 2783.

12. Gunther, H.; in *NMR Spectroscopy*, John Wiley and Sons, Chichester, 2nd ed., 1992, 115.

13. Karplus, M.J.; *J. Chem. Physics*, 1959, **30**, 11.

14. Torchia, D.A., *Macromolecules*, 1971, **4**, 440

15. Deber, C.M., Torchia, D.A., Blout, E.R., *J. Am. Chem. Soc*., 1971, **93**, 4893.

16. Pogliani, L., Ellenberger, Valat, J., *Org. Mag. Reson*., 1975, **7**, 61.

17. Pavia, D.L.; Lampman, G.M.; Lampman, G.S.; in *Introduction to Spectroscopy*, Saunders College Publishing, New York, 1979, 116.

18. White, D.W.; Karcher, B.A.; Jacobson, R.A.; Verkade, J.G.; *J. Am. Chem. Soc*., 1979, 101, **17**, 4921.

19. Cox, R.H.; Campbell, B.S.; Newton, M.G.; *J. Org. Chem*. 1972, **37**, 1557.

20. Cox, R.H.; Newton, M.G.; *J. Am. Chem. Soc*. 1972, **94**, 4212.

21. Bentrude, W.G.; Tan, H.W.; *J. Am. Chem. Soc*., 1976, **98**, 1850.

22. Pouchoulin, G.; Llinas, J.R.; Buono, G.; Vincent, E.; *J. Org. Magn. Reson*. 1976, **8**, 518.

23. Nielsen, J.; Dahl, O.; *J. Chem. Soc., Perkin Trans*., 1984, **2**, 553.

24. Verkade, J.G.; Quin, L.O.; in *Phosphorus-31 NMR Spectroscopy in Stereochemical Analysis*, VCH., Deerfield Beach, USA, 1987, 73.

24. Williams, D.H.; Fleming, I.; in *Spectroscopic Methods in Organic Chemistry*, 5th ed., McGraw-Hill Book, London, 1995, 91-99.

26. Block, F.; Hansen, W.W and Packard, M.E.; *Physics Riview*, 1946, **69**, 127.

27. Gorenstein, D.G.; in *Phosphorus-31, Principles and Apllication*, Academic Press, New York, 1984, 45-55.

28. Eliel, E.L.; Wilen, S.H.; in *Stereochemistry of Organic Compounds*, John Wiley and sons, INC, New York, 1994, 11, 13, 759.

29. Altona, C.; Giese, H.J., and Romers, C.; *Tetrahedron*, 1968, **24**, 13.

30. Duax, W.L., Wecks, C.M., and Rohrer, D.C., *Crystal Structure of Steroids, Top. Stereochem.*, 1976, **9**, 271.

31. Altona, C., Sundaralingam, M., *J. Am. Chem. Soc.*, 1972, **94**, 8205.

32. Altona,C., in *High Resolution NMR studies of Nucleic acids*, NATO, Advanced Study Inst., Ser.A, 1982, 45, 161.

33. Pitner, T.P., Edwards, W.B., Bassfield, R.L., and Whidby, J.F., *J. Am. Chem. Soc.* 1978, **100**, 246.

34. Aston, J.G., Schumann, S.C., Fink, H.L., and Doty, P.M., *J. Am. Chem. Soc.* 1941, **63**, 2029.

35. Pitzer, K.S., Donath, W.E., *J. Am. Chem. Soc.*, 1959, **81**, 3213.

36. Greenhouse, J.A., Strauss, H.L., *J. Chem. Phys.*, 1969, **50**, 124.

37. McCullough, J.P., *J. Chem. Phys.*, 1958, **29**, 966.

38. Fuchs, B., in *Conformation of Five-membered Rings, Top., Stereochem*, 1978, **10**, 1.

39. Riddel, F.G., in *The Conformational Analysis of Heterocyclic compounds*, Academic, New York, 1980.

40. Riddel, F.G., in *The Stereodynamics of Five-membered Nitrogen containing Rings*, In Lambert, J.B., and Takeuchi, Y., Eds., in *Cyclic Organonitrogen Stereodynamics*, VCH, New York, 1992, 159.

41. Willy, W.E., Binsch, G., and Eliel, E.L., *J. Am. Chem. Soc.*, 1970, **92**, 5394.

42. Anet, F.A.L., and Anet, R., in *Dynamic Nuclear Magnetic Resonance Spectroscopy*, Academic Press, New York, 1975, 54.

43. Hendrickson, J.B., *J. Am. Chem. Soc.*, 1961, **83**, 4543.

44. Hendrickson, J.B., *J. Am. Chem. Soc.*, 1961, **83**, 4537.

45. Dillen, J., and Giese, H.J., *J. Chem. Phys.*, 1979, **70**, 425.

46. Hendrickson, J.B., *J. Am. Chem. Soc.*, 1967, **89**, 7036.

47. Hendrickson, J.B., *J. Am. Chem. Soc.*, 1967, **89**, 7043.

48. Hendrickson, J.B., *J. Am. Chem. Soc.*, 1967, **89**, 7047.

49. Memert, J.M., Otto, M., and Widmer, H.M., in *Analytical Chemistry*, Wiley-VCH, Weinhiem, 1998, 89.

50. Ladd, M.F.C., Palmer, R.A., in *Structure Determination by X-ray Crystallography*, Plenum Press, New York. 2nd ed., 1985, 351.

51. Wan, H., Modro, T.A., *Synthesis.*,1996, **10**, 1227.

52. Bourne, S.A., Mbianda, X.Y., Modro, T.A., Nassimbeni, L.R., and Wan, H., *J. Chem. Soc., Perkin Trans.* 2, 1998, **2**, 87.

53. Mbianda, X.Y., Modro, T.A., and van Rooyen, P.H., *Chem. Commun.* 1998, 741.

54. Bourne, S.A., He, Z., Modro, T.A., and van Rooyen, P.H., *Chem. Commun.*, 1999, 853.

55. Johnson, C.K., ORTEP, *Report ORNL-3794*, Oak Ridge National Laboratory, Tennessee, USA, 1965.

56. Matirn, J.; Robert, J.B., *Org. Magn. Reson.* 1981, **15**, 87.

57. Martin, J., and Robert. J.B., *Org. Magn. Reson.*, 1981, vol.15, **1**, 87.

58. Costantino, M.G., da Silva, G.V.J., *Tetrahedron*, 1998, **54**, 11363.

59. The simulated results were obtained by subjecting the measured coupling constant to a computer simulation program in which case, if the measurements are correct, a replica of that particular spin system will be regenerated.

60. Modro. T.A., Modro, A.M., Bernatowitz, P., Schilf, W., and Stefaniak, L., *Mag. Reson. Chem.*, 1998, **36**, 212.

61. Henold, K.L., *Chem. Commun.*, 1970. 1340.

62. Silverstein, R.M., Webster, F.X., in *Spectroscopic Identification of Organic Compounds*, 6th Edition, John Wiley & Sons, New York, 1998, 166.

63. Du Plessies, M.P., Modro, T.A., Nassimbeni, L.R., *J. Org. Chem.*, 1992, **47**, 34.

64. Hendrickson, J.B., *J. Am. Chem. Soc.*, 1967, **89**, 7046.

65. Pouchert, C.J., Behuke, J., in *The Aldrich Library of ^{13}C and ^{1}H FT-NMR Spectra*, 1rst edition, Aldrich Chem. Co. Inc., Milwaukee, USA, 1993, Vol. **2**, 13359.

66. Castellano, S,, Bothner-By, A.A., *J. Chem. Phys.*, 1964, **41**, 3863-3869.

67. Khlopkov, V. N., Kirev, E.V., Shakhatani, A.G., Krasevin, A.O., CALM., ftp://block.cchem.berkerly.edu/pub/nmr/ms-dos

68. Marat, K., XSM., *The University of Matitoba NMR Spectral Simulation and Analysis Package*, 1996.

69. Sheldrick, G.M., *Acto Crystallogr.*, Sect. A, 1990, **46**, 467.

70. Sheldrick, G.M., SHELXL-93, *Program for the Refinement of Crystal Structures*, Universitat Gottingen, Germany, 1993.

71. Sheldrick, G.M., SHELX-97, *Program for Crystal Structure Analysis*, Univeristat Gottingen, Germany, 1997.

72. Sheldrick, G.M., SHELXL-86, *Program for Crystal Structure Analysis*, Universitat Gottingen, Germany, 1986.

73. Harchand, A.P., in *Methods in Stereochemical Analysis*, VCH, Deerfield, USA,

74. Verkade, J.G., Quin, L.D., Gallagher, J.G., in *Phosphorus-31 NMR Spectroscopy in*

Stereochemical Analysis, VCH, Deerfield, USA, 1987.

75. Laurens, S., Ichharam, V.H., Modro, T.A., Submitted for publication.